MASTERARBEIT / MASTER'S THESIS

Titel der Masterarbeit / Title of the Master's Thesis

„Beam loss monitoring at MedAustron synchrotron with available measurement methods"

verfasst von / submitted by

Raphael Neugebauer, BSc

angestrebter akademischer Grad / in partial fulfilment of the requirements for the degree of

Master of Science (MSc)

Wien, 2022 / Vienna, 2022

Studienkennzahl lt. Studienblatt / degree programme code as it appears on the student record sheet:	UA 066 876
Studienrichtung lt. Studienblatt / degree programme as it appears on the student record sheet:	Masterstudium Physik
Betreut von / Supervisor:	Dipl.-Phys. Dr. Eberhard Widmann

Acknowledgements

Abstract

At MedAustron hadron therapy is used to treat cancer patients. The available particles are protons and carbon ions which are accelerated in a synchrotron. When they reach the necessary energy for the deeper penetration of human tissue they are extracted from the synchrotron and guided on to an irradiation room (IR) where the treatment takes place. The number of particles that are injected into the synchrotron and that reach the IR are not the same, i.e. particles are lost in between. There is no active beam loss monitoring system for the accelerator chain therefore no exact information about the particle losses is available. Some of the particle losses are part of the accelerator design, but previous measurements have shown that loss points occur at unexpected locations as well. The aim of this thesis is to use equipment which is available at MedAustron to find loss points and test methods to characterize them. Measurements with thermoluminescent dosimeters (TLDs) were carried out to localize loss points and compare the occurring particle losses. With these measurements loss points at two unexpected locations of the synchrotron were detected. The chopper dump, a loss point by design in the high energy beam transfer line, expectedly produced secondary radiation as well and was used for field characterization measurements as well as for benchmarking FLUKA, a Monte Carlo (MC) code environment to simulate interactions of particles with matter, simulations. A vertical profile of the radiation field at the chopper dump was recorded, as well as at one of the unexpected loss points for comparison. The vertical profiles were remarkably different. At the unexpected loss point, the intensity distribution was largely symmetrical with a maximum at the beam height (h = 125 cm), while the intensity increased towards the floor at the chopper dump. A WENDI-II wide range rem counter (neutron detector) was used to estimate the ambient dose equivalent at the chopper dump in a 4-hour measurement shift. That measurement set-up was also simulated with FLUKA, resulting in good agreement with the detector measurements. The FLUKA simulation suggested that only 50% of the particles lost between the extraction and the IR, are lost at the chopper. Therefore, more detailed investigations of the particle losses in that section could be of interest in the future. In conclusion, the TLDs in combination with FLUKA can be used to find loss points and estimate the ambient dose equivalent at the loss points around the synchrotron. This thesis shows possible approaches, where the associated pitfalls are and areas for further research.

Kurzfassung

MedAustron ist ein Zentrum für Krebsbehandlung mit Hadronentherapie. Hierfür werden Protonen und Kohlenstoffionen in einem Synchrotron beschleunigt, sodass sie Energien erreichen mit denen sie bis zu etwa 30 cm in menschliches Gewebe eindringen können. Wenn die nötige Energie erreicht ist, werden die Teilchen aus dem Synchrotron extrahiert und in einen Bestrahlungsraum weitergeleitet, wo sie zur Behandlung verwendet werden. Die Anzahl der Teilchen, die in den Kreisbeschleuniger eingespeist werden, weicht ab von der Anzahl, die im Behandlungsraum ankommt. Das bedeutet, dass dazwischen Teilchen verloren gehen. Da es kein aktives *Beam Monitoring System* bei MedAustron gibt, stehen auch keine genauen Informationen zu den Teilchenverlusten zur Verfügung. Es gibt zwar Teilchenverluste die im Beschleunigerdesign eingeplant sind, allerdings haben 2019 durchgeführte Messungen ergeben, dass Teilchen auch an ungeplanten Orten verloren gehen. Das Ziel dieser Masterarbeit ist es diese Verlustpunkte zu lokalisieren und zu charakterisieren. Hierfür werden bei MedAustron verfügbare Methoden und Ausrüstung verwendet. Mit Thermolumineszenzdosimetern (TLDs) wurden Messungen zur Lokalisierung der Verlustpunkte durchgeführt und es wurden Vergleiche zwischen den Mengen an Verlusten zwischen den Verlustpunkten gezogen. Die Messungen brachten zwei unerwartete Verlustpunkte am Synchrotron zum Vorschein. Des Weiteren wurde Sekundärstrahlung am *Chopper Dump*, einem eingeplanten Verlustpunkt in der *High Energy Beam Transfer Line*, gemessen. Dieser wurde für weitere Messungen herangezogen. Am Chopper Dump, und zum Vergleich auch bei einem der ungeplanten Verlustpunkte wurde je ein vertikales Profil des Strahlenfeldes aufgenommen. Die Profile unterschieden sich voneinander insofern, dass am unerwarteten Verlustpunkt die Intensitätsverteilung größtenteils symmetrisch war, mit einem Maximum auf der Strahlhöhe (h = 125 cm), während die Teilchenintensität (Neutronen) beim Chopper Richtung Boden anstieg. Während einer vierstündigen Messschicht wurde mit einem *WENDI-II Wide Range Rem Counter* (Neutronensonde) die Umgebungs-Äquivalentdosis am Chopper aufgenommen. Der zugehörige Messaufbau wurde mit FLUKA, einem *Monte Carlo (MC) Code* zur Simulation von Wechselwirkungen zwischen Teilchen und Materie, simuliert. Das Ergebnis der Simulation stimmte gut mit dem Ergebnis der Messung mit dem Detektor überein. Des Weiteren lieferte die Simulation Hinweise darauf, dass nur die Hälfte der Teilchenverluste zwischen der Extraktion und den Bestrahlungsräumen am Chopper stattfinden, daher sind genauere Untersuchungen der Teilchenverluste in diesem Bereich in Zukunft notwendig. Zusammenfassend kann man sagen, dass die TLDs in Kombination mit FLUKA geeignet sind um Verlustpunkte am Synchrotron zu finden und die Umgebungs-Äquivalentdosis an diesen Stellen abzuschätzen. Diese Masterarbeit stellt mögliche Ansätze dafür vor, zeigt mögliche damit zusammenhängende Schwierigkeiten auf und weist auf Bereiche für zukünftige Forschung hin.

Contents

Contents

1. Introduction

1.1. Motivation for this Thesis

MedAustron uses a synchrotron to accelerate protons and carbon ions for cancer treatment and research (only protons). However, MedAustron synchrotron does not have an active beam loss monitoring system. Calculations for the general radiation exposure coming from the synchrotron and the required shielding which is needed to meet the Austrian law for radiation protection in such facilities have been performed by Jägerhofer [1]. While these general calculations exist, there is no detailed knowledge about the particle losses around the synchrotron. There are three main reasons why more knowledge on this topic is desirable.

The first reason is efficiency: it is of interest for the patients and the operators to have a system which is running with maximal efficiency. This is not the case, when there are particle losses at locations where they are not expected or planned. There are loss-points which are planned, e.g. beam dumps that have a function which is required for the regular operation of the facility. These kind of loss points are planned and not preventable since they serve an important role in the functioning of the whole system. On the other hand, measurements from 2019 have indicated, that there are loss points occurring at positions which were not previously calculated by MedAustron's beam physicists and are not planned. These loss points minimize the efficiency of the system and since they are unexpected it is also of interest for the operators to know why they occur and did not appear in the previous calculations.

The second reason why, especially unplanned, beam losses are of interest is, that in case components of the synchrotron are changed, e.g. beam diagnostic devices, they should not be placed at locations with a high exposure to radiation since electronic devices can react sensitive to radiation through single event upsets or have another kind of malfunction due to the exposure.

The third reason is workers safety. At loss points some of the the materials of the components become activated. Every three weeks a service slot takes place, where the synchrotron is turned off and maintenance of the system is done. Although activations in the synchrotron where measured to be negligible for the safety of the workers it is still of interest for radiation protection to know where to expect exposure to radiation while the synchrotron is turned off since it is their responsibility that all exposure is always within the limits given by law.

The aim of this thesis is to reevaluate the previous measurements for the locations of the loss points also with respect to the composition of the radiation fields and to perform a more detailed characterization of a known loss point to gain more knowledge about the

profile of the radiation field. Furthermore testing and comparison of methods at a known loss point was carried out to develope a strategy for characterization of the unknown loss points.

1.2. MedAustron

EBG MedAustron GmbH is a company specialized in cancer treatment via hadron therapy and research. It is based in Wr. Neustadt in Lower Austria, ∼50 km south of Vienna. There are only six comparable facilities around the world which offer a similar treatment. At MedAustron particle therapy is performed with protons and carbon ions. At the
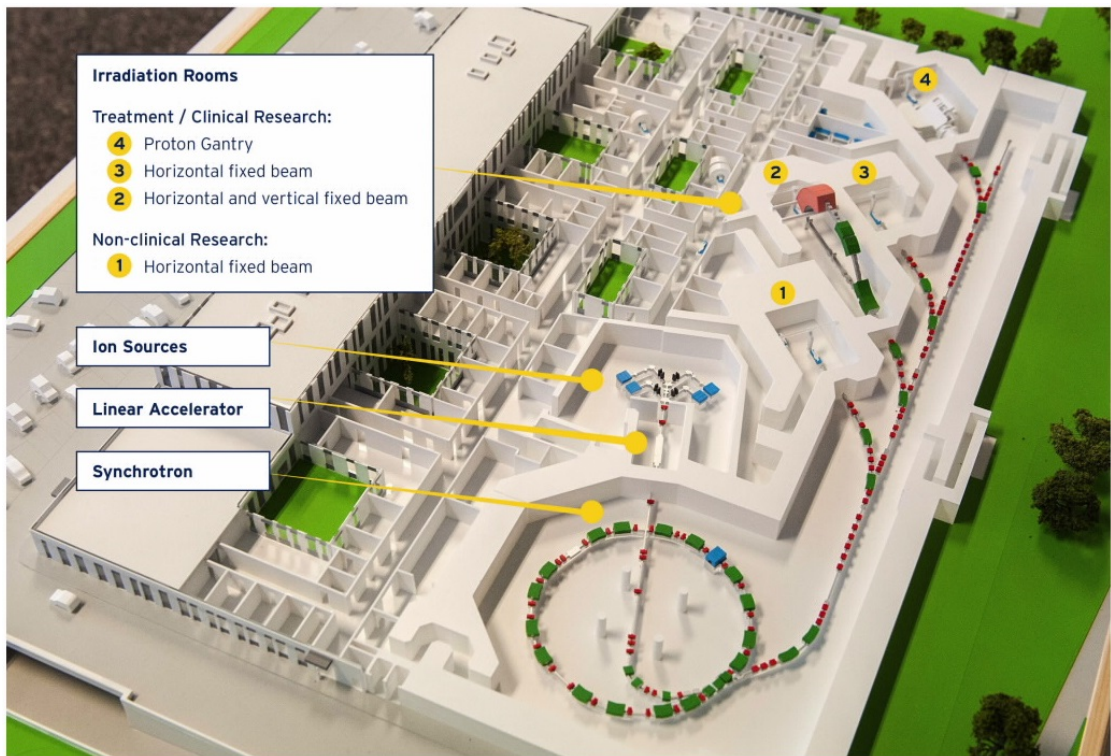
Figure 1.1.: Overview of the of MedAustron facility [2].

moment there are two treatment rooms available, irradiation room 2 (IR2) and IR3, where both have a horizontal beamline and IR2 has an additional vertical beamline. IR1 is only used for research purposes. A third room for treatment (IR4) will be ready for operation this year. It contains a proton gantry which will allow arbitrary angles for the beamline. An overview of the facility is given in Figure 1.1. The particles which are used for the treatment and research are provided by the ion sources. The carbon ions are extracted from CO_2 tanks and the protons come from H_2 tanks. The gases are heated

up to become a plasma, where the ions are extracted by the application of electric fields. In the linear accelerator (LINAC) the particles are accelerated to 7 MeV/u. From there they get passed on to the synchrotron which has a diameter of ∼25 m and accelerates the particles up to 2/3 of the speed of light. When the particles reach the desired energy they are extracted from the synchrotron and led to the IR they were prepared for. For cancer therapy protons between 60-250 MeV and carbon ions between 120-400 MeV are used (approximate penetration depth of up to ∼30 mm). For research purposes protons with energies up to 800 MeV can be produced.

1.3. Hadron Therapy

Hadron therapy uses heavy charged particles, like protons or carbon ions for cancer treatment. These particles need to reach a certain energy level to be able to penetrate a tissue to the required depth. To reach this energy, an accelerator facility which meets these requirements is needed. Considering that a facility like MedAustron demands a high energy supply and a lot of resources, one might ask what the advantage of hadron therapy is, in contrast to cancer treatment with X-rays. When protons and heavy charged particles
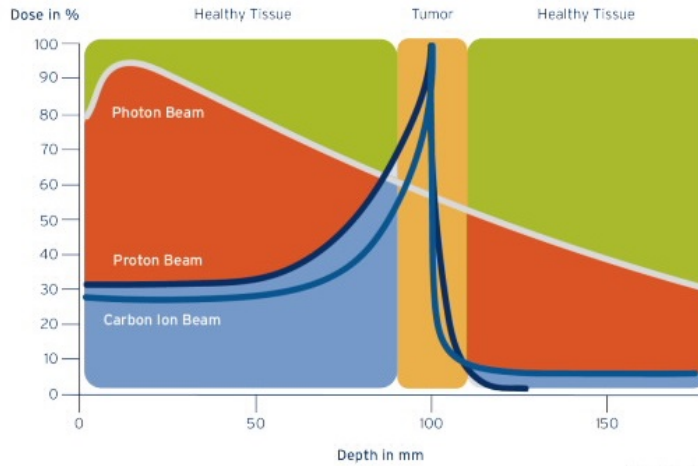
Figure 1.2.: Bragg curve of protons and carbon ions [2].

pass through matter they lose their energy mostly via ionization. This is described by the Bethe-Bloch equation. The Bragg curve is the graph which represents the energy loss rate, or Linear Energy Transfer (LET) as a function of the distance the particles travel through the matter. The energy loss is primarily dependent on Z^2 of the stopping matter but also inversely proportional to the square of the projectiles' velocity

$$-\frac{dE}{dx} \propto \frac{1}{v^2}.$$ (1.1)

This means the highest energy loss takes place right before the particle comes to a stop [3]. This is also displayed in Figure 1.2, where one can see the energy deposition of

protons and carbon ions in comparison to photons in the same tissue. The x-axis shows the penetration depth in mm, where there is a tumor at 100 mm. The particles used in hadron therapy deposit most of their energy exactly at this depth, while most of the healthy tissue is spared (dose level is at ∼30% before the tumor and below 10% behind the tumor). The photon beam on the other hand deposits most amount its energy in the healthy tissue before the tumor and still deposits energy in the healthy tissue behind the tumor. Hence, the main advantage of hadron therapy in comparison with conventional radiation therapy is that the dose in surrounding healthy tissue is minimized, reducing side effects such as damage to sensitive neighboring areas or reducing the probability of secondary cancers caused by radiation. This makes hadron therapy an important tool for treating cancer in sensitive areas (head, neck etc.) and for treating children. Patients who have already had treatment with photons and can not undergo the side effects of radiation with photons again also have indications for treatment with hadron therapy.

2. Theoretical Background

2.1. Physical Quantities

For the better understanding of the physical background of radiation and dosimetry, a few physical quantities as described by Knoll [4] will be introduced in this section.

2.1.1. Fluence

In general the *fluence* is defined as

$$\Phi = \frac{\mathrm{d}N}{\mathrm{d}a} \, [\mathrm{cm}^{-2}]. \tag{2.1}$$

Here $\mathrm{d}N$ marks the differential number of particles that are incident on a sphere with the differential cross-sectional area $\mathrm{d}a$. For a monodirectional beam the fluence is just the number of particles per unit area which is orthogonal to the beam. The fluence is therefore measured in the unit cm^{-2}.

2.2. Dosimetric Quantities

2.2.1. Absorbed Dose

The *absorbed dose D* is defined as the energy coming from any kind of radiation which is absorbed per unit mass of the absorber. It is measured in the SI units J/kg which is also known as gray (Gy).

$$D = \frac{E}{m} \left[\frac{\mathrm{J}}{\mathrm{kg}}\right] \tag{2.2}$$

2.2.2. Dose Equivalent

When living organisms are taken into consideration, the effects of radiation might be very different for the same amount of energy per unit mass absorbed. For example the biological damage created by radiation can differ a lot if the energy is deposited by heavy charged particles or electrons. This difference is related to the *linear energy transfer* (LET) which has large values for heavy charged particles and is smaller for electrons, while the amount of deposited energy per unit mass remains the same.
To take these differences into account the *dose equivalent H* was introduced. It is the product of the the absorbed dose D and the dimensionless quality factor Q

$$H = DQ \left[\frac{\mathrm{J}}{\mathrm{kg}}\right]. \tag{2.3}$$

The quality factor increases with the LET. For instance, for beta particles and other fast electrons the absorbed dose and the dose equivalent are more or less equal, hence $Q = 1$, while for alpha particles $Q \approx 20$. For neutrons Q depends a lot on the energy, but is mostly also larger than 1, since neutrons deliver most of their energy in the form of heavy charged particles. The SI unit for H is the same as for D but is called *sievert* (Sv) in this case, which makes it easier to distinguish between absorbed dose and dose equivalent. The International Commission on Radiation Protection (ICRP) denoted the *equivalent dose* in their report ICRP Publication 60 [5] as follows

$$H_{T,R} = w_R \cdot D_{T,R}. \tag{2.4}$$

Here $D_{T,R}$ is the absorbed Dose averaged over a tissue or organ T which was exposed to the radiation R and w_R is the weighting factor which takes the biological effects of radiation R into account.

Radiation weighting factors, $w_\mathbf{R}$.

Radiation type	Radiation weighting factor, $w_\mathbf{R}$
Photons	1
Electrons and muons	1
Protons and charged pions	2
Alpha particles, fission fragments, heavy ions	20
Neutrons	A continuous curve as a function of neutron energy

Table 2.1.: This table shows the values for the weighting factor w_R for different particles and energies as given in the ICRP report 116 [6].

In case different kinds of radiation are involved, the sum over all radiation types must be taken and the dose equivalent becomes

$$H_T = \sum_R H_{T,R} = \sum_R w_R \cdot D_{T,R}. \tag{2.5}$$

The function for the energy dependent weighting factor w_R for neutrons in Table 2.1 is given as follows:

$$w_R = \begin{cases} 2.5 + 18.2 \, e^{-[\ln(E_n)]^2/6}, & E_n < 1\,\mathrm{MeV} \\ 5.0 + 17.0 \, e^{-[\ln(2E_n)]^2/6}, & 1\,\mathrm{MeV} \leq E_n \leq 50\,\mathrm{MeV} \\ 2.5 + 3.25 \, e^{-[\ln(0.04E_n)]^2/6}, & E_n > 50\,\mathrm{MeV} \end{cases} \tag{2.6}$$

The function for the energy dependence of w_R for neutrons is displayed in Figure 2.1
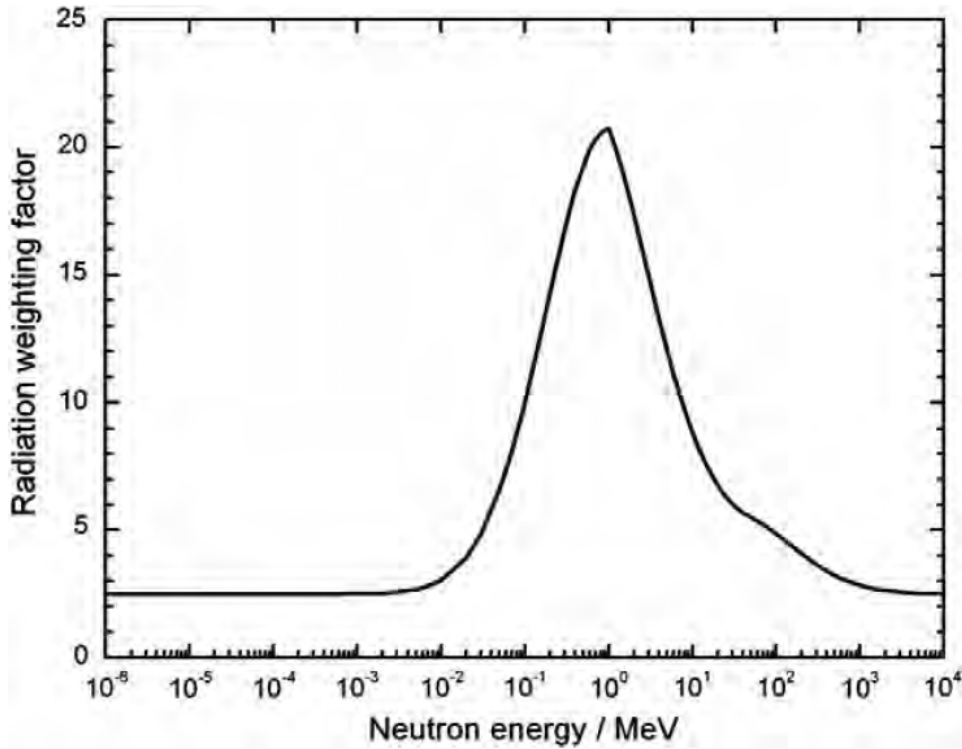
Figure 2.1.: w_R for neutrons as a function of the neutron energy [6] .

2.2.3. Ambient dose equivalent H*(10)

The ambient dose equivalent H*(10) is an operational quantity for area monitoring. At a point in the radiation field it is defined as the dose equivalent which would be produced by the corresponding expanded and aligned field in the ICRU sphere at a depth of 10 mm on the radius opposing the direction of the aligned field [6]. Its unit is sievert. The ambient dose equivalent is a relevant quantity because operational quantities are measurable unlike the effective dose (see section 2.2.5) for example. Measurement devices which are used for dose monitoring are calibrated in the terms of operational quantities.
The ICRU sphere which is used to define the ambient dose equivalent is a tissue equivalent sphere prescribed by the ICRU with a diameter of 30 cm and the following composition (by mass): 76.2% Oxygen, 10.1% Hydrogen, 11.1% Carbon, 2.6% Nitrogen. Its total density is 1 g/cm^3 [7].

7

2.2.4. Fluence-to-Dose Conversion

(a)

(b)
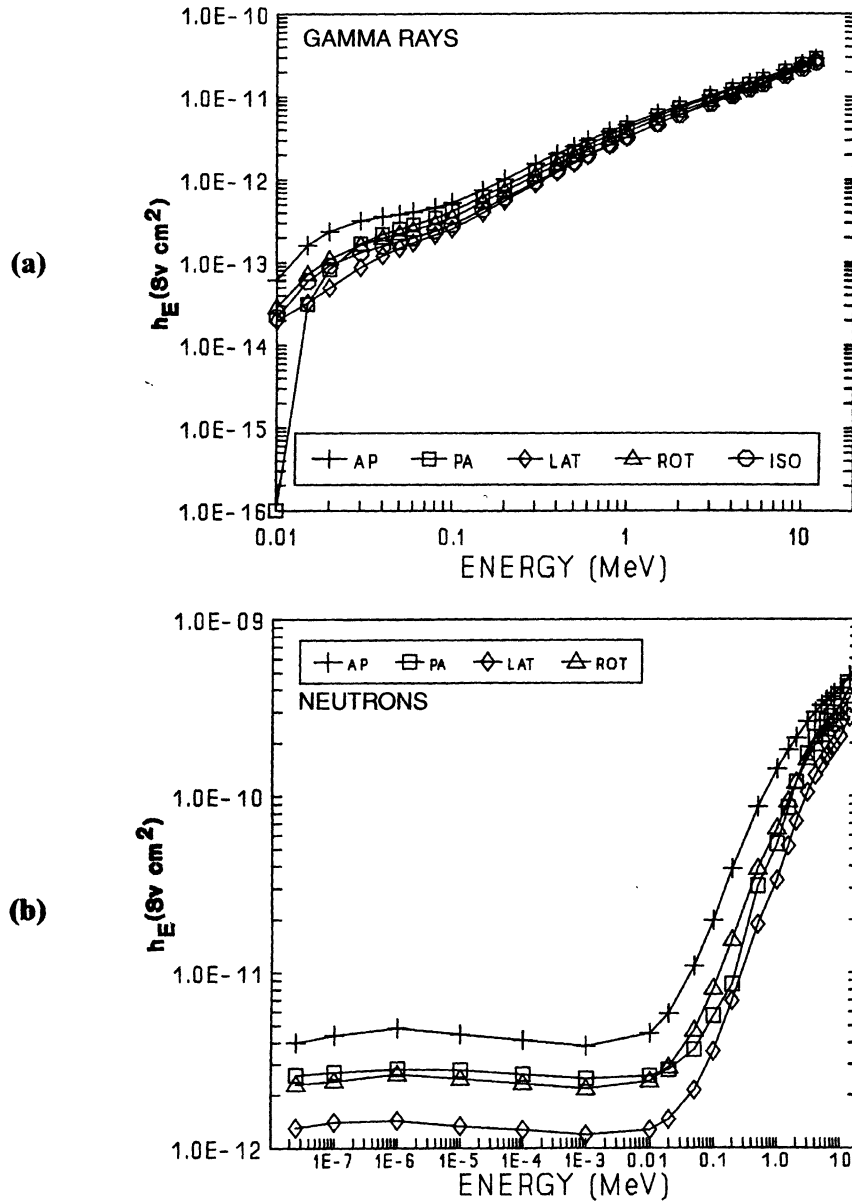
Figure 2.2.: Energy dependence of the fluence-to-dose conversion factor h_E for gamma particles (a) and neutrons (b). The different labels refer to different assumed directions of the incident particle flux. AP - frontal exposure of the body, PA - rear exposure, LAT - exposure from the side, ROT - uniform rotation of the body about its axis, perpendicular to the directional flux and ISO - isotropic incident flux [4].

Most radiation detectors record a number of counts which is created by interactions of incoming particles with the detector volume and therefore more closely related to fluence than to dose. Therefore, a fluence-to-dose conversion is convenient for better interpretation of detector measurements. A conversion from fluence to dose must pay respect to the energy-dependent probabilities of the production of ionizing secondary radiation, the energy that is deposited by this radiation and the quality factor Q which is connected to it. Furthermore, the direction of incidence and the different radiosensitivity of various organs and tissues of the body need to be taken into account. Altogether, the *effective dose equivalent H_E*, which estimates the overall biological effect on the whole body of the exposure to the particle fluence is given by

$$H_E = h_E \phi \tag{2.7}$$

where h_E is the fluence-to-dose factor, dependent on all the previously mentioned properties. An energy dependence of h_E for gammas and neutrons is displayed in figure 2.2.

2.2.5. Effective Dose

There is a weighting factor not only for the radiation type, but also for the exposed tissue, which is denoted by w_T. If that is taken into account as well, one gets the *effective dose E* which is calculated by

$$E = \sum_T w_T \cdot H_T. \tag{2.8}$$

The effective dose here should provide the same information as the effective dose calculated as a product of the fluence-to-dose conversion and the fluence, hence it estimates all effects on the mass which is exposed to radiation. Obviously the tissue-weighting factors are greater for tissues and organs which are more sensitive to radiation. They are also normalized, meaning when considering the radiation on a whole body they sum up to unity and the effective dose then becomes equivalent to the dose equivalent.

It should be noted that these quantities are defined via calculations and can not be measured. What they can provide is guidance for the approximation of potential effects when exposure to radiation needs to be considered.

For measurements, operational quantities like the ambient dose equivalent (see section 2.2.3) are used.

3. Methods

In this thesis three methods were evaluated: simulations with the Monte Carlo (MC) code FLUKA [8], measurements with thermoluminescent dosimeters (TLDs) and measurements with a wide range REM counter capable of measuring high energy neutrons.

3.1. FLUKA

Generally speaking, codes using MC simulations are very useful in the matter of radiation protection. In the case of this thesis FLUKA, a MC code developed at CERN was used, which is introduced on the official website as follows: "FLUKA is a general purpose tool for calculations of particle transport and interactions with matter, covering an extended range of applications spanning from proton and electron accelerator shielding to target design, calorimetry, activation, dosimetry, detector design, Accelerator Driven Systems, cosmic rays, neutrino physics, radiotherapy etc [9, 8, 10]." For the operation with FLUKA *flair* was used which is an interface to work with FLUKA (flair = FLuka Advanced InteRface) [11]. One of its main advantages is the wide range of opportunities of graphical representation of the created geometries and generally a more intuitive usability in the creation of geometries and the handling of the processes. In this thesis FLUKA was used to implement simplified geometries of parts of the synchrotron and have them run with a given beam (e.g. a 250 MeV proton beam), to determine the deposited dose at certain points or to gain some knowledge about the neutron fluence. A more detailed explanation on how the use of FLUKA via flair works will be given later.

3.2. Thermoluminescent Dosimeters (TLDs)

3.2.1. Thermoluminescence

Some crystalline materials have the property of being able to store energy from ionizing radiation which they were exposed to. This stored energy can later be released through emission of the energy as light which is described by the term luminescence. There are different methods which may be used to trigger the emission of the absorbed energy and one of them is via the exposure of the material to heat which is then thermoluminescence [12]. Typically, materials used for thermoluminescence are insulators which have a crystalline structure with some impurities in it (occurring naturally or artificially). When exposed to ionizing radiation, shell electrons from the atoms in the crystal are exited. In an insulator's band structure, the valence band which is filled up with electrons and the empty conduction band are separated by a gap where there are no allowed energy levels

for the electrons. When the insulator is doped with other materials or has some natural impurities, energy levels within the forbidden region appear. When ionizing radiation excites the electrons and lifts them up to the conduction band, some of the electrons get trapped in the energy levels in the forbidden region, where they remain in a metastable region until they receive external energy in the form of heat. That way they can leave the traps and recombine with the holes. While the recombination takes place, visible light is emitted [12, 13]. The principle is visualized in Figure 3.1.
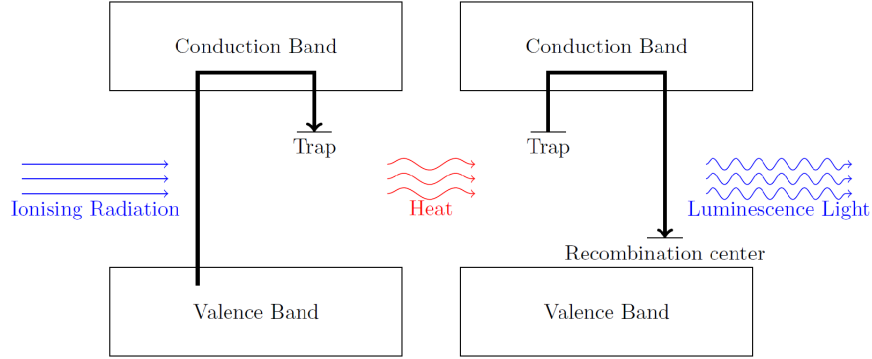
Figure 3.1.: Ionizing radiation elevates an electron to the conduction band and it gets trapped (left). Applying heat releases the electron from the trap, it recombines and light is emitted (right) (©Adrian Thummerer).)

Figure 3.1 shows only one energy level that can function as a trap, but usually there are multiple energy levels with different activation energies where electrons can get trapped (see Figure 3.2). As a consequence the energy required to release an electron from a trapped state is dependent on the energy level of the trap and results in the shape of the glow curve of thermoluminescent materials (see Figure 3.3).
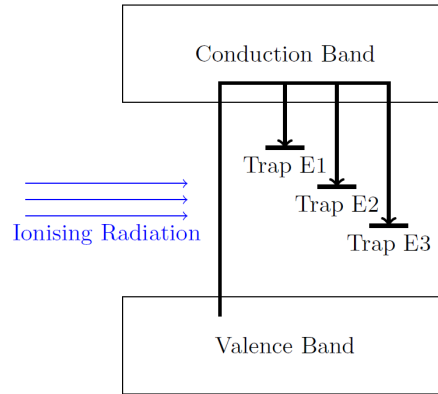
Figure 3.2.: Multiple energy levels functioning as traps between the conduction band and the valence band (©Adrian Thummerer).

Randall and Wilkins [14] provided a basic and simplified theoretical model to describe thermoluminescence in 1945. In this model the shape of a glow peak results from the light, emitted by a single electron trap. This means each peak results from electrons trapped at the same energy level. The model is a *first-order-kinetics* model, since the possibility of electrons leaving a trap and then getting trapped again at another level is not considered. The intensity of the emitted light as a function of the temperature is then given by

$$I(T) = s \cdot n_0 \cdot \exp\left(\frac{-E_t}{kT}\right) \cdot \exp\left[-\frac{s}{\beta}\int_{T_0}^{T} \exp\left(\frac{-E_T}{k\theta}\right)d\theta\right], \tag{3.1}$$

with the frequency factor s, the number of trapped electrons n_0, the activation energy of the specific trap E_t, the Boltzmann constant k, the temperature T, the linear heating rate β and the starting temperature T_0. A characteristic glow curve is displayed in Figure 3.3, where the individual peaks correspond to the different energy levels of the traps. As one can see, some of the peaks may overlap.
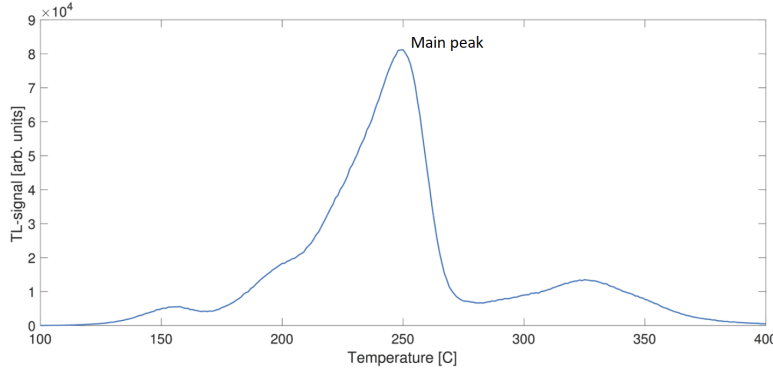
Figure 3.3.: Glow curve of a TLD-100 with markings at the visible peaks (©Adrian Thummerer).

As already stated, the glow curve is a function of the temperature. The peaks which occur at lower temperatures are the traps which are closest to the conduction band, since the least energy is required to elevate the electrons trapped there. Hence the high temperature peaks correspond to the deeper traps. The glow curve resulting from the heating process is a superposition of all the peaks.
Thermoluminescent materials can be used for dosimetry, because the emitted light during the heating process is proportional to the absorbed dose. It is a relative dosimetric method which is used in medical applications, for personal, environmental and space dosimetry. There are different approaches to analyze the glow curve. One could naively integrate the whole glow curve, which would make the measurement a time dependent process, since some electrons which are trapped in the region close to the conduction band might already be released at room temperature. This type of thermal fading is not an issue for the traps where a higher activation energy is necessary. One could also only use the main peak in Figure 3.3 and make a region of interest (ROI) analysis, where the area around

the main peak is taken into consideration for the dose analysis. The other visible peaks are negligible in this analysis.

Since the TLD sensitivity varies with the radiation quality, the TLDs would need to be calibrated for each field where they are used. For the measurements performed in this thesis, the time resolution was three weeks for most measurements, during which the quality of the radiation varied. Therefore the measurements represent the average radiation over three weeks.

Before each measurement the TLDs need to undergo the so-called *annealing* process, which is a thermal treatment, where the TLDs spend a certain of amount time in an oven with specified temperatures to get all the electrons out of the traps and re-establish the traps.

3.2.2. TLD properties

During this thesis TLDs of the types TLD 600 and TLD 700 were used. They consist of a lithium fluorine crystal doped with magnesium and titanium (LiF:Mg,Ti). The types 600 and 700 mean that the ratio of $^6Li/^7Li$ is not natural but enriched either by ^6Li or ^7Li. TLD 600 contains 95.62% of the ^6Li isotope in the LiF part and the TLD 700 99.99% of ^7Li [15]. As a consequence, they have different sensitivities to different particles. The TLD 600 are sensitive to thermal neutron and gamma radiation, while the TLD 700 are only sensitive to gamma radiation [16]. Hence, when a radiation field consists mainly of neutrons and photons which is the case in the MedAustron synchrotron hall [1], it is possible to measure a relatively accurate neutron number by subtracting the counts from the TLD 700 from the TLD 600.

Figure 3.4.: The Risø TLD reader.

The TLDs have a diameter of 4.5 ± 0.1 mm and a thickness of 0.9 ± 0.1 mm. For the measurements they were put into little plastic bags in groups of three or four which were then mounted to the desired measurement location. For the evaluation of the TLDs a Risø DA20 TL/OSL reader from DTU Nutec, Denmark was used (see Figure 3.4).
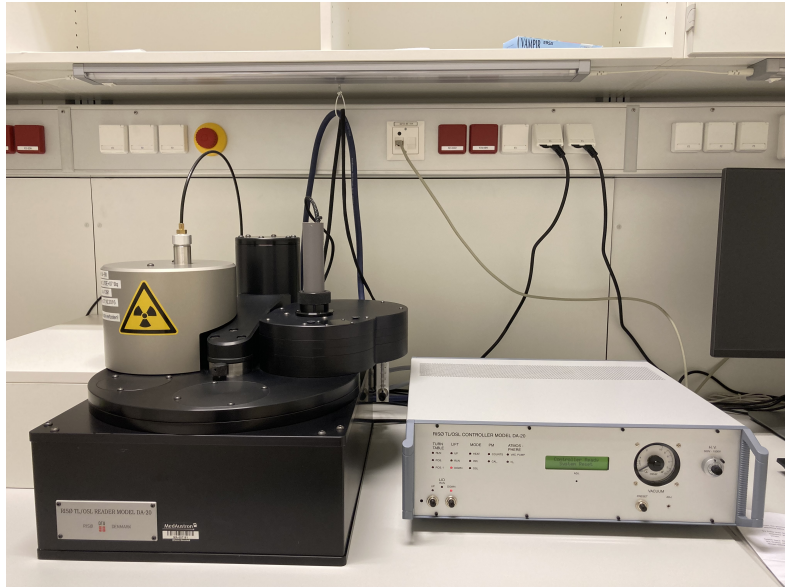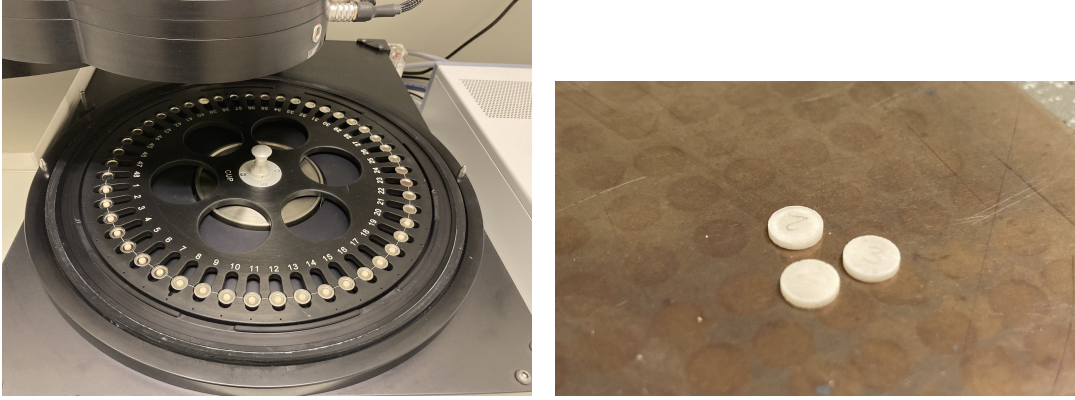
Figure 3.5.: The disc for the TLD placements of the reader (left) and three TLD 700 (right).

3.3. WENDI-II rem Counter

For real time monitoring of ambient dose equivalent rates, a FHT-762 WENDI-II rem counter by Thermo Scientific was used. The WENDI-II rem counter is a wide range neutron rem counter, which means it is able to detect neutrons up to an energy of 5 GeV. It is an extension of a neutron rem counter of the classical Andersson-Braun (A-B) type. The usual energy range of a classical A-B type rem meter is between thermal neutrons up to neutrons with a kinetic energy of about 10 MeV. The basic construction of an A-B rem counter consists of a gas filled counter tube (filled boronfluoride with BF_3 or ^{3}He) surrounded by a moderator shell. The gases used inside the counter tube have their cross section maxima in the region of thermal neutrons. For neutrons with a higher kinetic energy (>10 MeV), the moderator shell is usually not capable of the required moderation, i.e. to slow the neutrons down to thermal energies. Typical materials for the moderator shell contain a lot of hydrogen, like polyethylene or paraffin [1].

To create a wider range of detectable neutron energies, a layer of a high-Z material (e.g. tungsten) inside the moderator shell can be used. In this layer, high energy neutrons can cause spallation reactions which produce slower neutrons [17].

3.3.1. Reaction in the counter tube

The WENDI-II rem counter uses a counter tube which is filled with ^{3}He. For thermal neutrons, the gas has a high cross section for (n,p) reactions. ^{3}He reacts the following way with (thermal) neutrons

$$^{3}_{2}He + ^{1}_{0}n \rightarrow ^{3}_{1}H + ^{1}_{1}p. \tag{3.2}$$

The Q-value which marks the amount of energy which is released by the reaction is $Q = 764\,\text{keV}$. The energy is split up as kinetic energy in opposite directions between the

reaction products:

$$E_p = 573 \, \text{keV} \qquad \text{and} \qquad E_{3H} = 191 \, \text{keV}.$$

Figure 3.6 shows the cross section for the described reaction.
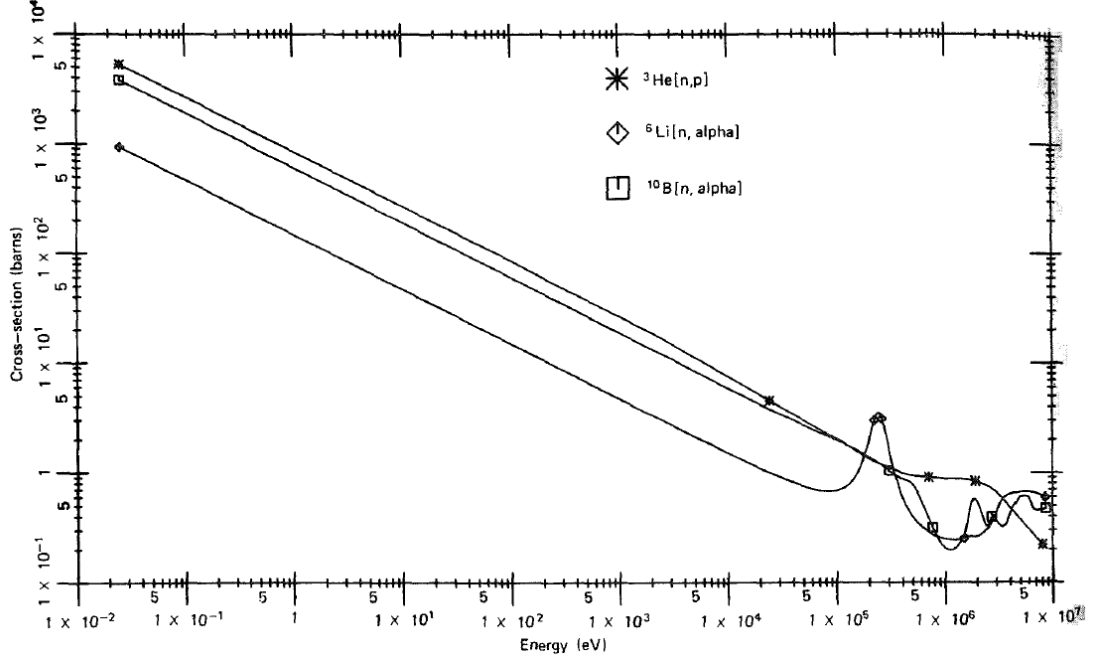
Figure 3.6.: Cross section for ^{3}He(n,p)^{3}H and other gases used in neutron detection [4].

For ^{3}He the value for the cross section, like for the other gases, falls with a $1/v$ energy dependence. For thermal neutrons, the cross section is at 5330 barns, which is significantly higher than for the other gases displayed [4].
Figure 3.6 shows that the cross section for the reaction is decreasing for neutron energies higher than thermal neutrons, which also leads to a decreasing detector efficiency. For this reason the counter tube of the detector is surrounded by a layer of polyethylene, which contains a high amount of hydrogen and works well as a moderator. A schematic representation of the process is displayed in figure 3.7. It shows two detectors with different thicknesses of the moderator shell. Neutrons of the type (1) represent fast incoming neutrons which are moderated successfully and get detected afterwards. The ones labeled with (2) are partially or fully moderated but escape the moderator without reaching the detector. History (3) represents neutrons which are parasitically captured by the moderator [4]. For a high detector efficiency the goal is to reduce processes of the type (2) and (3).

16
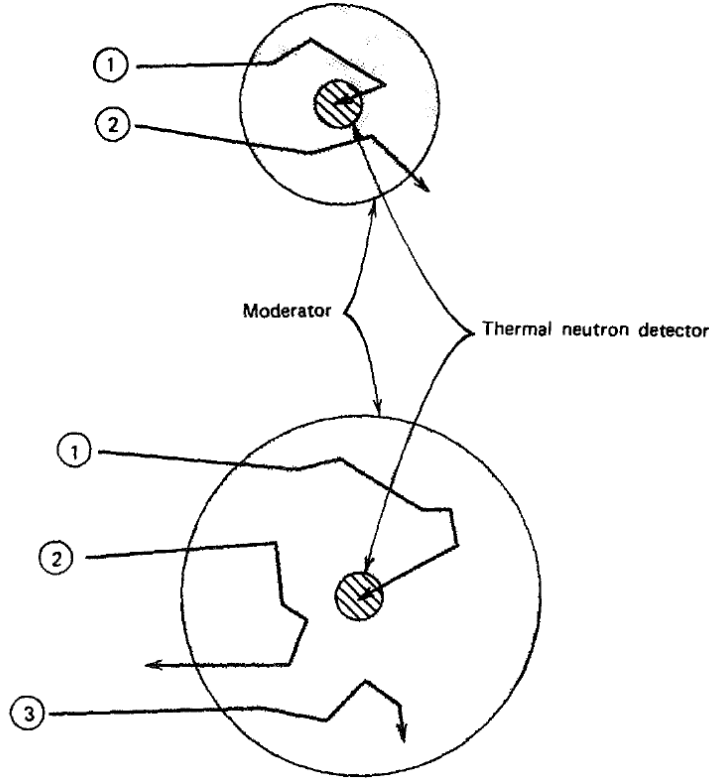
Figure 3.7.: Schematic representation of neutron histories in a moderated detector. The counter tube in the center is surrounded by a moderator. (1), (2) and (3) show different possible histories for incoming neutrons. [4].

For a source with homogeneous neutron energies the response of the detector may easily be adjusted by choosing the appropriate thickness of the moderator shell. For radiation fields with a continuum of neutron energies a response over the full energy range is desired. This is determined via the response function of a detector which describes the number of counts [cts] per incident fluence [cm/cm^3] (=[1/cm^2]) as a function of the neutron energy. According to ICRP, the appropriate operational quantity to use for the calibration of rem counters is the ambient dose equivalent [H*(10)] [1], which is given by

$$H^*(10) = \int h_\Phi(E)\Phi(E)dE \tag{3.3}$$

where h_Φ is the fluence-to-ambient-dose-equivalent conversion function, which was described in section 2.2.4, and $\Phi(E)$ is the neutron fluence in the given neutron field. In that field, the response of the detector R is then given by

$$R = \int Cd_\Phi(E)\Phi(E)dE \tag{3.4}$$

with the rem counters' response function $d_\Phi(E)$ [cts/cm^2] and a calibration constant C [Sv/cts]. For a good neutron detector $d_\Phi(E)$ and $h_\Phi(E)$ match well in their energy

response [18]. Figure 3.8 shows the fluence-to-ambient-dose-equivalent conversion function for neutrons, which was determined by Pelliccioni [19].
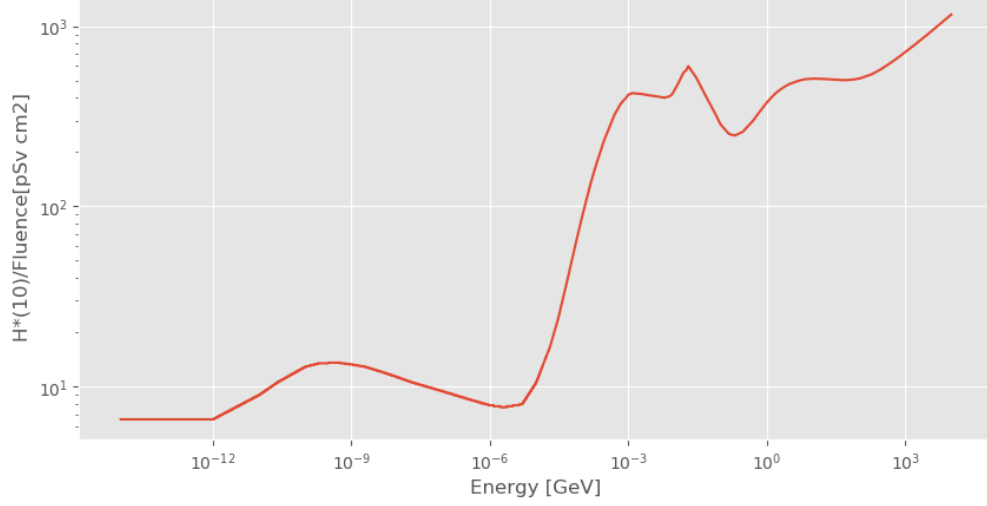
Figure 3.8.: Fluence-to-ambient-dose-equivalent conversion function for neutrons by Pelliccioni [19].
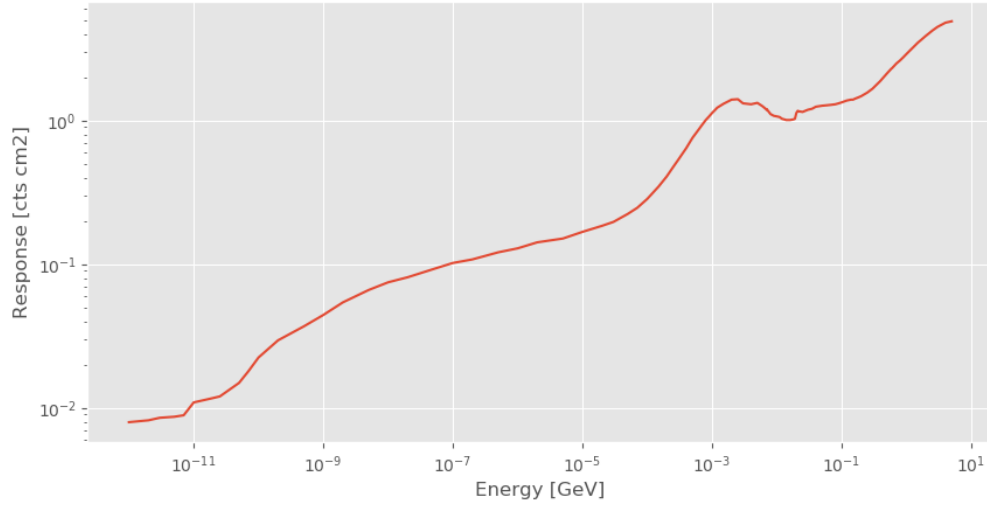
Figure 3.9.: Response function of the neutron detector [20].

For detectors where the moderation happens only through a material rich in hydrogen the response function decreases for energies above 10 MeV. In 1990, Biratti et al. [17] found a way to increase the response of neutron detectors for higher neutron energies, by including a layer of a material with a high Z-value into the moderating shell. High

energy neutrons react with the heavy material via inelastic processes like evaporation and produce low energy neutrons which get detected by the counter tube. Lower energy neutrons pass through this layer without moderation because only elastic processes take place. In the FHT-762 WENDI-II rem counter, which was used in this thesis, a layer of tungsten powder with a tap density of 10.71 g/cm^3 [1] is in the moderator shell. This sets the upper limit of the detector's energy range to 5 GeV. The response function of the detector, which was determined by Jägerhofer [1] is displayed in Figure 3.9. As one can see, the response increases up to energies of GeV.
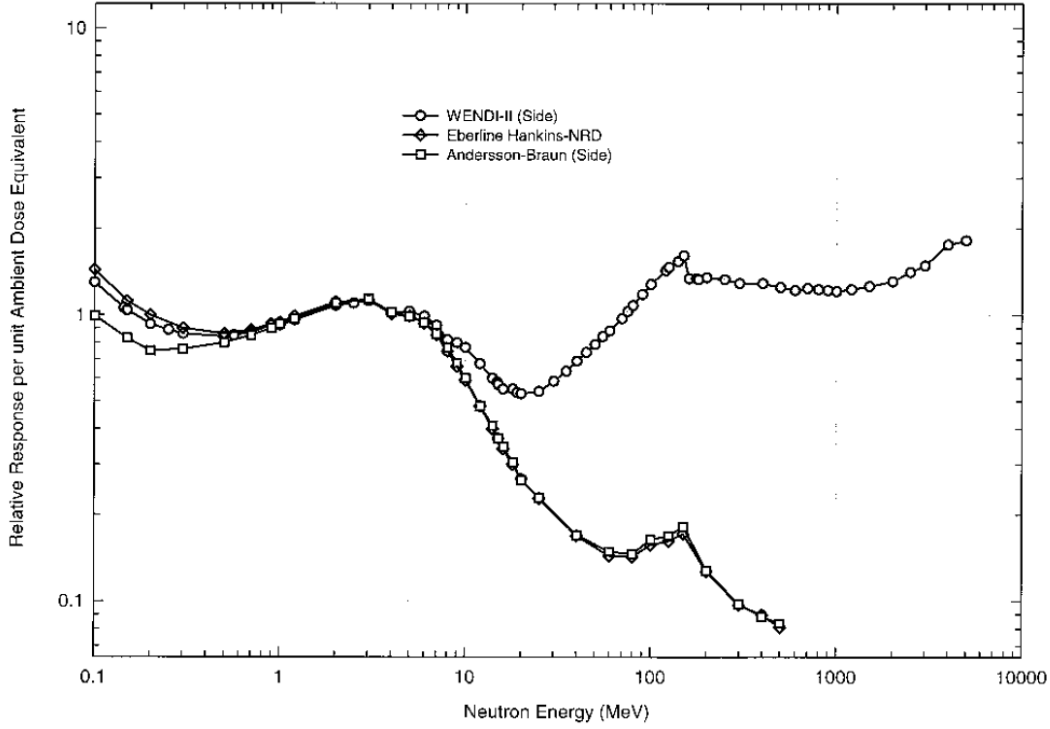
Figure 3.10.: Comparison of different response functions of A-B rem meters and the WENDI-II rem counter [18].

Figure 3.10 shows a comparison of responses between A-B type rem meters and a WENDI-II rem counter. There is a very clear difference in the responses from 10 MeV upwards, which is due to the added tungsten layer.

Figure 3.11 shows a schematic cross section of the used detector. In the center is the counter tube which is surrounded by the polyethylene moderator shell. The darker part in the moderator shell is the tungsten layer which surrounds the counter tube like a cup. The layer is open to the top, which needs to be considered, when using the detector for measurements, because the position of the detector has an influence on its response, since only fast neutrons that pass the tungsten can actually be detected.
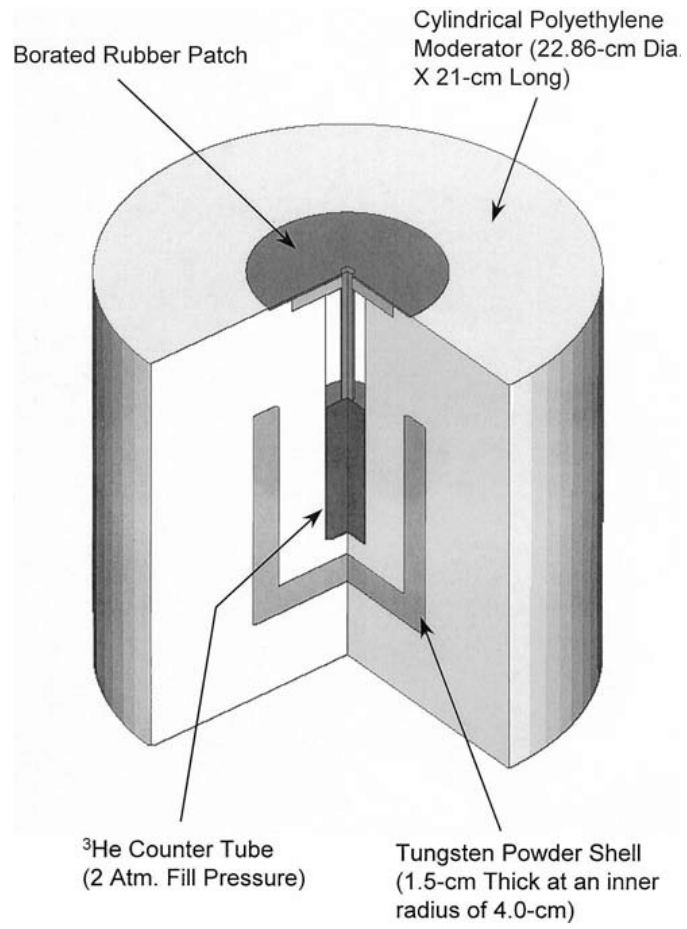
Figure 3.11.: Schematic representation of the WENDI-II rem counter [18].

4. TLD Measurements

4.1. Measurements around the synchrotron

To receive a more precise knowledge about the loss points around the synchrotron, locations with more or less regular distances between them (one measurement point at each dipole magnet) were chosen as measurement points. Previous measurements from 2019 already gave some indications for where to expect more particles of secondary radiation but they could not be used for direct comparison, because those measurements were carried out with TLD 100 which have different sensitivities to photons and neutrons and therefore can not be compared directly to measurements with TLD 600 and TLD 700.
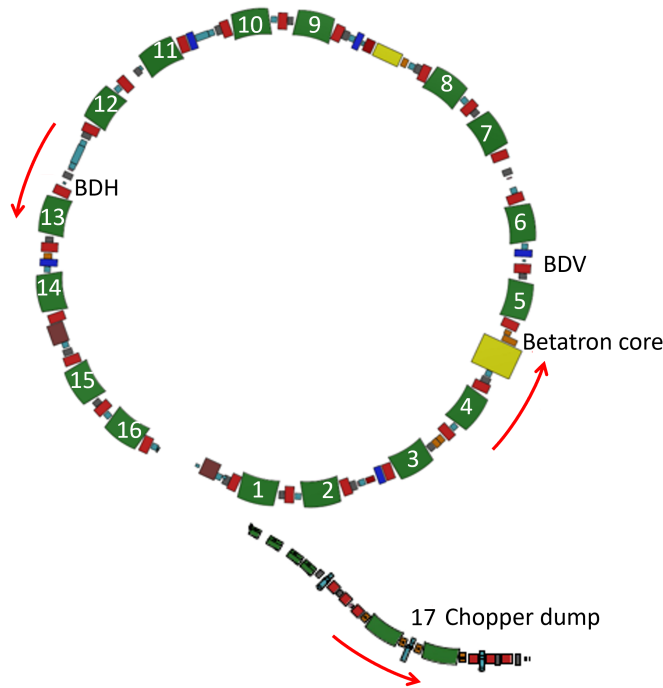
Figure 4.1.: Schematic representation (not to scale) of the TLD positions around the synchrotron for the measurement of loss points. They were numbered counterclockwise starting at the extraction at each dipole (green). One additional set was located at the chopper. The red arrows indicate the beam direction.

Due to the limited possibilities of places where one can affix the TLDs they were located at each dipole magnet of the synchrotron and one set of TLDs was put up right next to the chopper. The chopper is a safety device which is located after the extraction from the synchrotron. It contains a beam dump (a tungsten block) in the beam line. Before and after the chopper are two magnets. When they are turned on, the beam is guided around the beam dump of the chopper. When they are turned off the beam runs directly into the dump. If any beam properties do not match the requirements for the patients treatment, the magnets are turned off and the beam is dumped at the chopper, instead of reaching IR. The chopper is also used to chop off the beginning and end of each spill to provide spills with the required homogeneous intensity and energy.

At each measurement location two groups of four TLDs of each type were put into plastic bags and put on a custom plastic stand (made by Michael Deutsch) with a rubber band. The number of four TLDs for each location comes from the limited number of available TLDs (approximately 100 pieces per kind) and the attempt to approximate the reliability and reduce the statistical uncertainties. Figure 4.1 shows the approximate TLD positioning around the synchrotron. Some of the important loss points which are going to be discussed later are marked.

The TLDs were then left in the synchrotron hall for three weeks in July 2021. That is the time period between two service slots where the usual maintenance is taken care of and it is possible to enter the synchrotron hall, since the accelerator is turned off. Figure 4.2 shows one of the identical plastic stands which were used and how the TLDs were mounted to it. At the dipole magnets the TLDs were positioned on a similar kind of platform. All the TLDs were positioned at beam height, where the highest dose can be expected. Obviously they cannot all be in the exact same spot so their count results were averaged later. Although their position in the bags seems a bit random, it was taken care that they do not overlap to avoid any kind of shielding effects which would result in higher uncertainties.
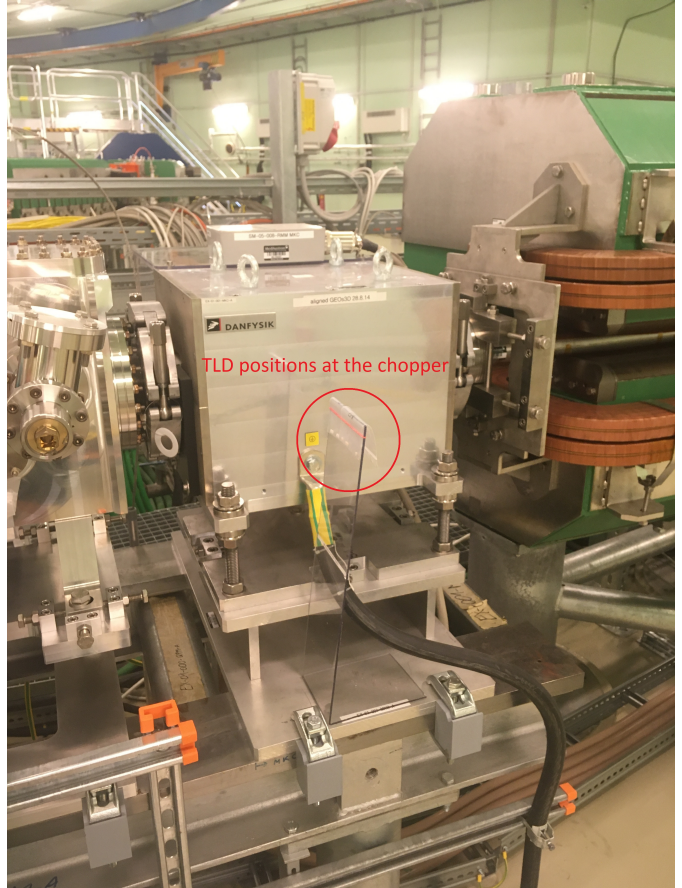
Figure 4.2.: TLD positioning at the chopper.

4.1.1. Results and Discussion

The TLDs spent three weeks inside the synchrotron hall and were measured afterwards with the Risø TLD reader. For the measurement of the TLDs the "Risø sequence editor" software was used which stores the recorded data in .binx and .sec files. After that the "Risø analyst" software was used to translate the .binx files into .txt files and export them. The .txt files were then loaded into a python script written by Michael Deutsch which I modified for my settings. The python script analyses the glow curve via the ROI method and yields a number of counts as a result.
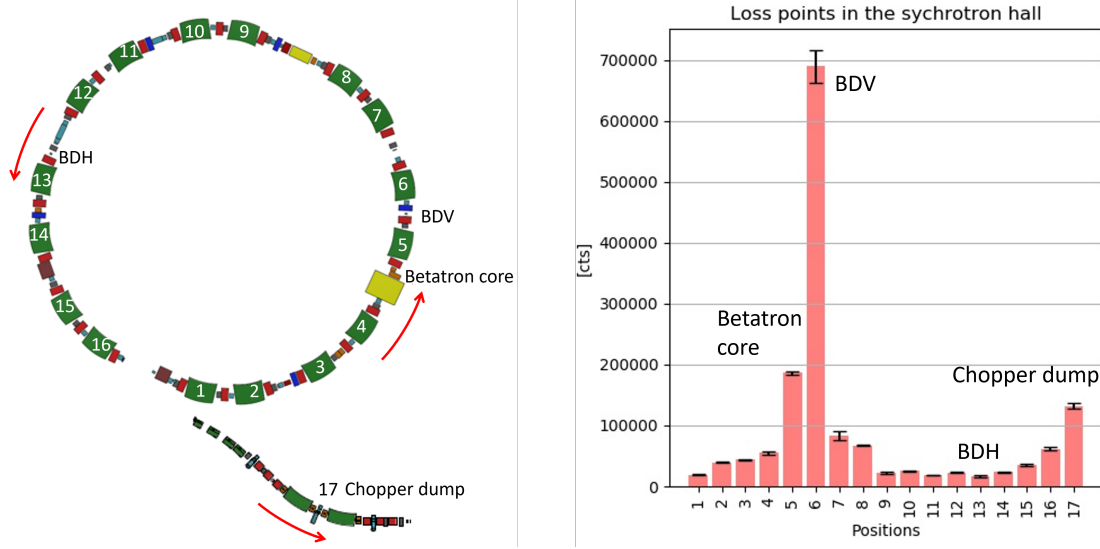
Figure 4.3.: Comparison of the recorded counts at each position around the synchrotron and the chopper, measured by the TLD 600 (right), with the positions as reference (left).

Figure 4.3 shows the average of the absolute counts measured by four TLD 600s for each position with the standard deviation as the error bars. The TLD 600 are sensitive to photons as well as to (thermal) neutrons and therefore measure the highest measurable number of counts with respect to the available TLD types. The loss point where the most secondary radiation is measured, is at position 6, in the vicinity of the BDV. The BDV is a vertical beam dump which acts as a sparingly used, actively triggered safety device. The loss point with the second highest count number (position 5) appears to be next to the betatron core which is a device to initiate the slow beam extraction. Interestingly, at the BDH (position 13), a horizontal beam dump which is supposedly used more than the BDV, a very low number of counts was recorded, suggesting few particles are lost here. This is an indication, that the BDV gets hit by the beam even when not activated, while the BDH does not. The loss point with the third highest count number is at the chopper dump (position 17), where the particle losses are intended. When looking at

the individual contribution of each loss point to the total losses of the synchrotron, it becomes clear that the chopper still represents almost 10% of the secondary radiation of all measured positions in the synchrotron hall. Since one of the main goals of this thesis is to develop a method for better dosimetric mapping of the loss points, the chopper was chosen as point for further investigations, because it is one of the expected loss points (i.e. how exactly the losses occur is known), it is easily accessible for further measurements and it is also not too complicated to implement into a FLUKA simulation. Figure 4.4 shows the recorded counts of the positions, split up into the different radiation types.
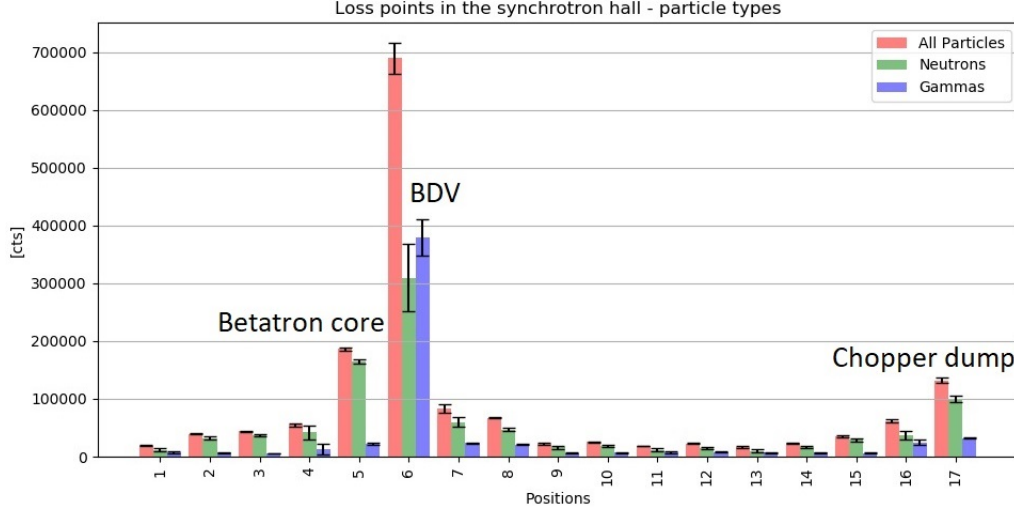
Figure 4.4.: Comparison the recorded counts of the TLD 600 (All Particles) the TLD 700 (Gammas) and their difference (Neutrons).

The TLD 600 measurement is labeled with *All Particles*, while the TLD 700 measurement is labeled with *Gammas*. The green bars, which are labeled with *Neutrons* are the difference between the TLD 600 and the TLD 700 measurements with a larger uncertainty due to error propagation. It becomes clear that the ratio of the TLD 600 result and the TLD 700 result is not the same for all positions. This means the secondary radiation field compositions are varying as well. The neutron-count is usually much higher than the gamma-count. The exception is the betatron core, where the gamma-count contributes to more than half of the total counts measured by the TLD 600. In general, these results support the assumption that the secondary radiation produced by the synchrotron consists mainly of neutrons, but a homogeneous radiation field cannot be assumed. Therefore, detailed measurements have to be carried out at every point where a more precise knowledge about the composition of the radiation fields is desired.

4.2. Vertical measurements

4.2.1. Chopper

Figure 4.5.: TLD positions for measuring a vertical profile at the chopper. The red arrow indicates the beam direction.

The measurements around the synchrotron have shown the chopper to be one of the loss points contributing close to 10% of the secondary radiation, in comparison with the other loss points. For a more detailed characterization of the loss point, a vertical profile of the secondary radiation was recorded in a later three-week period. In that case, the TLDs were mounted to an aluminum pole reaching up to the highest point where electronic devices are located which is at ~185 cm and was the deciding factor for the upper limit of the vertical profile. Bags containing four TLD 600 and 700 each were mounted to five different positions on the pole. For this measurement also TLD 100 were used to receive information about their comparability to the other TLD types. In contrast to the TLD 600 and 700, in the TLD 100 the ratio of ^{6}Li/^{7}Li in the LiF is natural and not enriched with either isotope. In Figure 4.5 one can see the TLD positions at the pole. Position 1 is the highest with a height of $h_1 = (185 \pm 0.5)$ cm and position 5 is the lowest with a height of $h_5 = (4 \pm 0.5)$ cm. As one can see the positions are not equidistant. Position 1 was chosen to be at the height of the highest positioned electrical device and position 5 is the closest possible position

to the floor. Position 3 is not exactly between them but at the same level as the beam ($h_3 = (125 \pm 0.5)$ cm). Position 2 is exactly in the middle between position 1 and 3 at a height of $h_2 = (155 \pm 0.5)$ cm and position 4 is in the middle between the positions 3 and 5 at a height of $h_4 = (62 \pm 0.5)$ cm. The position of the pole is marked by a distance of $d_1 = (44 \pm 2)$ cm to the closer edge of the chopper's vacuum tank and by a distance of $d_2 = (33 \pm 2)$ cm to the center of the SFX which is attached to the vacuum tank. The higher uncertainties for d_1 and d_2 are due to the higher inaccuracy when measuring the distances with a measuring tape.

4.2.2. Vertical Beam Dump (BDV)

For a comparison with the vertical profile of the chopper another loss point, with also a high contribution to the secondary radiation (more than 10%) was chosen for a vertical profile. A similar setup was installed to have a relative comparison of the vertical profiles at the BDV. A pole with five measurements positions was set up next to the BDV and left there for a time period of three weeks. The heights of the positions match the vertical measurements at the chopper, with exception of position 4 ($h_4 = (64 \pm 0.5)$ cm) and position 5 ($h_5 = (10 \pm 0.5)$ cm). The distance to the beamline varied for the different positions because the available rack was not completely vertical. The distance to the beamline was $b_1 = (80 \pm 2)$ cm for the first position, $b_2 = (76 \pm 2)$ cm, $b_3 = (73 \pm 2)$ cm, $b_4 = (68 \pm 2)$ cm and $b_5 = (60 \pm 2)$ cm. The rack is placed to the right of the BDV when looking at Figure 4.6, with a distance of $d_1 = (54 \pm 2)$ cm.
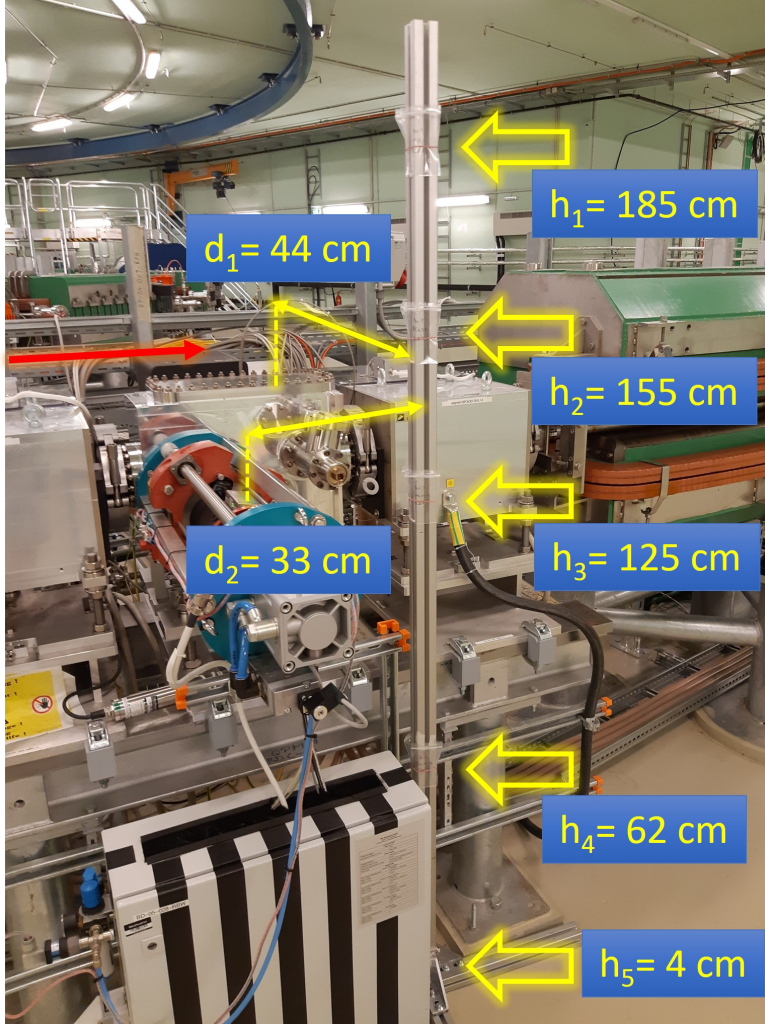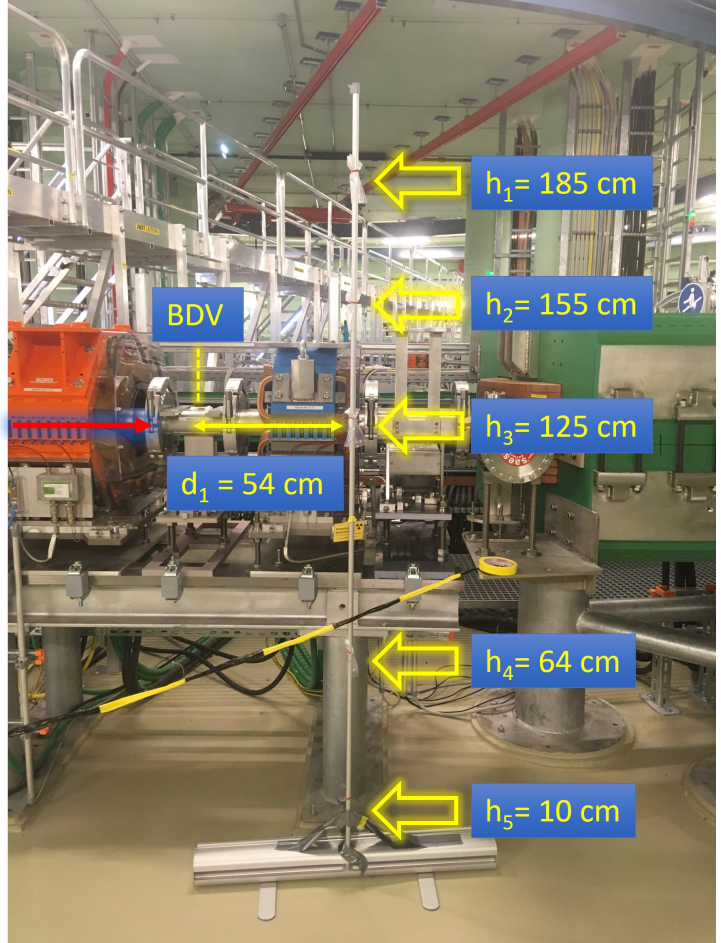

Figure 4.6.: TLD positions for measuring a vertical profile at the BDV. The red arrow indicates the beam direction.

4.2.3. Results and Discussion

Figure 4.7 shows the counts for each position of the vertical profile resolved for every TLD type and also for the difference of the TLD 600 and the TLD 700 count.
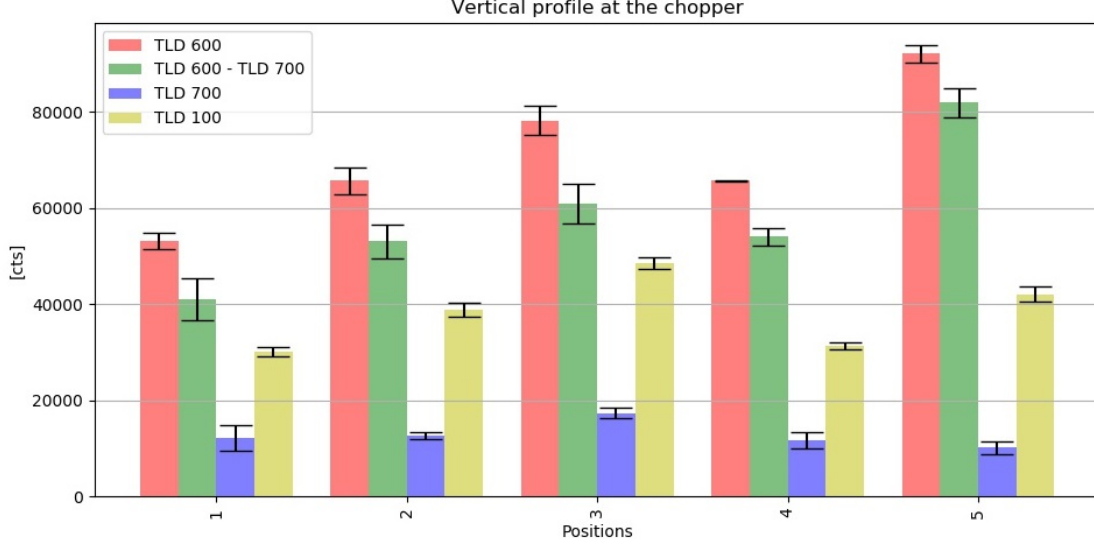
Figure 4.7.: Comparison for all TLD measurements and the calculated neutron counts ($=$ TLD 600 - TLD 700) for the vertical profile of the chopper. Positions: $h_1 = (185 \pm 0.5)\,\text{cm}$, $h_2 = (155 \pm 0.5)\,\text{cm}$, $h_3 = (125 \pm 0.5)\,\text{cm}$, $h_4 = (62 \pm 0.5)\,\text{cm}$, $h_5 = (4 \pm 0.5)\,\text{cm}$.

As expected, the recorded amount of secondary radiation is higher at the positions closer to the beam and lower with further distance from the beam, with exception to position 5 where an unexpectedly high amount of neutrons was recorded. When looking at the gamma-count (TLD 700 in Figure 4.7) there are no surprises in the results. The different behavior of the different radiations here shows that it is very important to use TLDs with different radiation specific sensitivities to receive a better knowledge of the radiation fields produced at certain positions. The TLD 100 show a similar profile to the one of the TLD 600. They were not used in further experiments though, because they have a mixed sensitivity for neutrons and gamma-particles which is unknown. This means they do not really serve for any comparison purposes, since the ratio of neutrons and gammas they record is unknown and will not be found out via calculations. There is also no known calibration for any kind of radiation field for the TLD 100 available at MedAustron so they were not put to further use in this thesis, as all measurement results must be put in to relation here. Of course, calibrated TLD 100 still serve very well for dosimetry, for example for personal dosimetry.

Figure 4.8 shows the results for the vertical profile at the chopper (a) in comparison to the profile at the BDV (b). The unexpected neutron count close to the floor at the chopper

was one of the reasons in the first place why an additional measurement at the BDV was performed.

(a) Chopper

(b) BDV
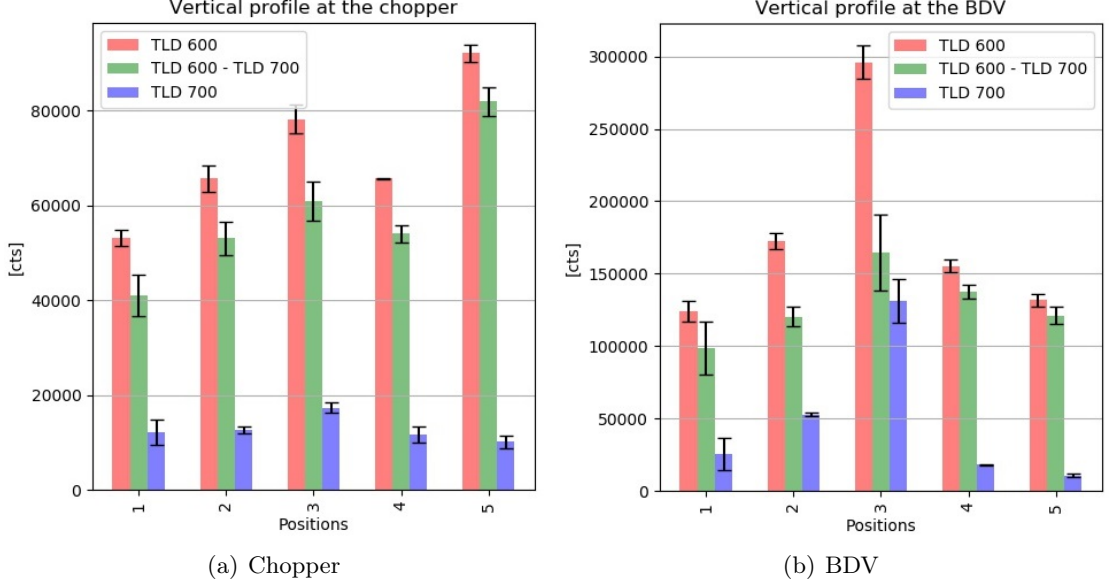
Figure 4.8.: Comparison of TLD 600 and TLD 700 measurements and the calculated neutron counts for the vertical profile at the chopper (left) and at the BDV (right).

The measurements of the BDV show that the extraordinary high neutron count close to the floor measured next to the chopper cannot be replicated at the BDV. The neutron count at the floor is higher than at the higher positions, but by far not comparable to the low position at the chopper, it is clearly less and not more than at the position which is closest to the beam.

The high neutron count close to the floor at the chopper is unexpected, therefore a repetition of these vertical measurements was performed to exclude any errors in the preparation and set up of the first vertical measurements.

4.2.4. Repetition of the vertical measurements

To substantiate the results at the two loss points the measurements were repeated, this time simultaneously, hence they also saw the same beam profile during the three week measurement period. Figure 4.9 shows the new setup. This time two identical racks were available, therefore the horizontal distance to the beamline was the same for all the positions for each rack. The distance to the beamline was $b_1 = (73 \pm 2)\,\text{cm}$ at the chopper and $b_2 = (58 \pm 2)\,\text{cm}$ at the BDV. The heights of the positions were the same for both
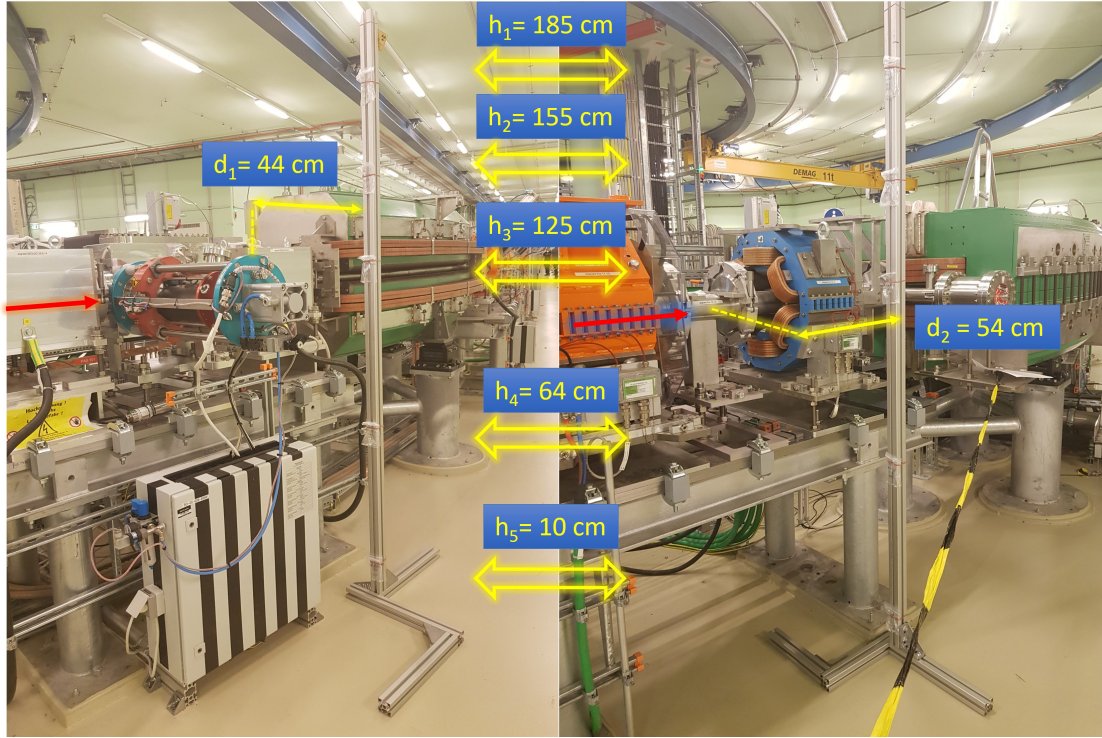
measurements.

Figure 4.9.: Measurement set up for the second measurements at the chopper and the BDV. The red arrows indicate the beam directions (©Claudia Lenauer).

4.2.4.1. Results and discussion

Figure 4.10 shows the results of the second three week measurement at the chopper. There are a few unexpected things to these results. Firstly, the standard deviation for the gamma-count at position 1 is unexpectedly high, as a consequence the same is true for the neutron count. This is due to the fact, that one of the four TLDs at position 1 was an outlier. It recorded a particle count of $N_1 = 32887$ [cts], while the others recorded between $N_2 = 10046$ [cts] and $N_4 = 7365$ [cts]. This results in a mean value which is too large, compared to the positions 2-5 and in a very large standard deviation. Figure 4.10 (b) shows a box-and-whisker-plot of the four TLD 700. The box-and-whisker-plot identifies outliers at positions 1 and 3. The outlier at position 1 is a clear outlier and will be subsequently removed from further calculations and plots. Position 3, however, is not so clear: past experience in using TLDs suggests this outlier is within the expected uncertainty range. In any case, outlier identification with four data points per sample needs to be treated with caution. Since removing the outlier at position 3 would also not meaningfully change the results, it will not be removed.

The exact reason for the outlier at position 1 TLD is unclear, possibly an error in the annealing process resulted in electrons still being trapped from earlier exposure which then were released during the measurement process. The outlier TLD distorts the results, but there are still three TLDs left from this position which can be used to calculate the mean value for position 1, therefore the calculations were done again without the outlier TLD.

Figure 4.11 shows the results of the second chopper measurement again (a), but with the corrected data for the gamma- and neutron count for position 1, and the results of the second vertical profile at the BDV (b). The standard deviation of the TLD 700 at position 1 is still higher than for the other positions, because only three TLDs were used for the analysis while the mean of the other positions was calculated with four TLDs, hence the statistical uncertainty is lower.

(a) All positions

(b) TLD 700: Outlier TLD
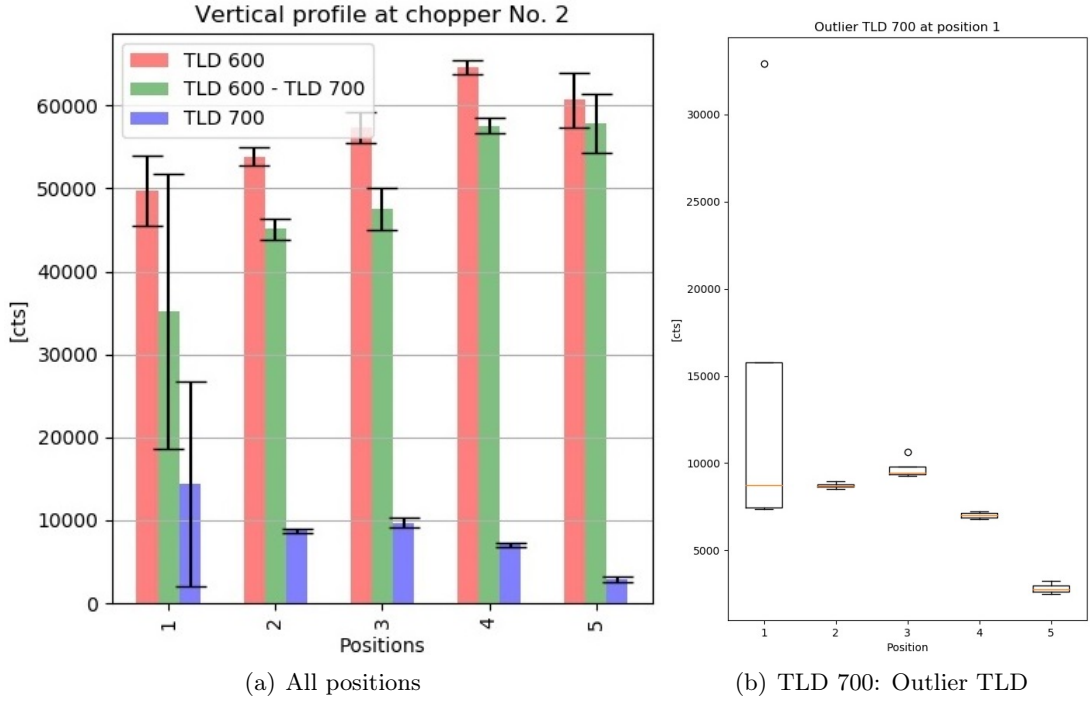
Figure 4.10.: Comparison of the second TLD 600 and TLD 700 measurements and the calculated neutron counts for the vertical profile of the chopper (left) and box-and-whisker-plot of the gamma count of each position (right).

It should be noted that, for this measurement, the highest TLD 600 count was recorded at position 4 and not position 5 as in the previous measurement. When compared to Figure 4.8 one can see how only position 4 makes an exception in the second measurement while position 5 still has more counts than position 3. However, this outcome is a little different from the first vertical measurement at the chopper, the trend and unexpected

higher particle count close to the floor was measured again.

Figure 4.11 also shows the measurement results for the second vertical profile which was measured at the BDV. Although there are some variances in the gamma-count and therefore also in the neutron count, the overall picture remains the same. The highest amount of any particle is found at the position closest to the beamline, while more distance to the beamline results in a decreasing particle count. This means the higher particle count closer to the floor was only measured at the chopper, which was recorded in both measurements. The reason for this peculiar occurrence was not investigated further in this thesis, but remains to be examined in more detail in the future.

(a) Chopper

(b) BDV
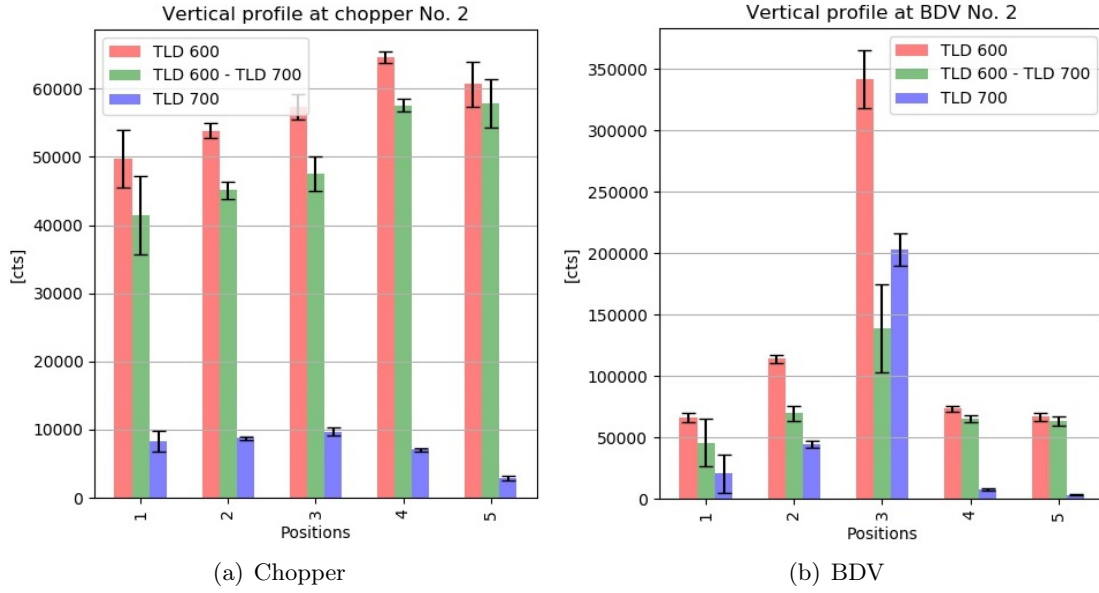
Figure 4.11.: Vertical profile of the second measurement at the chopper with the corrected date for the TLD 700 (left) and vertical profile of the second measurement at the BDV (right).

Figure 4.12 shows a summary of the previously discussed results. It shows the result of all measurements separated into the particle types with neutrons on the left (a) and gammas on the right (b). In the graphic displaying the neutrons, one can very well see the differences in the distribution between the chopper and the BDV. The particle count for both particle types is much higher at the BDV which was already seen in the comparison of the total particle counts of all positions in the synchrotron. The comparison of the results by particle types also open a new perspective on the results and raise questions for further investigations, like what a more detailed distribution of the radiation fields would look like and the reasons for the differences in the distributions.

(a) Neutrons

(b) Gammas
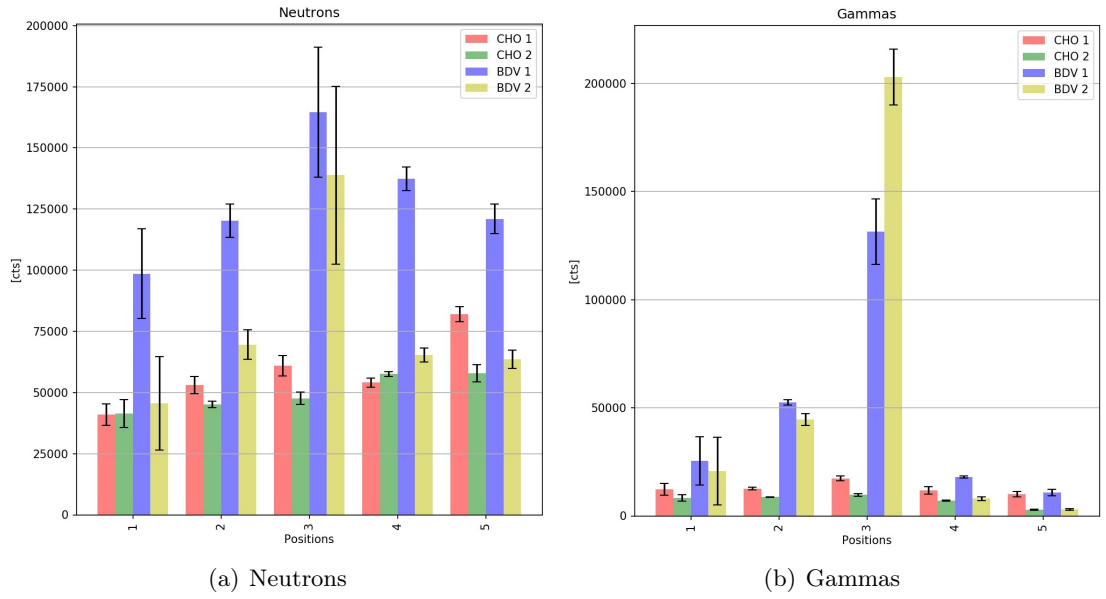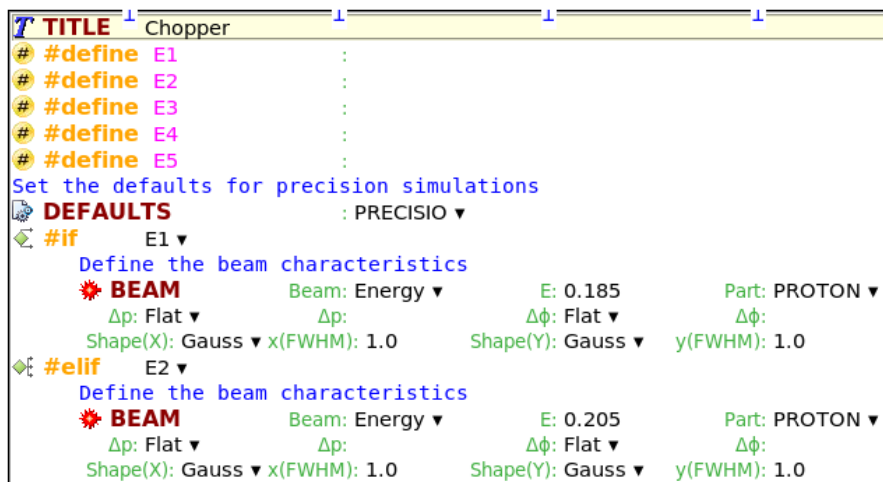
Figure 4.12.: Comparison of all vertical profiles separated by particle types. CHO 1 marks the first measurement at the chopper, CHO 2 the second, BDV 1 the first measurement at the BDV and so on.

5. Chopper dump

5.1. Implementation of the Chopper into FLUKA

The chopper was chosen to get implemented into FLUKA since the mechanism of the particle loss is well known, it has a fairly simple geometry and good access for measurement, as was seen in the sections of the TLD measurements. This will also be used as an example to demonstrate the basic steps which need to be made to use FLUKA via flair for the implementation of the desired real-life geometry.

Figure 5.1.: Defining the properties of the used beam in flair

Basically, FLUKA works with *cards*, where certain properties for the simulation are specified. For example, there is a card for the beam properties, which will be explained shortly. There are cards for the geometric bodies which are used, there are cards for the materials and so on. This is going to be explained with more detail in the following section.

In Figure 5.1 the definition of the beam properties in the given simulation is displayed. In the top rows one can see that beams with five different energies (named E1-E5) can be chosen. This provides the option that an arbitrary amount between one and five simulations with the different beam energies can be run simultaneously. On the displayed figure only the properties of the lowest two energies are shown. The two beams match in all properties but the energies E, which is $E1 = 185\,\mathrm{MeV}$ in the first case and $E2 = 205\,\mathrm{MeV}$ in the second case. FLUKA uses GeV as the unit for energy. The direction of the beam

is by default headed along the z-axes (in positive z direction, see Figure 5.2) therefore the shape in x and y direction has to be chosen, where a Gauss shape with $FWHM = 1$ cm was picked. All length scales are measured in cm in FLUKA. In the measurement which is simulated here a proton beam was used, therefore the particle type is set to *PROTON*.

```
Define the beam position
🌀 BEAMPOS              x: 0.            y: 0.            z: 40.
                    cosx:            cosy:            Type: POSITIVE ▾
🏠 GEOBEGIN         Accuracy:        Option: ▾        Paren:
                    Geometry: ▾      Out: ▾           Fmt: COMBNAME ▾
      Title:
      Black body
   🔵 SPH blkbody      x: 0.0           y: 0.0           z: 0.0
                    R: 100000.0
      Void sphere
   🔵 SPH void         x: 0.0           y: 0.0           z: 0.0
                    R: 10000.0
      Wendi
   🟡 RCC wendi        x: -10.5         y: 50.0          z: 170.0
                    Hx: 21.0         Hy: 0.           Hz: 0.
                    R: 12.5
```

Figure 5.2.: Defining the geometric properties of the simulation.

Figure 5.2 shows the properties of the beamp position in the first few rows. As there are no x- and y-coordinates, the beam still lies on the z-axis and the start of the beam is moved 40 cm into the positive z direction. With cosx and cosy an arbitrary angle for the beam direction could be selected.

In the geometry section (marked by GEOBEGIN) one can only see the first three entries. The first two are basic to any FLUKA simulation. The *Black Body* is a sphere (SPH) creating a shell around everything else and is there for simplicity reasons, since it 'swallows' every particle that travels far enough, hence no 'infinite' calculations need to be performed for any particle. The black body sphere has a radius of $r = 100000$ cm. If one would implement a geometry of a large building the radius of the black body sphere would need to be considerably larger. The *Void sphere* is a smaller sphere placed inside the black body sphere, because an environment where the particles can travel and interact needs to be created. The body with the name *Wendi* assigned to it is the first object of the implemented geometry. It is a cylinder where one can choose the size with the radius R and the the height Hx in this case and the placement, by choosing x-, y- and z-coordinates. There is a few more basic bodies to select from, like cuboids, spheres, planes, wedges etc. With those simple and some more complex geometric bodies many real life geometries can be simulated by adding and subtracting them to obtain the desired bodies. After every body was created, bodys which belong together and are made of the same material (e.g. form a device) are assigned to a region. Figure 5.3 shows how then the materials are assigned to the regions. For every *ASSIGNMA* card a material is selected and the according region is selected, for example *BLCKHOLE* to *BLKBODY*, *AIR* to *VOID*, *ALU* to *REG_ALU* and so on. Of course, not every possible material exists in flair, therefore some materials have to be put together by using a *COMPOUND* card.
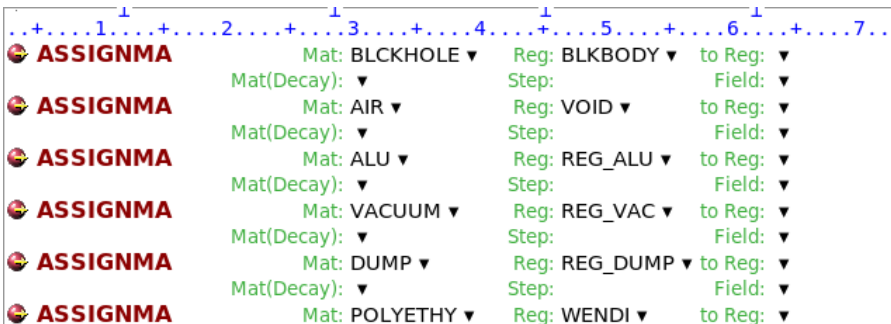
Figure 5.3.: Assigning material to the regions.

Here one can choose the elements the material contains, their mass or atomic ratios and the density of the material. This way a new material is created which can be assigned to a region just like every other material.
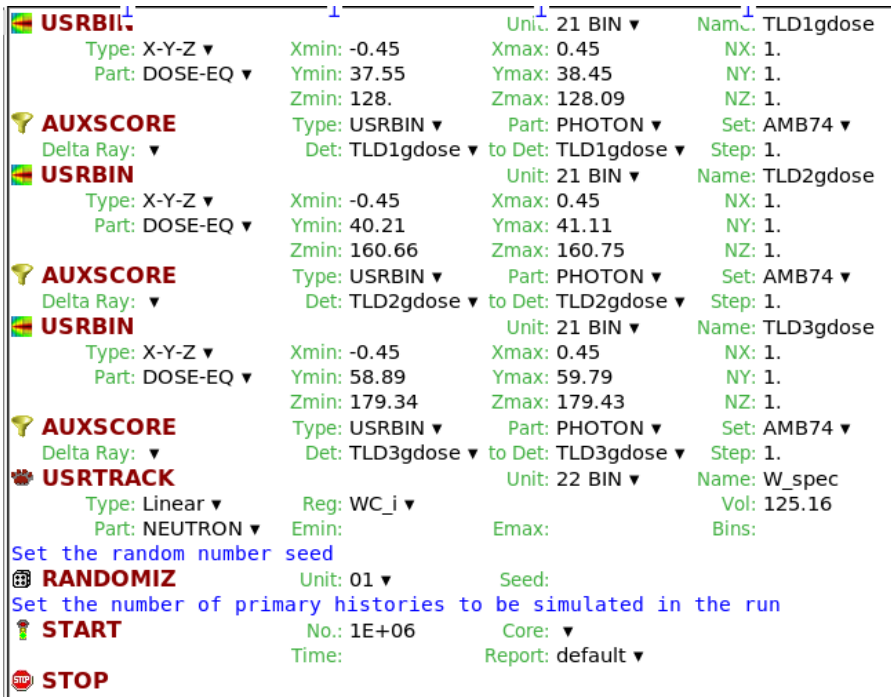
Figure 5.4.: Defining the desired scoring options.
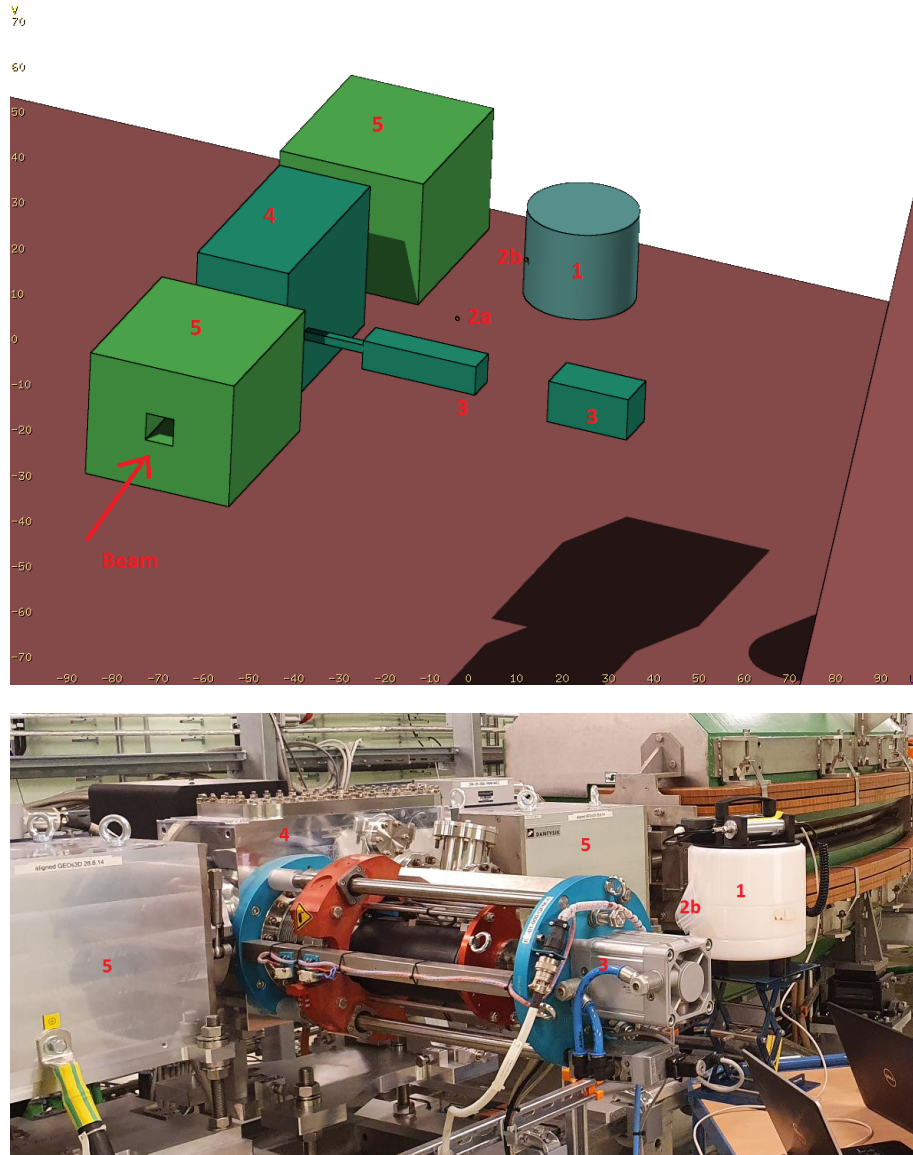
Figure 5.5.: First Figure: 3D-model of the geometry implemented into FLUKA. 1) Wendi-
II rem counter. 2a) and 2b) placement of TLDs at different measurements.
3) Aluminum parts of the SFX. 4) Casing of the Chopper with a beam dump
inside. 5) Magnets before and after the chopper to prefix the beam path.
Second Figure: Photo of the same setup with the exception that the TLD at
2a is not there (ⒸLukas Jägerhofer).

After defining the beam properties, creating the geometry, defining the regions and
assigning materials to it, one has to define what should actually be calculated when
running a simulation. To do so bins are created (see Figure 5.4) at the desired locations

in the geometry where one wants to gain knowledge about certain physical quantities. For the shape of the bins there also exist a few different options, like cuboids, cylinders etc. The first *USRBIN* in Figure 5.4 shows that the *Type: X-Y-Z* was chosen which means the bin has the form of a cuboid where all the coordinates can be chosen freely. *Part: DOSE-EQ* means that the output of the simulation is the dose equivalent for the defined region, which will be given in pSv/primary. This refers to the dose equivalent that results of one primary particle, which is a the dose equivalent per proton in this simulation. This means to calculate the dose equivalent for a given geometry, the number of incident particles is required. The *AUXSCORE* card provides the possibility to filter the recorded quantity for a selected particle type in the same region of the above USRBIN. In the case of the first USRBIN AUXSCORE scores the number of photons. The *USRTRACK* card scores the neutron fluence in this case which is given in $\text{cm}^{-2}\text{GeV}^{-1}$/primary. The *START* card defines the number of primaries that are used for the simulation, which is 1 million in this case.

Figure 5.5 shows a 3D model of the FLUKA geometry that was implemented into FLUKA and a photo of the real world setup. Obviously, the FLUKA model is a simplification of the real version, which is not a problem since the uncertainties in other parts of the process are much higher than in the accuracy of the geometry.

The geometry was built with the blue print of each component, meaning that sizes, distances and material thicknesses are implemented very accurately. The simplifications mainly occur in the form details which is obvious when comparing, for example, the complicated real beam diagnostic component SFX to the modeled SFX ("3" in Figure 5.5).

5.2. Measurements with the WENDI-II rem counter at the Chopper

The WENDI-II wide range rem counter was used during a five-hour shift in May 2021. Usually, the synchrotron hall can only be entered every three weeks, but on some occasions short measurements like the one performed here are possible. The counter was placed on a small platform next to the chopper (see Figure 5.6), such that the center of the counter tube is at the height of the beamline ($h = 125$ cm measured from the floor).

Figure 5.6.: WENDI-II rem counter at the chopper with a bag containing TLDs taped to it (©Lukas Jägerhofer).

During the shift, a 250 MeV proton beam was produced. While the WENDI-II rem counter was placed there, the beam was running from 00:31:58 a.m. ± 10 sec. to 04:40:58 a.m. ± 20 sec, hence the measurement time was $\Delta t = (14940 \pm 30)$ s. The counter records different dose values during the measurement. There is an accumulated ambient dose equivalent which is estimated and displayed during the measurement and can be read off

the display right after the measurement. This recorded dose was

$$H_{\text{WENDI-II}} = (18.9 \pm 0.1)\,\text{mSv}.$$

The WENDI-II rem counter also records the neutron and photon dose equivalent per time every five seconds and stores them into a .log file (units are $\mu\text{Sv/h}$). When taking the average neutron and photon dose and normalizing it for the recorded time, the estimated dose should match $H_{WENDI-II}$. The dose can be calculated by

$$H_{\text{WENDI-II-log}} = \Delta t \cdot \frac{1}{N} \sum_{t=0}^{T} H_t, \tag{5.1}$$

where Δt is the measurement time, N is the number of recorded dose values and H_t are the dose values recorded every five seconds. The result is

$$H_{\text{WENDI-II-log}} = (16.54 \pm 0.04)\,\text{mSv}.$$

This is $\sim 12.5\%$ less than the accumulated dose. When looking at the plot of the ambient dose equivalent per unit of time as a function of the time, some gaps appear which cannot be explained by a lack of radiation, since there was a beam for the whole period of Δt. It is not completely certain what happened there, but most likely the computer which was storing the measurement values into the .log file had some problems and was not storing the dose.
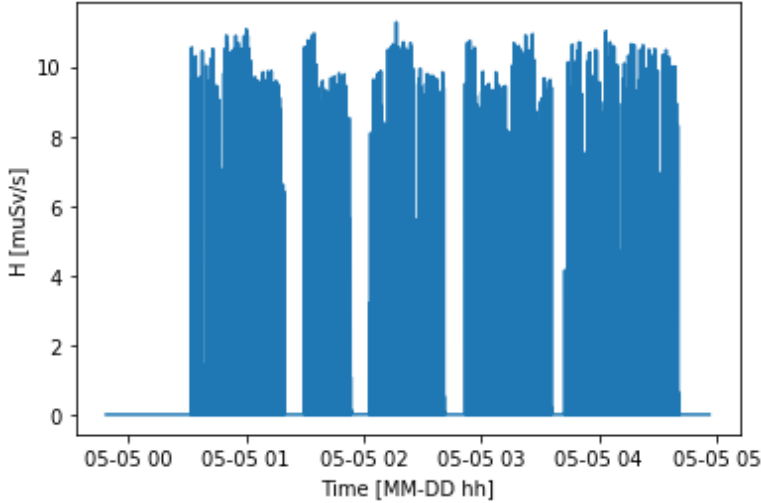
Figure 5.7.: Ambient dose equivalent per unit of time as a function of the time.

To even this error out, the average dose value in $\mu\text{Sv/s}$ was calculated and interpolated for the missing data points. That way the corrected ambient dose equivalent per unit of time integrated over time yields

$$H_{\text{WENDI-II-log-corr}} = (18.53 \pm 0.71)\,\text{mSv}.$$

This matches with $H_{\text{WENDI-II}}$ when considering the range of the uncertainty.
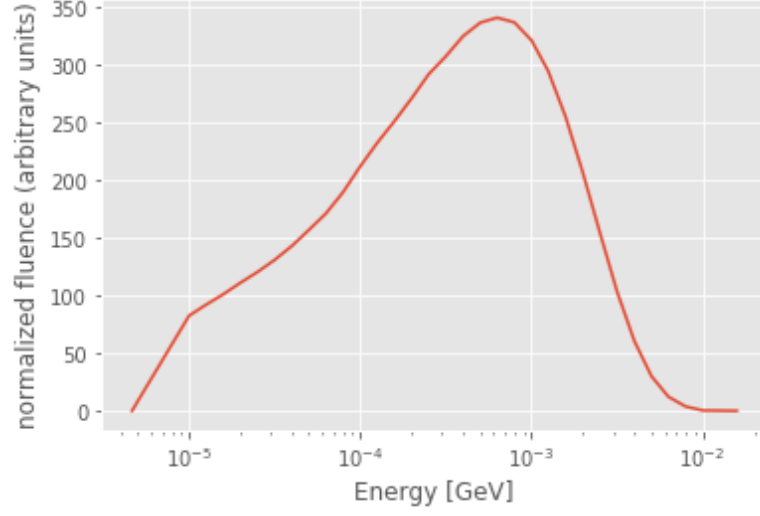
Figure 5.8.: The neutron fluence spectrum of the ^{252}Cf source which was used for the calibration of the WENDI-II rem counter.
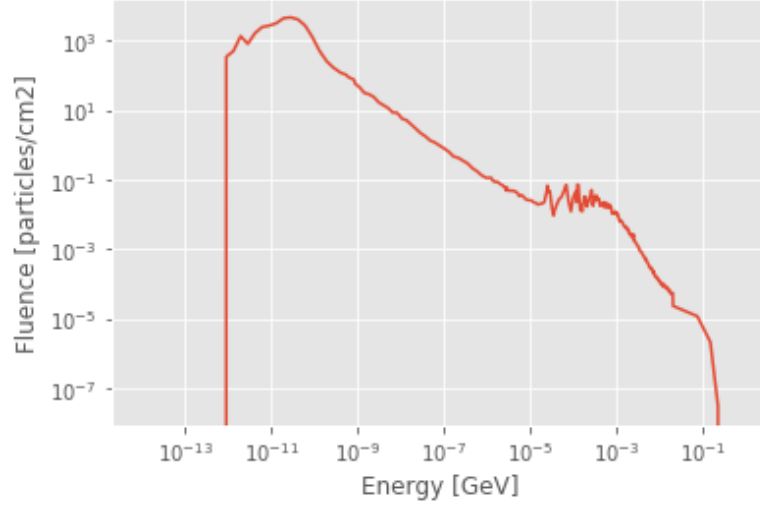
Figure 5.9.: The neutron fluence spectrum in the WENDI-II volume, estimated by FLUKA.

As was already shown by Jägerhofer [1], the dose equivalent recorded by the rem counter may necessitate to be corrected by a *field correction factor* f_{cor}. This is due to the fact, that the response function of the WENDI-II was calibrated in the field of an open ^{252}Cf source (see Figure 5.8). The neutron fluence spectrum of the ^{252}Cf source shows that the

peak of the spectrum is right below 1 MeV.

The neutron fluence spectrum at the measurement location was estimated via FLUKA (see Figure 5.9) and shows that most of the neutrons are in the region of thermal neutrons, hence the WENDI-II rem counter might underestimate the dose equivalent. Therefore a correction factor needs to be calculated to consider the effects of a different radiation field to the detector's response.

To receive the field correction factor, first the *field calibration factor* [cts/μSv] (f_{cal}) needs to be computed by the following method: The neutron fluence spectrum of the radiation field occurring at the chopper in the WENDI-II volume has to be convolved with the response function of the WENDI-II, which tells us the number of counts in the actual field conditions (by integrating the function resulting from the convolution). The neutron fluence spectrum also needs to be convolved with the fluence-to-ambient-dose-equivalent conversion function for neutrons by Pelliccioni [19] which yields the exact H*(10) dose in the volume (by integrating the function resulting from the convolution). The ratio of the number of counts and the H*(10) dose yields the field calibration factor in cts/μSv.
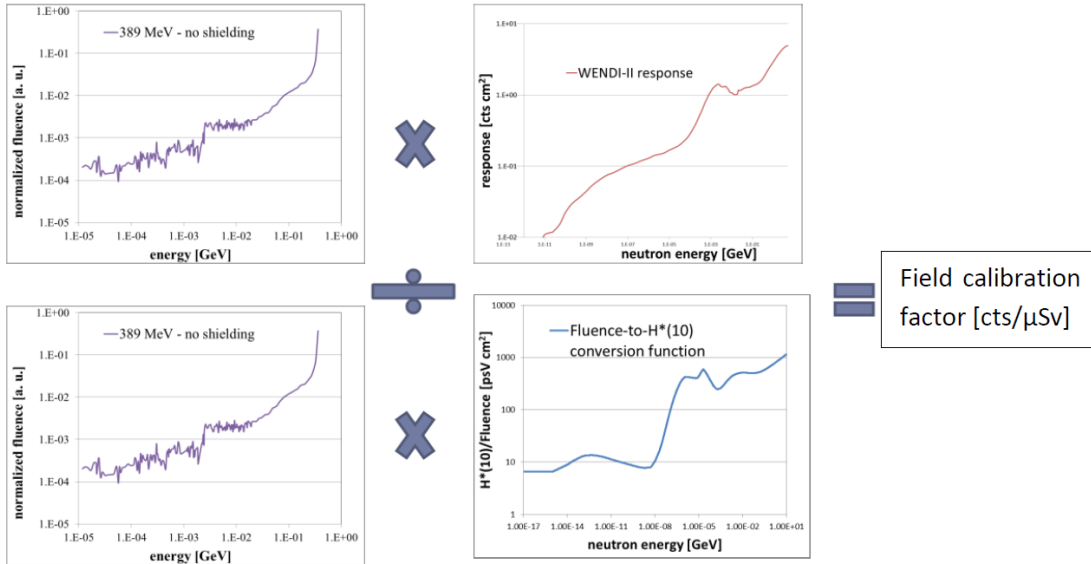
Figure 5.10.: Visualization of the method to obtain the field calibration factor by Jäger-hofer 2012 [1].

Figure 5.10 shows a visualization of the described method. For the calculations in this thesis, the spectrum displayed in Figure 5.9 is used instead of the 389 MeV neutron spectrum with no shielding, which was used by Jägerhofer and is displayed in Figure 5.10. To obtain the field correction factor, the sensitivity factor of the WENDI-II rem counter which is given by the manufacturer as 3024 cts/μSv has to be divided by the field

calibration factor.

$$f_{\text{cor}} = \frac{3024[\text{cts}/\mu\text{Sv}]}{f_{\text{cal}}[\text{cts}/\mu\text{Sv}]} \tag{5.2}$$

Finally, the corrected accumulated dose of the detector is determined by

$$H_{\text{WENDI−II−corrected}} = H_{\text{WENDI−II}} \cdot f_{\text{cor}}. \tag{5.3}$$

The field calibration factor then is $f_{\text{cal}} = (2809.4 \pm 142.3)\,\text{cts}/\mu\text{Sv}$ which yields a field correction factor of

$$f_{\text{cor}} = \frac{3024[\text{cts}/\mu\text{Sv}]}{2809.4[\text{cts}/\mu\text{Sv}]} = 1.076 \pm 0.055$$

and a corrected ambient dose equivalent of

$$H_{\text{WENDI−II−corr}} = 18.9\,\text{mSv} \cdot 1.076 = (\mathbf{20.34 \pm 1.05})\,\mathbf{mSv}.$$

The field correction factor induces a change of the ambient dose equivalent value of only 7.6%, i.e. the accuracy of the dose recorded by the neutron detector for the existing radiation field was already in very good agreement with the value after the correction. A similar conclusion could be drawn in Theis et al. [21] where field calibration studies for ionization chambers in mixed high-energy radiation fields were performed and a similar discrepancy between the field of the calibration source and the radiation field during the measurement occurred.

With the assumption that the radiation field around the synchrotron does not vary significantly, it can be concluded that field correction factors are negligible for measurements with the neutron detector anywhere around the synchrotron. Although the composition of the radiation fields might change, the energy range remains the same, since the primary particles come with a limited maximum energy and the reactions with the synchrotrons components are also limited to the used materials. Therefore, a similar spectral distribution of the neutron energies can be expected around the synchrotron. To support this statement, further investigations are necessary.

5.3. Comparison of different methods and conclusions about the chopper

In section 5.1, a detailed description on the implementation of the geometry at the measurement location was provided. This implementation not only resulted in a neutron fluence spectrum in the volume of the detector, but also an estimate for the dose the detector was exposed to, which provides a value to compare with.
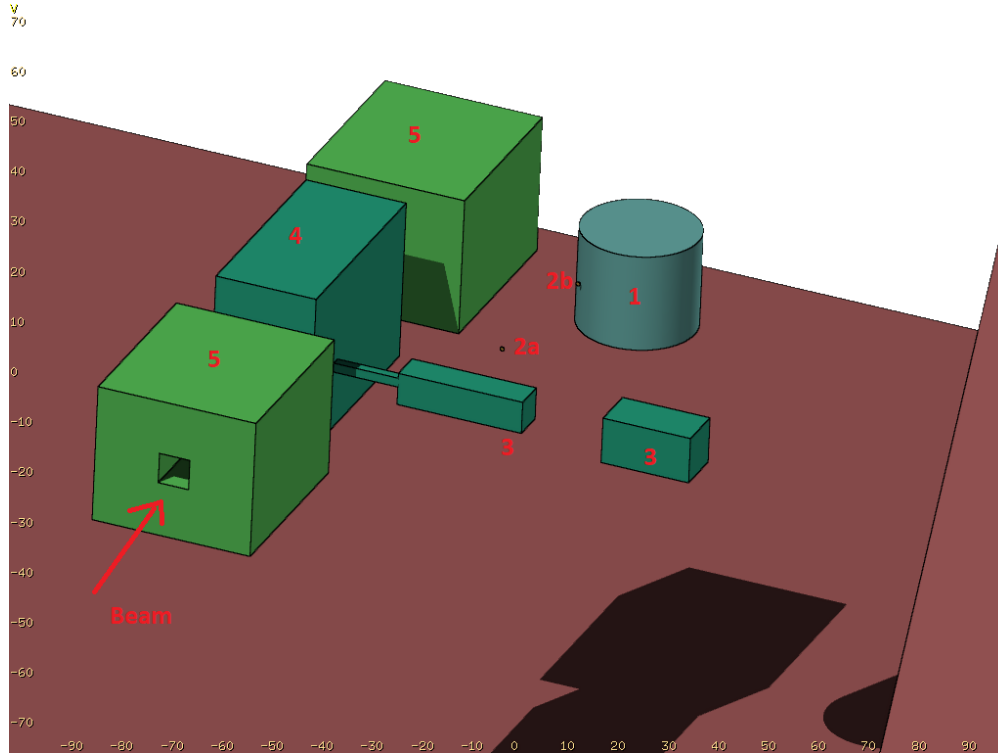
Figure 5.11.: 3D model of the geometry around the chopper in FLUKA.

Figure 5.11 shows a 3-D model of the geometry, with the detector (1), two TLDs (2a and 2b), the SFX (3), the chopper (4) and the two magnets before it and after it in the beamline (5). The red arrow indicates the direction of the beam.

The simulation was run with a 250 MeV proton beam and the ambient dose equivalent in the WENDI-II volume was scored via region scoring. The simulation is run with an arbitrary number of primary particles, which determines the time the computer takes to compute the simulation and also the uncertainty of the results. For the simulation calculated here, 10^6 primary particles were used which led to a computation time of ~ 4 hours and the uncertainty of the result was given with 0.29%. The resulting dose equivalent of the FLUKA simulation was given as

$$H_{\mathrm{FLUKA}} = 1.12 \cdot 10^{-2} \, \mathrm{pSv/primary} \pm 0.29\%.$$

That result by itself does not provide much information unless it is normalized to yield a dose comparable to the measurement of the detector. The normalization formula is given by

$$H_{\text{F}}\,[\text{mSv}] = H_{\text{FLUKA}}\left[\frac{\text{pSv}}{\text{primary}}\right]\cdot 10^{-9}\left[\frac{\text{mSv}}{\text{pSv}}\right]N\left[\frac{\text{primaries}}{\text{spill}}\right]\Delta t\,[\text{s}]\frac{1}{5\left[\frac{\text{s}}{\text{spill}}\right]}\cdot\frac{1}{2} \quad (5.4)$$

with the dose from FLUKA H_{FLUKA} provided above, the factor 10^{-9} to convert from pSv to mSv, N as the number of primaries per spill and Δt as the measurement time. The factor $1/2$ comes from the fact that there is five seconds of beam and then five seconds no beam, hence the detector is exposed to radiation only half of the time. The factor $1/5$ is there because one spill lasts five seconds, this means the amount of particles which are in one spill come in a time window of five seconds which needs to be considered as well when multiplying by the measurement time Δt.

Since the values for Δt and H_{FLUKA} have already been determined the only variable which remains unclear is N, which is the actual number of particles which get "lost" in the chopper. The number of particles lost in the chopper is uncertain, therefore a proper estimation needs to be found.

For the measurement shift with the WENDI-II rem counter some particle numbers are known. Firstly, the average number of particles per spill which are extracted from the synchrotron is $N_{\text{extraction}} = (12.6 \pm 0.34)\cdot 10^9$ and secondly the number of particles per spill which reach the irradiation room (IR) is at $N_{\text{IR}} = (9.8 \pm 0.33)\cdot 10^9$. With the assumption that the chopper is the only loss-point between the extraction and the IR, one can just take the difference and assume that $N_{\text{chopper}} = (2.8 \pm 0.34)\cdot 10^9$ is the number of particles per spill which are absorbed by the chopper's beam dump. The uncertainties for these numbers are the standard deviations of the values they were averaged from. Inserting N_{chopper} into equation 5.4 yields an estimated dose equivalent of

$$H_{\text{F}_1} = (46.22 \pm 5.52)\,\text{mSv}.$$

This is more than double the dose equivalent measured by the detector. Assuming the detector measurement is correct, this could mean either the FLUKA simulation cannot provide a better accuracy, given the implemented geometry is just an approximation of the real-world example, or there are particle losses at other points as well. This would mean that not just at the chopper, but also at other points between the extraction and the irradiation room, some of the particles get "lost" i.e., cause some reactions. The particle loss at the chopper is energy dependent but there is no exact information on the amount of particle loss for a defined energy or particle type. The assumed particle loss by MedAustrons beam physicists is $\sim 10\%$ but there are no measurements backing this information.

To get a better understanding of the particle loss at the chopper, equation 5.4 is calculated with $N_{\text{extraction}}$ and different assumptions on the quantity of the particle losses at the chopper. The results of these calculations are displayed in table 5.1. They show the closest matching between H_{F_2} and $H_{\text{WENDI-II-corr}}$ comes up when a 10% particle loss at

Particle loss [%]	Dose Equivalent $H_{\mathrm{F_2}}$ [mSv]	Deviation from $H_{\mathrm{WENDI-II-corr}}$ [%]
5	10.50 ± 0.29	-48.37
7.5	15.75 ± 0.43	-22.57
10	$\mathbf{20.99 \pm 0.57}$	$+3.20$
12.5	26.24 ± 0.71	$+29.01$
15	31.49 ± 0.86	$+54.82$
17.5	36.74 ± 1.00	$+80.63$
20	41.99 ± 1.14	$+106.44$

Table 5.1.: Estimated dose values according to different assumptions of particle loss at the chopper.

the chopper is assumed, which also matches with the expected amount of particle loss. The table also shows that for the calculation of $H_{\mathrm{F_1}}$ a particle loss of at least 20% needs to be assumed. This means that only $\sim 50\%$ of the particle losses between the extraction and the irradiation room take place at the chopper and the rest somewhere else between these two locations. A more detailed examination of the particle losses there remains to be done in the future.

Other than that, the conclusion can be drawn, that the FLUKA simulations work well for a dose estimation at a certain location, which becomes obvious by the comparison of $H_{\mathrm{F_2}}$ for 10% particle loss and $H_{\mathrm{WENDI-II-corr}}$, which match with respect to their uncertainties. This makes FLUKA a powerful tool for dose estimations at other locations as well, when a measurement with the neutron detector is not possible. The WENDI-II neutron counter can only be used for short measurement periods (i.e., several hours), but there are very few opportunities for short measurements. For the usual three week period between opportunities to access the synchrotron area, TLDs calibrated by FLUKA simulations are the best option.

6. Conclusions and Outlook

The TLD measurements have shown where the loss points around the synchrotron are located and confirmed that the radiation field in the synchrotron hall consists mainly of neutrons. These measurements have shown very high particle losses at the BDV where no beam impact is anticipated. While there were large amounts of particle losses at the BDV there were very little particle losses measured at the BDH where more losses are expected. The chopper dump, an expected loss point, could be confirmed as such and proved to contribute about 10% to the measured particle losses.

For further investigation of the radiation field in the vicinity of the chopper, a vertical profile was recorded which showed an unexpected large amount of neutrons close to the floor. As a consequence, a vertical profile was also recorded in the vicinity of the BDV where this occurrence did not appear. To exclude errors in the measurement method, those measurements were repeated and the results were replicated. The reason for the unexpected neutron count close to the floor at the chopper was not investigated further but since it was recorded twice one can conclude that this is not an appropriate location for sensitive electronic devices.

To get a better idea of the dose values which occur at the loss points, the ambient dose equivalent next to the chopper was recorded during a ∼4-hour measurement with a WENDI-II rem counter. To verify the measurement with the neutron detector and to compare the methods, the geometry of the chopper and its surroundings was implemented into FLUKA and simulated. The required field calibration of the WENDI-II rem counter, which was performed with the neutron fluence spectrum, obtained via FLUKA, resulted in a small correction for the radiation fields occurring in the vicinity of the chopper. The recorded ambient dose equivalent and the calculated value from the FLUKA simulation were in good agreement, under the assumption that the particle losses at the chopper amount to ∼10%, as is expected by MedAustron's beam physicists. This lead to the understanding that about half of the particles which are lost between the extraction and the IR do not get lost at the chopper.

This thesis contributed to the better understanding of the particle losses at MedAustron synchrotron. Areas for further research were identified. The positions of the unexpected loss points at the synchrotron provide a starting point for MedAustron's beam physicists to find the reasons for the occurrence of the particular loss points. Also, the particle losses between the extraction and the IR remain to be investigated further.

The TLDs have served as reliable method for a qualitative comparison of different locations. A future task will be to create a setting in which TLD measurements can be reliably compared to FLUKA simulations and get a dose assigned to the number of counts they recorded. If one could argue that the radiation fields in the synchrotron hall do not vary significantly over the course of a three-week period, a calibration of the TLDs

could be carried out. If the TLDs are calibrated, they can be used for further detailed measurements at the unexpected loss points.

Soon MedAustron will have a system which allows active beam loss monitoring at two positions. This active beam loss monitoring system has a time resolution allowing identification of which parts of a spill are lost. Hopefully, this will make the dose mapping and understanding of the loss points much easier in combination with the methods already available at MedAustron.

Bibliography

[1] **Jägerhofer, L.** *Shielding and Radiation studies for MedAustron.* Dissertation, Technische Universität Wien, 2012.

[2] **EBG MedAustron GmbH**.

[3] Bragg Curves and Peaks. `https://www.bnl.gov/nsrl/userguide/bragg-curves-and-peaks.php`. Accessed: 2022-02-24.

[4] **Knoll, G.F.** *Radiation Detection and Measurement.* Willey & Sons, New York, 3rd edition, 2000.

[5] **International Commission on Radiation Units and Measurements**. Fundamental quantities and units for ionizing radiation. ICRU Report 60, 1998.

[6] **International Comission on Radiological Protection**. Conversion Coefficients for Radiological Protection Quantities for External Radiation Exposures. ICRP Publication 116, Ann. ICRP 40(2-5), 2010.

[7] **International Commission on Radiological Protection**. Conversion Coefficients for use in Radiological Protection against External Radiation. ICRP Report 74, 1996.

[8] **Böhlen, T.T., Cerutti, F., Chin, M.P.W., Fassò, A., Ferrari, A., Ortega, P.G., Mairani, A., Sala, P.R., Smirnov, G. and Vlachoudis, V.** The FLUKA Code: Developments and Challenges for High Energy and Medical Applications. *Nuclear Data Sheets*, (120):211–214, 2014.

[9] `http://www.fluka.org/`. Accessed: 2021-12-09.

[10] **Ferrari, A., Sala, P.R., Fassò, A. and Ranft, J.** FLUKA: a multi-particle transport code, 2005. INFN/TC_05/11, SLAC-R-773.

[11] `http://www.fluka.org/flair/`. Accessed: 2021-12-10.

[12] **Sunta, C. M.** *Unrevealing Thermoluminescence.* Springer, New Delhi, 2015.

[13] **Chen, R. and McKeever, S. W. S.** *Theory of Thermoluminescence and Related Phenomena.* World Scientific, Singapore, 1997.

[14] **Randall, J. T. and Wilkins, M. H. F.** Phosphorence and electron traps. I. the study of trap distributions. *Proceedings of the Royal Society*, (184):366–389, 1945.

Bibliography

[15] **El-Faramawy, N., Chopra, V., Rawash, S., El-Hafez, A.A., Dhoble, S.J.**
Response of TLD-600/TLD-700 and CR-39 to neutrons for medical dosimetry. *Luminescence*, (36):1257–1264, 2021. https://doi.org/10.1002/bio.4051.

[16] **Cavalieri, T.A., Castro, V.A. and Siqueira, P.T.D.** Differences in TLD600 and TLD700 Glow Curves derived from Distict (sic) Mixed Gamma/Neutron Field Irradiations. Recife, PE, Brazil, 11 2013. Associacao Brasileira de Energia Nuclear - ABEN, Instituto de Pesquisas Energéticas e Nucleares (IPEN / CNEN - SP).

[17] **Biratarri, C., Ferrari, A., Nuccetelli, C., Pellicioni, M., Silari, M.** An Extended Range Neutron Rem Counter. *Nuclear Instruments and Methods in Physics Research*, (A297):250–257, 1990.

[18] **Olsher, H., Hsu, H., Beverding, A., Kleck, J.H., Casson, W.H., Vasilik, D.G. and Devine, R.** WENDI: An Improved Neutron REM Meter. *Health Physics*, 79(2):170–181, 2000.

[19] **Pellicioni, M.** Overview of Fluence-To-Effective Dose and Fluence-To-ambient Dose Equivalent Conversion Coefficients for High Energy Radiation calculated using the FLUKA Code. *Radiation Protection Dosimetry*, 88(4):279–297, 2000.

[20] **Jägerhofer, L., Feldbaumer, E., Theis, C., Roesler, S.and Vincke, H.** A new method to calculate the response of the WENDI-II rem counter using the FLUKA Monte Carlo Code. *Nuclear Instruments and Methods in Physics Research Section A: Accelerators, Spectrometers, Detectors and Associated Equipment*, 691:81–85, 2012.

[21] **Theis, C., Forkel-Wirth, D., Fuerstner, M., Mayer, S., Otto, Th., Roesler, S. and Vincke, H.** Field Calibration Studies for Ionisation Chambers in Mixed High-Energy Radiation Fields. *Radiation Protection Dosimetry*, 126(1-4):299–305, 2007.

Acronyms

A-B Andersson-Braun. 15

BDH Beam Dump Horizontal. 23

BDV Beam Dump Vertical. 23

CERN Conseil Européen pour la Recherche Nucléaire. 11

EBG Errichtungs und Betriebs Gesellschaft. 2

flair Fluka Advanced Interface. 11

FLUKA Fluktuierende Kaskade. 11

ICRP International Commission on Radiation Protection. 6

ICRU International Commission on Radiation Units and Measurements. 7

IR Irradiation Room. 2

LET Linear Energy Transfer. 3

LINAC Linear Accelerator. 3

MC Monte Carlo. 11

ROI Region Of Interest. 13

SFX Scintillating Fiber Hodoscope. 26

TLD Thermoluminescence Dosimeter. 11

List of Tables

List of Figures

A. Appendix

A.1. Convolution Results

The following two sections show the result files of the convolutions performed for the calculation of f_{cal}. The column with the title "dPhi [1/cm2]" contains the spectrum of the neutron fluence, calculated in FLUKA. The column "Fluence Uncertainty [%]" contains the according uncertainties. The "Response [C cm2]" column contains either the fluence-to-ambient-dose-equivalent conversion function by Pellicioni or the WENDI-II response function. "Response Uncertainty [%]" is the according uncertainty and "Convolution-Result [C]" and "rel. Uncertainty [%]" are self explanatory. The last rows of both files each contain the convolution integral, which was used to calculate f_{cal}.

A.1.1. Convolution of the neutron fluence spectrum with the fluence-to-ambient-dose-equivalent conversion function for neutrons by Pelliccioni

```
Energy (GeV) dPhi [1/cm2] Fluence Uncertainty [%] Response[C cm2] Response Uncertainty [%]
Convolution-Result [C] rel. Uncert [%]
4.47e-014 0.00000000e+000 0.0000 6.600000000000e+000 0.0000 0.00000000e+000 0.0000
2.42e-013 0.00000000e+000 0.0000 6.600000000000e+000 0.0000 0.00000000e+000 0.0000
3.55e-013 0.00000000e+000 0.0000 6.600000000000e+000 0.0000 0.00000000e+000 0.0000
5.19e-013 0.00000000e+000 0.0000 6.600000000000e+000 0.0000 0.00000000e+000 0.0000
7.61e-013 0.00000000e+000 0.0000 6.600000000000e+000 0.0000 0.00000000e+000 0.0000
1.11e-012 1.48358523e-010 0.7076 6.700000000000e+000 0.0000 9.94002101e-010 0.7076
1.63e-012 3.18501341e-010 0.5684 7.063769808730e+000 0.0000 2.24982016e-009 0.5684
2.39e-012 1.25031249e-009 0.3328 7.400000000000e+000 0.0000 9.25231241e-009 0.3328
3.50e-012 1.09902674e-009 0.2031 7.800000000000e+000 0.0000 8.57240860e-009 0.2031
5.13e-012 3.25481712e-009 0.1310 8.200000000000e+000 0.0000 2.66895004e-008 0.1310
7.52e-012 7.16775654e-009 0.1026 8.690413867706e+000 0.0000 6.22907708e-008 0.1026
1.10e-011 1.15474129e-008 0.0750 9.208414311346e+000 0.0000 1.06333362e-007 0.0750
1.61e-011 1.98952182e-008 0.0593 9.800000000000e+000 0.0000 1.94973138e-007 0.0593
2.36e-011 4.04898406e-008 0.0369 1.049274943135e+001 0.0000 4.24849752e-007 0.0369
3.46e-011 6.28061523e-008 0.0339 1.110000000000e+001 0.0000 6.97148291e-007 0.0339
5.07e-011 8.00118324e-008 0.0282 1.170000000000e+001 0.0000 9.36138439e-007 0.0282
7.43e-011 7.82628848e-008 0.0370 1.239661675727e+001 0.0000 9.70194989e-007 0.0370
1.09e-010 5.40899624e-008 0.0340 1.300000000000e+001 0.0000 7.03169512e-007 0.0340
1.59e-010 3.16707171e-008 0.0477 1.330000000000e+001 0.0000 4.21220538e-007 0.0477
2.34e-010 2.33136642e-008 0.0532 1.350000000000e+001 0.0000 3.14734467e-007 0.0532
3.42e-010 2.17317584e-008 0.0527 1.360000000000e+001 0.0000 2.95551915e-007 0.0527
4.69e-010 1.40922788e-008 0.0684 1.360000000000e+001 0.0000 1.91654992e-007 0.0684
5.76e-010 1.00007272e-008 0.0755 1.350000000000e+001 0.0000 1.35009817e-007 0.0755
6.53e-010 5.13046866e-009 0.1227 1.350000000000e+001 0.0000 6.92613269e-008 0.1227
7.54e-010 1.28911487e-008 0.0767 1.340000000000e+001 0.0000 1.72741393e-007 0.0767
8.55e-010 3.22341842e-009 0.1702 1.340000000000e+001 0.0000 4.31938069e-008 0.1702
9.93e-010 1.47241757e-008 0.0806 1.330000000000e+001 0.0000 1.95831537e-007 0.0806
1.28e-009 1.44988515e-008 0.0633 1.320000000000e+001 0.0000 1.91384840e-007 0.0633
```

```
1.64e-009 1.30054086e-008 0.0863 1.300000000000e+001 0.0000 1.69070312e-007 0.0863
2.10e-009 1.52552518e-008 0.0874 1.288783364401e+001 0.0000 1.96607147e-007 0.0874
2.70e-009 1.64104019e-008 0.0835 1.260000000000e+001 0.0000 2.06771064e-007 0.0835
3.47e-009 1.48691436e-008 0.0568 1.234558704188e+001 0.0000 1.83568306e-007 0.0568
4.45e-009 1.58071319e-008 0.0641 1.210000000000e+001 0.0000 1.91266297e-007 0.0641
5.72e-009 1.68391158e-008 0.0647 1.190000000000e+001 0.0000 2.00385478e-007 0.0647
7.34e-009 1.60574824e-008 0.0655 1.160000000000e+001 0.0000 1.86266796e-007 0.0655
9.42e-009 1.99007668e-008 0.0646 1.140000000000e+001 0.0000 2.26868741e-007 0.0646
1.21e-008 1.75717153e-008 0.0709 1.110000000000e+001 0.0000 1.95046040e-007 0.0709
1.55e-008 2.00131053e-008 0.0533 1.086497643035e+001 0.0000 2.17441917e-007 0.0533
1.99e-008 1.95303988e-008 0.0588 1.060000000000e+001 0.0000 2.07022227e-007 0.0588
2.56e-008 1.88531055e-008 0.0614 1.040000000000e+001 0.0000 1.96072298e-007 0.0614
3.29e-008 1.80869603e-008 0.0406 1.020000000000e+001 0.0000 1.84486995e-007 0.0406
4.22e-008 1.89243640e-008 0.0813 1.000000000000e+001 0.0000 1.89243640e-007 0.0813
5.42e-008 1.84925559e-008 0.0733 9.814121546922e+000 0.0000 1.81488192e-007 0.0733
6.96e-008 2.07502447e-008 0.0664 9.700000000000e+000 0.0000 2.01277373e-007 0.0664
8.94e-008 2.19841957e-008 0.0784 9.500000000000e+000 0.0000 2.08849859e-007 0.0784
1.15e-007 2.29928216e-008 0.0551 9.300000000000e+000 0.0000 2.13833240e-007 0.0551
1.47e-007 2.36902799e-008 0.0487 9.100000000000e+000 0.0000 2.15581547e-007 0.0487
1.89e-007 2.22823117e-008 0.0658 8.900000000000e+000 0.0000 1.98312574e-007 0.0658
2.43e-007 2.62455909e-008 0.0457 8.800000000000e+000 0.0000 2.30961200e-007 0.0457
3.12e-007 2.80593225e-008 0.0539 8.600000000000e+000 0.0000 2.41310173e-007 0.0539
4.01e-007 2.97153370e-008 0.0550 8.400000000000e+000 0.0000 2.49608831e-007 0.0550
5.14e-007 2.81390304e-008 0.0642 8.300000000000e+000 0.0000 2.33553952e-007 0.0642
6.61e-007 2.91663251e-008 0.0539 8.100000000000e+000 0.0000 2.36247233e-007 0.0539
8.48e-007 2.86684404e-008 0.0457 8.000000000000e+000 0.0000 2.29347523e-007 0.0457
1.09e-006 3.10844663e-008 0.0500 7.900000000000e+000 0.0000 2.45567284e-007 0.0500
1.30e-006 1.49697060e-008 0.0682 7.800000000000e+000 0.0000 1.16763707e-007 0.0682
1.43e-006 1.34780919e-008 0.0817 7.800000000000e+000 0.0000 1.05129117e-007 0.0817
1.55e-006 6.78601916e-009 0.1005 7.800000000000e+000 0.0000 5.29309495e-008 0.1005
1.62e-006 7.00221966e-009 0.0873 7.800000000000e+000 0.0000 5.46173134e-008 0.0873
1.75e-006 1.54700620e-008 0.0728 7.700000000000e+000 0.0000 1.19119477e-007 0.0728
1.94e-006 1.61936532e-008 0.0751 7.700000000000e+000 0.0000 1.24691130e-007 0.0751
2.14e-006 1.59280450e-008 0.0781 7.700000000000e+000 0.0000 1.22645946e-007 0.0781
2.36e-006 1.67530066e-008 0.0697 7.791646919970e+000 0.0000 1.30533512e-007 0.0697
2.55e-006 7.93704570e-009 0.1094 7.800000000000e+000 0.0000 6.19089564e-008 0.1094
2.68e-006 8.28212774e-009 0.0646 7.800000000000e+000 0.0000 6.46005964e-008 0.0646
2.80e-006 5.79931889e-009 0.1138 7.800000000000e+000 0.0000 4.52346874e-008 0.1138
2.95e-006 1.02855496e-008 0.0855 7.800000000000e+000 0.0000 8.02272865e-008 0.0855
3.19e-006 1.57224024e-008 0.0653 7.906165988097e+000 0.0000 1.24303923e-007 0.0653
3.53e-006 1.72809972e-008 0.0542 7.900000000000e+000 0.0000 1.36519878e-007 0.0542
3.90e-006 1.87360846e-008 0.0516 7.900000000000e+000 0.0000 1.48015069e-007 0.0516
4.20e-006 1.02112372e-008 0.0917 7.900000000000e+000 0.0000 8.06687739e-008 0.0917
4.42e-006 1.02714632e-008 0.1076 8.000000000000e+000 0.0000 8.21717053e-008 0.1076
4.76e-006 2.20256736e-008 0.0581 8.000000000000e+000 0.0000 1.76205389e-007 0.0581
5.26e-006 2.22656906e-008 0.0564 8.162194664980e+000 0.0000 1.81736901e-007 0.0564
5.89e-006 2.51691015e-008 0.0574 8.500000000000e+000 0.0000 2.13937362e-007 0.0574
6.67e-006 3.06154426e-008 0.0419 8.985784259553e+000 0.0000 2.75103762e-007 0.0419
7.56e-006 2.97834421e-008 0.0532 9.400000000000e+000 0.0000 2.79964355e-007 0.0532
8.57e-006 2.89130605e-008 0.0471 9.899045252998e+000 0.0000 2.86211694e-007 0.0471
9.71e-006 3.16864974e-008 0.0553 1.040729047562e+001 0.0000 3.29770583e-007 0.0553
1.10e-005 3.56132117e-008 0.0435 1.119941045693e+001 0.0000 3.98846976e-007 0.0435
1.25e-005 3.57244008e-008 0.0538 1.209356844780e+001 0.0000 4.32035487e-007 0.0538
1.41e-005 3.83992610e-008 0.0435 1.322233102309e+001 0.0000 5.07727740e-007 0.0435
1.60e-005 3.90782008e-008 0.0461 1.440758312098e+001 0.0000 5.63022426e-007 0.0461
1.81e-005 4.67288196e-008 0.0317 1.553434880709e+001 0.0000 7.25901783e-007 0.0317
2.03e-005 4.26686420e-008 0.0339 1.679364310234e+001 0.0000 7.16561945e-007 0.0339
2.16e-005 1.28499701e-008 0.0962 1.770589221874e+001 0.0000 2.27520185e-007 0.0962
2.27e-005 5.02754357e-008 0.0376 1.850926231452e+001 0.0000 9.30561227e-007 0.0376
```

```
2.39e-005 2.57732124e-008 0.0479 1.944147354024e+001 0.0000 5.01069228e-007 0.0479
2.45e-005 3.53725905e-008 0.0423 1.978886783617e+001 0.0000 6.99983519e-007 0.0423
2.54e-005 8.68651851e-008 0.0244 2.051622961383e+001 0.0000 1.78214608e-006 0.0244
2.71e-005 9.04086947e-008 0.0294 2.156447712955e+001 0.0000 1.94961623e-006 0.0294
2.99e-005 1.77984727e-007 0.0205 2.369948202706e+001 0.0000 4.21814584e-006 0.0205
3.30e-005 3.60340390e-008 0.0301 2.631905237446e+001 0.0000 9.48381760e-007 0.0301
3.47e-005 8.17882679e-009 0.0742 2.780952949100e+001 0.0000 2.27449325e-007 0.0742
3.56e-005 9.11181579e-009 0.1083 2.853969074864e+001 0.0000 2.60048405e-007 0.1083
3.84e-005 6.19549462e-008 0.0364 3.094452630260e+001 0.0000 1.91716646e-006 0.0364
4.35e-005 1.07987516e-007 0.0292 3.537759075187e+001 0.0000 3.82033816e-006 0.0292
4.93e-005 1.73049520e-007 0.0177 4.049182105483e+001 0.0000 7.00709021e-006 0.0177
5.45e-005 1.32160081e-007 0.0202 4.528038774093e+001 0.0000 5.98425970e-006 0.0202
5.80e-005 1.16755667e-007 0.0245 4.855821181985e+001 0.0000 5.66944642e-006 0.0245
6.10e-005 1.41882683e-007 0.0245 5.136749754504e+001 0.0000 7.28815835e-006 0.0245
6.49e-005 2.71444042e-007 0.0172 5.510259469927e+001 0.0000 1.49572710e-005 0.0172
7.17e-005 6.43085553e-007 0.0107 6.162898363330e+001 0.0000 3.96327090e-005 0.0107
8.13e-005 2.48768321e-007 0.0142 7.047510859355e+001 0.0000 1.75319744e-005 0.0142
9.21e-005 1.43199388e-007 0.0199 8.051857912313e+001 0.0000 1.15302113e-005 0.0199
1.04e-004 4.04837098e-007 0.0133 9.198446119767e+001 0.0000 3.72387223e-005 0.0133
1.14e-004 2.61108263e-007 0.0176 1.005181674673e+002 0.0000 2.62461241e-005 0.0176
1.20e-004 1.40337609e-007 0.0211 1.055887642418e+002 0.0000 1.48180747e-005 0.0211
1.26e-004 4.64203856e-007 0.0154 1.108316691276e+002 0.0000 5.14484882e-005 0.0154
1.32e-004 4.72997262e-007 0.0109 1.164321589823e+002 0.0000 5.50720924e-005 0.0109
1.39e-004 1.73897002e-007 0.0155 1.223247509879e+002 0.0000 2.12719074e-005 0.0155
1.46e-004 9.79519821e-008 0.0272 1.287786205634e+002 0.0000 1.26141211e-005 0.0272
1.54e-004 1.12621474e-007 0.0258 1.345670533841e+002 0.0000 1.51551398e-005 0.0258
1.60e-004 4.97304710e-008 0.0345 1.394925651409e+002 0.0000 6.93703097e-006 0.0345
1.64e-004 8.15863994e-008 0.0311 1.426385906883e+002 0.0000 1.16373690e-005 0.0311
1.68e-004 8.62810820e-008 0.0310 1.455990748934e+002 0.0000 1.25624457e-005 0.0310
1.72e-004 1.04578514e-007 0.0293 1.489609959004e+002 0.0000 1.55781196e-005 0.0293
1.79e-004 2.85368336e-007 0.0176 1.536298166537e+002 0.0000 4.38410852e-005 0.0176
1.88e-004 3.14186692e-007 0.0153 1.607578817299e+002 0.0000 5.05079870e-005 0.0153
1.97e-004 2.67118797e-007 0.0159 1.679527822783e+002 0.0000 4.48633452e-005 0.0159
2.08e-004 1.76036427e-007 0.0187 1.749019989274e+002 0.0000 3.07891230e-005 0.0187
2.18e-004 2.30817638e-007 0.0200 1.818105803746e+002 0.0000 4.19650886e-005 0.0200
2.29e-004 2.78764173e-007 0.0182 1.892227888420e+002 0.0000 5.27485343e-005 0.0182
2.41e-004 3.96327902e-007 0.0181 1.966367960536e+002 0.0000 7.79326488e-005 0.0181
2.53e-004 4.52649464e-007 0.0129 2.041100798920e+002 0.0000 9.23903183e-005 0.0129
2.66e-004 6.78624338e-007 0.0115 2.123317666273e+002 0.0000 1.44093505e-004 0.0115
2.77e-004 2.24402960e-007 0.0188 2.187831638450e+002 0.0000 4.90955896e-005 0.0188
2.84e-004 1.27901189e-007 0.0219 2.231716477874e+002 0.0000 2.85439190e-005 0.0219
2.91e-004 1.50810743e-007 0.0245 2.276944482008e+002 0.0000 3.43387689e-005 0.0245
2.98e-004 2.01173530e-007 0.0214 2.318489191274e+002 0.0000 4.66418655e-005 0.0214
3.06e-004 2.40813882e-007 0.0228 2.356700215601e+002 0.0000 5.67526128e-005 0.0228
3.14e-004 1.97084340e-007 0.0156 2.396951224892e+002 0.0000 4.72401549e-005 0.0156
3.25e-004 4.41119504e-007 0.0137 2.454135357304e+002 0.0000 1.08256697e-004 0.0137
3.42e-004 6.13579106e-007 0.0092 2.532812700138e+002 0.0000 1.55408095e-004 0.0092
3.60e-004 4.71871973e-007 0.0109 2.612719381776e+002 0.0000 1.23286905e-004 0.0109
3.78e-004 4.93505329e-007 0.0080 2.699733427188e+002 0.0000 1.33233283e-004 0.0080
3.98e-004 5.67927491e-007 0.0087 2.784895611107e+002 0.0000 1.58161878e-004 0.0087
4.18e-004 3.79587743e-007 0.0166 2.873492165843e+002 0.0000 1.09074241e-004 0.0166
4.39e-004 3.93884685e-007 0.0115 2.967942107246e+002 0.0000 1.16902694e-004 0.0115
4.62e-004 4.78797483e-007 0.0154 3.063220791612e+002 0.0000 1.46666241e-004 0.0154
4.86e-004 5.21478185e-007 0.0149 3.161957569579e+002 0.0000 1.64889189e-004 0.0149
5.04e-004 2.84748967e-007 0.0118 3.232415047949e+002 0.0000 9.20426847e-005 0.0118
5.17e-004 2.93294209e-007 0.0169 3.268687124627e+002 0.0000 9.58687005e-005 0.0169
5.30e-004 2.12248395e-007 0.0232 3.306941320045e+002 0.0000 7.01892989e-005 0.0232
5.43e-004 2.71115384e-007 0.0185 3.343250691525e+002 0.0000 9.06406695e-005 0.0185
5.64e-004 5.20005957e-007 0.0120 3.401694170315e+002 0.0000 1.76890123e-004 0.0120
```

```
5.93e-004 6.17778158e-007 0.0135 3.477825298556e+002 0.0000 2.14852451e-004 0.0135
6.23e-004 6.44793309e-007 0.0107 3.559145904628e+002 0.0000 2.29491347e-004 0.0107
6.55e-004 5.02936138e-007 0.0137 3.641410922072e+002 0.0000 1.83139715e-004 0.0137
6.89e-004 6.66252152e-007 0.0133 3.724665083747e+002 0.0000 2.48156613e-004 0.0133
7.24e-004 6.39430920e-007 0.0111 3.783530146835e+002 0.0000 2.41930616e-004 0.0111
7.62e-004 5.97287927e-007 0.0126 3.831427785489e+002 0.0000 2.28846556e-004 0.0126
8.01e-004 4.26366956e-007 0.0156 3.881482483836e+002 0.0000 1.65493587e-004 0.0156
8.42e-004 4.75437041e-007 0.0141 3.931383565334e+002 0.0000 1.86912537e-004 0.0141
8.85e-004 4.87530318e-007 0.0111 3.982557265032e+002 0.0000 1.94161741e-004 0.0111
9.30e-004 5.64785069e-007 0.0142 4.049644142688e+002 0.0000 2.28717855e-004 0.0142
9.58e-004 9.44429934e-008 0.0365 4.093647669208e+002 0.0000 3.86616340e-005 0.0365
9.70e-004 1.75737154e-007 0.0181 4.112177859360e+002 0.0000 7.22662432e-005 0.0181
9.90e-004 2.80712898e-007 0.0199 4.144718724885e+002 0.0000 1.16347601e-004 0.0199
1.03e-003 5.15615887e-007 0.0117 4.174187536679e+002 0.0000 2.15227741e-004 0.0117
1.08e-003 5.57924091e-007 0.0129 4.196268905141e+002 0.0000 2.34119952e-004 0.0129
1.14e-003 4.33867162e-007 0.0146 4.223431982184e+002 0.0000 1.83240845e-004 0.0146
1.18e-003 1.90538476e-007 0.0188 4.241797135591e+002 0.0000 8.08225562e-005 0.0188
1.21e-003 2.13167338e-007 0.0188 4.248712681946e+002 0.0000 9.05686771e-005 0.0188
1.26e-003 4.21081513e-007 0.0141 4.245443745038e+002 0.0000 1.78767788e-004 0.0141
1.32e-003 4.26119681e-007 0.0148 4.241006245508e+002 0.0000 1.80717623e-004 0.0148
1.39e-003 4.03578512e-007 0.0148 4.236226160781e+002 0.0000 1.70964985e-004 0.0148
1.46e-003 3.68374971e-007 0.0129 4.231117279343e+002 0.0000 1.55863771e-004 0.0129
1.51e-003 1.78909917e-007 0.0167 4.227549829993e+002 0.0000 7.56350591e-005 0.0167
1.55e-003 1.67691514e-007 0.0197 4.224723458277e+002 0.0000 7.08450272e-005 0.0197
1.59e-003 1.79254796e-007 0.0173 4.222784947151e+002 0.0000 7.56954456e-005 0.0173
1.63e-003 1.88436894e-007 0.0166 4.219762106699e+002 0.0000 7.95158864e-005 0.0166
1.69e-003 3.45400176e-007 0.0169 4.216381726605e+002 0.0000 1.45633899e-004 0.0169
1.78e-003 3.27835939e-007 0.0149 4.210826518464e+002 0.0000 1.38046027e-004 0.0149
1.85e-003 1.80051111e-007 0.0241 4.208009477021e+002 0.0000 7.57656782e-005 0.0241
1.90e-003 1.61389859e-007 0.0234 4.204702052514e+002 0.0000 6.78596270e-005 0.0234
1.94e-003 1.40841541e-007 0.0259 4.202767097133e+002 0.0000 5.91924194e-005 0.0259
1.99e-003 1.49669899e-007 0.0228 4.199805539191e+002 0.0000 6.28584472e-005 0.0228
2.07e-003 2.79713137e-007 0.0133 4.193497395738e+002 0.0000 1.17297631e-004 0.0133
2.18e-003 2.77679416e-007 0.0152 4.182748513263e+002 0.0000 1.16146316e-004 0.0152
2.25e-003 9.28965366e-008 0.0252 4.176499615202e+002 0.0000 3.87982349e-005 0.0252
2.29e-003 8.35346704e-008 0.0333 4.173220891268e+002 0.0000 3.48608632e-005 0.0333
2.33e-003 8.94062398e-008 0.0330 4.170407210431e+002 0.0000 3.72860427e-005 0.0330
2.36e-003 4.56816042e-008 0.0504 4.167454533255e+002 0.0000 1.90376009e-005 0.0504
2.38e-003 5.18247199e-008 0.0320 4.166303044347e+002 0.0000 2.15917488e-005 0.0320
2.41e-003 9.65321206e-008 0.0290 4.163491786502e+002 0.0000 4.01910691e-005 0.0290
2.45e-003 1.08561448e-007 0.0280 4.160483540395e+002 0.0000 4.51668117e-005 0.0280
2.53e-003 2.25720849e-007 0.0184 4.153160512565e+002 0.0000 9.37454918e-005 0.0184
2.66e-003 2.36715367e-007 0.0193 4.143566970387e+002 0.0000 9.80845977e-005 0.0193
2.79e-003 2.20810796e-007 0.0155 4.133720286684e+002 0.0000 9.12770067e-005 0.0155
2.94e-003 2.05736984e-007 0.0181 4.123537239601e+002 0.0000 8.48364114e-005 0.0181
3.05e-003 9.99222853e-008 0.0305 4.117501369844e+002 0.0000 4.11430146e-005 0.0305
3.13e-003 9.44271444e-008 0.0340 4.114447128999e+002 0.0000 3.88515493e-005 0.0340
3.21e-003 9.07433475e-008 0.0260 4.110473258213e+002 0.0000 3.72998103e-005 0.0260
3.29e-003 9.22233711e-008 0.0294 4.107438509165e+002 0.0000 3.78801826e-005 0.0294
3.41e-003 1.65007357e-007 0.0191 4.101868467689e+002 0.0000 6.76838475e-005 0.0191
3.59e-003 1.59481521e-007 0.0208 4.095067870370e+002 0.0000 6.53087653e-005 0.0208
3.77e-003 1.59694654e-007 0.0244 4.088261998642e+002 0.0000 6.52873584e-005 0.0244
3.97e-003 1.48413163e-007 0.0338 4.081156145674e+002 0.0000 6.05697290e-005 0.0338
4.17e-003 1.38982378e-007 0.0234 4.074306730443e+002 0.0000 5.66256839e-005 0.0234
4.38e-003 1.31737593e-007 0.0258 4.067460555373e+002 0.0000 5.35837463e-005 0.0258
4.55e-003 6.72827041e-008 0.0263 4.063004760478e+002 0.0000 2.73369947e-005 0.0263
4.66e-003 6.20113674e-008 0.0257 4.058875236772e+002 0.0000 2.51696404e-005 0.0257
4.78e-003 5.80677005e-008 0.0406 4.055922843279e+002 0.0000 2.35518113e-005 0.0406
4.90e-003 6.20256483e-008 0.0346 4.053130377486e+002 0.0000 2.51398039e-005 0.0346
```

```
5.09e-003 1.12917542e-007 0.0221 4.045125744274e+002 0.0000 4.56765657e-005 0.0221
5.35e-003 1.07545247e-007 0.0253 4.031380481529e+002 0.0000 4.33555811e-005 0.0253
5.63e-003 1.00316787e-007 0.0266 4.017293131719e+002 0.0000 4.03001940e-005 0.0266
5.84e-003 4.35067980e-008 0.0416 4.007717255323e+002 0.0000 1.74362945e-005 0.0416
5.99e-003 4.37682076e-008 0.0378 4.000801520638e+002 0.0000 1.75107912e-005 0.0378
6.14e-003 4.70164859e-008 0.0387 4.007227168973e+002 0.0000 1.88405740e-005 0.0387
6.30e-003 4.72070983e-008 0.0296 4.015831793013e+002 0.0000 1.89575766e-005 0.0296
6.46e-003 4.42864777e-008 0.0380 4.023804046745e+002 0.0000 1.78200108e-005 0.0380
6.56e-003 1.43818788e-008 0.0815 4.029116262048e+002 0.0000 5.79462618e-006 0.0815
6.62e-003 1.44966206e-008 0.0633 4.031814750247e+002 0.0000 5.84476886e-006 0.0633
6.68e-003 1.34439374e-008 0.0809 4.034750169684e+002 0.0000 5.42429287e-006 0.0809
6.79e-003 4.19464681e-008 0.0439 4.040094825112e+002 0.0000 1.69467709e-005 0.0439
6.96e-003 3.93566581e-008 0.0416 4.047981338978e+002 0.0000 1.59315017e-005 0.0416
7.14e-003 4.14898318e-008 0.0321 4.055872498290e+002 0.0000 1.68277468e-005 0.0321
7.32e-003 3.65948532e-008 0.0376 4.063295051351e+002 0.0000 1.48695686e-005 0.0376
7.50e-003 3.84691425e-008 0.0445 4.070730309674e+002 0.0000 1.56597504e-005 0.0445
7.69e-003 3.23922999e-008 0.0584 4.078036496726e+002 0.0000 1.32096981e-005 0.0584
7.89e-003 3.31303408e-008 0.0449 4.085809021160e+002 0.0000 1.35364245e-005 0.0449
8.09e-003 3.27832719e-008 0.0657 4.099814763307e+002 0.0000 1.34405342e-005 0.0657
8.29e-003 3.32776827e-008 0.0461 4.123319117430e+002 0.0000 1.37214505e-005 0.0461
8.50e-003 3.39844091e-008 0.0488 4.146893769845e+002 0.0000 1.40929734e-005 0.0488
8.72e-003 3.31514081e-008 0.0448 4.169600960320e+002 0.0000 1.38228143e-005 0.0448
8.94e-003 3.02528438e-008 0.0518 4.193664018343e+002 0.0000 1.26870262e-005 0.0518
9.16e-003 3.20980787e-008 0.0419 4.233498429722e+002 0.0000 1.35887166e-005 0.0419
9.39e-003 3.20646780e-008 0.0686 4.279826235658e+002 0.0000 1.37231250e-005 0.0686
9.63e-003 3.06737269e-008 0.0435 4.327388493480e+002 0.0000 1.32737133e-005 0.0435
9.88e-003 2.93781240e-008 0.0450 4.376121725256e+002 0.0000 1.28562247e-005 0.0450
1.01e-002 2.99308336e-008 0.0471 4.431435091079e+002 0.0000 1.32636546e-005 0.0471
1.04e-002 2.74197587e-008 0.0632 4.476785067025e+002 0.0000 1.22752366e-005 0.0632
1.06e-002 2.88986649e-008 0.0491 4.524522290287e+002 0.0000 1.30752653e-005 0.0491
1.09e-002 2.99081808e-008 0.0443 4.592636541303e+002 0.0000 1.37357404e-005 0.0443
1.12e-002 2.70727555e-008 0.0574 4.643295406914e+002 0.0000 1.25706801e-005 0.0574
1.15e-002 2.64758439e-008 0.0537 4.697060748889e+002 0.0000 1.24358647e-005 0.0537
1.18e-002 3.10652870e-008 0.0547 4.752251273319e+002 0.0000 1.47630050e-005 0.0547
1.21e-002 2.85767733e-008 0.0430 4.810139606771e+002 0.0000 1.37458269e-005 0.0430
1.24e-002 2.58873214e-008 0.0413 4.875163590524e+002 0.0000 1.26204927e-005 0.0413
1.27e-002 2.63712103e-008 0.0528 4.941900064148e+002 0.0000 1.30323886e-005 0.0528
1.30e-002 2.68729627e-008 0.0443 5.012438464724e+002 0.0000 1.34699072e-005 0.0443
1.33e-002 2.83871013e-008 0.0568 5.062799846439e+002 0.0000 1.43718212e-005 0.0568
1.37e-002 3.00569304e-008 0.0490 5.138003469646e+002 0.0000 1.54432613e-005 0.0490
1.40e-002 3.02773579e-008 0.0441 5.202815848116e+002 0.0000 1.57527518e-005 0.0441
1.44e-002 2.65495043e-008 0.0509 5.278602632599e+002 0.0000 1.40144284e-005 0.0509
1.47e-002 2.90301035e-008 0.0323 5.343200237058e+002 0.0000 1.55113656e-005 0.0323
1.51e-002 2.84538135e-008 0.0435 5.417105315258e+002 0.0000 1.54137304e-005 0.0435
1.55e-002 2.75522254e-008 0.0531 5.475209714524e+002 0.0000 1.50854212e-005 0.0531
1.59e-002 2.59999921e-008 0.0539 5.534294805964e+002 0.0000 1.43891621e-005 0.0539
1.63e-002 2.51894245e-008 0.0465 5.573026501699e+002 0.0000 1.40381330e-005 0.0465
1.67e-002 2.82734255e-008 0.0597 5.599319406156e+002 0.0000 1.58311940e-005 0.0597
1.71e-002 2.78314769e-008 0.0544 5.633805822058e+002 0.0000 1.56797137e-005 0.0544
1.76e-002 2.57466725e-008 0.0573 5.669149078382e+002 0.0000 1.45961725e-005 0.0573
1.80e-002 2.45185368e-008 0.0712 5.696439798328e+002 0.0000 1.39668369e-005 0.0712
1.85e-002 2.35755885e-008 0.0506 5.773957138220e+002 0.0000 1.36124438e-005 0.0506
1.89e-002 2.63284209e-008 0.0576 5.838096683227e+002 0.0000 1.53707867e-005 0.0576
1.94e-002 2.69083162e-008 0.0551 5.907005583793e+002 0.0000 1.58947574e-005 0.0551
1.98e-002 2.01056283e-008 0.0616 5.971939538685e+002 0.0000 1.20069596e-005 0.0616
3.82e-002 1.25383062e-006 0.0071 4.571028131269e+002 0.0000 5.73129504e-004 0.0071
1.03e-001 8.73832560e-007 0.0110 2.826194235185e+002 0.0000 2.46962054e-004 0.0110
1.79e-001 1.57471996e-007 0.0243 2.493399374589e+002 0.0000 3.92640576e-005 0.0243
2.53e-001 2.28004694e-009 0.1975 2.538521649451e+002 0.0000 5.78794852e-007 0.1975
```

```
3.26e-001 0.00000000e+000 0.0000 2.650157074236e+002 0.0000 0.00000000e+000 0.0000
3.99e-001 0.00000000e+000 0.0000 2.802727283180e+002 0.0000 0.00000000e+000 0.0000
4.73e-001 0.00000000e+000 0.0000 2.933256533834e+002 0.0000 0.00000000e+000 0.0000
5.46e-001 0.00000000e+000 0.0000 3.073269992438e+002 0.0000 0.00000000e+000 0.0000
6.19e-001 0.00000000e+000 0.0000 3.209405323299e+002 0.0000 0.00000000e+000 0.0000
6.92e-001 0.00000000e+000 0.0000 3.335355975337e+002 0.0000 0.00000000e+000 0.0000


Convolution integral: 1.08845875e-002  +- 0.165% (Max err: 1.803%)
```

A.1.2. Convolution of the neutron fluence spectrum with the response function of the WENDI-II rem counter

```
Energy (GeV) dPhi [1/cm2] Fluence Uncertainty [%] Response[C cm2] Response Uncertainty [%]
Convolution-Result [C] rel. Uncert [%]
4.47e-014 0.00000000e+000 0.0000 3.843776246083e-004 0.0000 0.00000000e+000 0.0000
2.42e-013 0.00000000e+000 0.0000 2.072933723326e-003 0.0000 0.00000000e+000 0.0000
3.55e-013 0.00000000e+000 0.0000 3.021647617985e-003 0.0000 0.00000000e+000 0.0000
5.19e-013 0.00000000e+000 0.0000 4.377779193402e-003 0.0000 0.00000000e+000 0.0000
7.61e-013 0.00000000e+000 0.0000 6.256811740853e-003 0.0000 0.00000000e+000 0.0000
1.11e-012 1.48358523e-010 0.7076 8.552082683125e-003 0.0000 1.26877435e-012 0.7076
1.63e-012 3.18501341e-010 0.5684 7.630726676821e-003 0.0000 2.43039668e-012 0.5684
2.39e-012 1.25031249e-009 0.3328 8.311065640705e-003 0.0000 1.03914292e-011 0.3328
3.50e-012 1.09902674e-009 0.2031 8.639009703176e-003 0.0000 9.49450270e-012 0.2031
5.13e-012 3.25481712e-009 0.1310 8.672393445328e-003 0.0000 2.82270547e-011 0.1310
7.52e-012 7.16775654e-009 0.1026 9.188316960281e-003 0.0000 6.58596189e-011 0.1026
1.10e-011 1.15474129e-008 0.0750 1.227232831105e-002 0.0000 1.41713642e-010 0.0750
1.61e-011 1.98952182e-008 0.0593 1.043492992481e-002 0.0000 2.07605208e-010 0.0593
2.36e-011 4.04898406e-008 0.0369 1.190253101199e-002 0.0000 4.81931583e-010 0.0369
3.46e-011 6.28061523e-008 0.0339 1.296274551956e-002 0.0000 8.14140169e-010 0.0339
5.07e-011 8.00118324e-008 0.0282 1.500187522615e-002 0.0000 1.20032753e-009 0.0282
7.43e-011 7.82628848e-008 0.0370 1.864534069353e-002 0.0000 1.45923815e-009 0.0370
1.09e-010 5.40899624e-008 0.0340 2.415153637434e-002 0.0000 1.30635569e-009 0.0340
1.59e-010 3.16707171e-008 0.0477 2.584684551996e-002 0.0000 8.18588133e-010 0.0477
2.34e-010 2.33136642e-008 0.0532 3.271101053228e-002 0.0000 7.62613516e-010 0.0532
3.42e-010 2.17317584e-008 0.0527 3.341270533071e-002 0.0000 7.26116840e-010 0.0527
4.69e-010 1.40922788e-008 0.0684 3.386867964087e-002 0.0000 4.77286878e-010 0.0684
5.76e-010 1.00007272e-008 0.0755 3.849315026717e-002 0.0000 3.84959495e-010 0.0755
6.53e-010 5.13046866e-009 0.1227 3.958996982218e-002 0.0000 2.03115099e-010 0.1227
7.54e-010 1.28911487e-008 0.0767 4.064199029152e-002 0.0000 5.23921941e-010 0.0767
8.55e-010 3.22341842e-009 0.1702 4.170694920128e-002 0.0000 1.34438948e-010 0.1702
9.93e-010 1.47241757e-008 0.0806 4.413032689892e-002 0.0000 6.49782688e-010 0.0806
1.28e-009 1.44988515e-008 0.0633 4.755099163732e-002 0.0000 6.89434766e-010 0.0633
1.64e-009 1.30054086e-008 0.0863 5.023713261490e-002 0.0000 6.53354437e-010 0.0863
2.10e-009 1.52552518e-008 0.0874 5.577775216677e-002 0.0000 8.50903654e-010 0.0874
2.70e-009 1.64104019e-008 0.0835 6.061274418167e-002 0.0000 9.94679493e-010 0.0835
3.47e-009 1.48691436e-008 0.0568 6.023029116629e-002 0.0000 8.95572848e-010 0.0568
4.45e-009 1.58071319e-008 0.0641 6.030769639129e-002 0.0000 9.53291714e-010 0.0641
5.72e-009 1.68391158e-008 0.0647 6.847270061148e-002 0.0000 1.15301973e-009 0.0647
7.34e-009 1.60574824e-008 0.0655 7.037628806023e-002 0.0000 1.13006601e-009 0.0655
9.42e-009 1.99007668e-008 0.0646 7.278171621121e-002 0.0000 1.44841196e-009 0.0646
1.21e-008 1.75717153e-008 0.0709 7.769043743879e-002 0.0000 1.36515425e-009 0.0709
1.55e-008 2.00131053e-008 0.0533 7.785604682418e-002 0.0000 1.55814126e-009 0.0533
1.99e-008 1.95303988e-008 0.0588 8.098239377273e-002 0.0000 1.58161844e-009 0.0588
2.56e-008 1.88531055e-008 0.0614 8.456871431300e-002 0.0000 1.59438290e-009 0.0614
3.29e-008 1.80869603e-008 0.0406 8.648159916546e-002 0.0000 1.56418925e-009 0.0406
4.22e-008 1.89243640e-008 0.0813 8.824866298097e-002 0.0000 1.67004982e-009 0.0813
5.42e-008 1.84925559e-008 0.0733 9.398056242296e-002 0.0000 1.73794081e-009 0.0733
6.96e-008 2.07502447e-008 0.0664 9.676969238920e-002 0.0000 2.00799479e-009 0.0664
```

```
8.94e-008 2.19841957e-008 0.0784 9.896988649741e-002 0.0000 2.17577336e-009 0.0784
1.15e-007 2.29928216e-008 0.0551 1.046409418141e-001 0.0000 2.40599050e-009 0.0551
1.47e-007 2.36902799e-008 0.0487 1.051004891230e-001 0.0000 2.48986001e-009 0.0487
1.89e-007 2.22823117e-008 0.0658 1.058674824093e-001 0.0000 2.35897224e-009 0.0658
2.43e-007 2.62455909e-008 0.0457 1.106266188239e-001 0.0000 2.90346098e-009 0.0457
3.12e-007 2.80593225e-008 0.0539 1.133704476125e-001 0.0000 3.18109795e-009 0.0539
4.01e-007 2.97153370e-008 0.0550 1.160435186107e-001 0.0000 3.44827226e-009 0.0550
5.14e-007 2.81390304e-008 0.0642 1.216710242658e-001 0.0000 3.42370465e-009 0.0642
6.61e-007 2.91663251e-008 0.0539 1.248664283595e-001 0.0000 3.64189484e-009 0.0539
8.48e-007 2.86684404e-008 0.0457 1.251895222971e-001 0.0000 3.58898836e-009 0.0457
1.09e-006 3.10844663e-008 0.0500 1.303789220684e-001 0.0000 4.05275921e-009 0.0500
1.30e-006 1.49697060e-008 0.0682 1.331461512188e-001 0.0000 1.99315874e-009 0.0682
1.43e-006 1.34780919e-008 0.0817 1.347472504588e-001 0.0000 1.81613582e-009 0.0817
1.55e-006 6.78601916e-009 0.1005 1.360166657402e-001 0.0000 9.23011700e-010 0.1005
1.62e-006 7.00221966e-009 0.0873 1.369278554901e-001 0.0000 9.58798922e-010 0.0873
1.75e-006 1.54700620e-008 0.0728 1.384556540905e-001 0.0000 2.14191755e-009 0.0728
1.94e-006 1.61936532e-008 0.0751 1.409867703960e-001 0.0000 2.28309087e-009 0.0751
2.14e-006 1.59280450e-008 0.0781 1.453487346912e-001 0.0000 2.31512119e-009 0.0781
2.36e-006 1.67530066e-008 0.0697 1.489957261185e-001 0.0000 2.49612638e-009 0.0697
2.55e-006 7.93704570e-009 0.1094 1.505734551303e-001 0.0000 1.19510839e-009 0.1094
2.68e-006 8.28212774e-009 0.0646 1.510449394988e-001 0.0000 1.25097348e-009 0.0646
2.80e-006 5.79931889e-009 0.1138 1.510677163111e-001 0.0000 8.76089861e-010 0.1138
2.95e-006 1.02855496e-008 0.0855 1.506596411180e-001 0.0000 1.54961720e-009 0.0855
3.19e-006 1.57224024e-008 0.0653 1.491789714414e-001 0.0000 2.34545181e-009 0.0653
3.53e-006 1.72809972e-008 0.0542 1.462554769002e-001 0.0000 2.52744049e-009 0.0542
3.90e-006 1.87360846e-008 0.0516 1.431880286637e-001 0.0000 2.68278303e-009 0.0516
4.20e-006 1.02112372e-008 0.0917 1.419253662885e-001 0.0000 1.44923358e-009 0.0917
4.42e-006 1.02714632e-008 0.1076 1.422494363856e-001 0.0000 1.46110985e-009 0.1076
4.76e-006 2.20256736e-008 0.0581 1.457664047839e-001 0.0000 3.21060326e-009 0.0581
5.26e-006 2.22656906e-008 0.0564 1.518184752428e-001 0.0000 3.38034320e-009 0.0564
5.89e-006 2.51691015e-008 0.0574 1.538705400517e-001 0.0000 3.87278323e-009 0.0574
6.67e-006 3.06154426e-008 0.0419 1.565677609934e-001 0.0000 4.79339130e-009 0.0419
7.56e-006 2.97834421e-008 0.0532 1.597125333799e-001 0.0000 4.75678899e-009 0.0532
8.57e-006 2.89130605e-008 0.0471 1.632618539055e-001 0.0000 4.72039986e-009 0.0471
9.71e-006 3.16864974e-008 0.0553 1.670797173344e-001 0.0000 5.29417103e-009 0.0553
1.10e-005 3.56132117e-008 0.0435 1.713303828908e-001 0.0000 6.10162520e-009 0.0435
1.25e-005 3.57244008e-008 0.0538 1.743234832720e-001 0.0000 6.22760199e-009 0.0538
1.41e-005 3.83992610e-008 0.0435 1.759727942229e-001 0.0000 6.75722526e-009 0.0435
1.60e-005 3.90782008e-008 0.0461 1.771148354764e-001 0.0000 6.92132910e-009 0.0461
1.81e-005 4.67288196e-008 0.0317 1.796731350487e-001 0.0000 8.39591351e-009 0.0317
2.03e-005 4.26686420e-008 0.0339 1.854319188210e-001 0.0000 7.91212815e-009 0.0339
2.16e-005 1.28499701e-008 0.0962 1.871918453127e-001 0.0000 2.40540961e-009 0.0962
2.27e-005 5.02754357e-008 0.0376 1.885180981007e-001 0.0000 9.47782951e-009 0.0376
2.39e-005 2.57732124e-008 0.0479 1.898067227762e-001 0.0000 4.89192899e-009 0.0479
2.45e-005 3.53725905e-008 0.0423 1.904509467129e-001 0.0000 6.73674336e-009 0.0423
2.54e-005 8.68651851e-008 0.0244 1.914376076027e-001 0.0000 1.66292632e-008 0.0244
2.71e-005 9.04086947e-008 0.0294 1.932147229519e-001 0.0000 1.74682909e-008 0.0294
2.99e-005 1.77984727e-007 0.0205 1.968507248850e-001 0.0000 3.50364226e-008 0.0205
3.30e-005 3.60340390e-008 0.0301 2.008559858319e-001 0.0000 7.23765243e-009 0.0301
3.47e-005 8.17882679e-009 0.0742 2.031280307228e-001 0.0000 1.66134898e-009 0.0742
3.56e-005 9.11181579e-009 0.1083 2.043338497795e-001 0.0000 1.86185240e-009 0.1083
3.84e-005 6.19549462e-008 0.0364 2.082181228049e-001 0.0000 1.29001426e-008 0.0364
4.35e-005 1.07987516e-007 0.0292 2.154466116085e-001 0.0000 2.32655445e-008 0.0292
4.93e-005 1.73049520e-007 0.0177 2.231385994124e-001 0.0000 3.86140276e-008 0.0177
5.45e-005 1.32160081e-007 0.0202 2.293596979341e-001 0.0000 3.03121962e-008 0.0202
5.80e-005 1.16755667e-007 0.0245 2.332971482080e-001 0.0000 2.72387642e-008 0.0245
6.10e-005 1.41882683e-007 0.0245 2.365608663482e-001 0.0000 3.35638903e-008 0.0245
6.49e-005 2.71444042e-007 0.0172 2.409334348941e-001 0.0000 6.53999454e-008 0.0172
7.17e-005 6.43085553e-007 0.0107 2.490652632030e-001 0.0000 1.60170273e-007 0.0107
```

```
8.13e-005 2.48768321e-007 0.0142 2.611362716211e-001 0.0000 6.49624318e-008 0.0142
9.21e-005 1.43199388e-007 0.0199 2.752185855930e-001 0.0000 3.94111331e-008 0.0199
1.04e-004 4.04837098e-007 0.0133 2.905110864836e-001 0.0000 1.17609665e-007 0.0133
1.14e-004 2.61108263e-007 0.0176 3.025418416366e-001 0.0000 7.89961747e-008 0.0176
1.20e-004 1.40337609e-007 0.0211 3.098890266677e-001 0.0000 4.34890850e-008 0.0211
1.26e-004 4.64203856e-007 0.0154 3.176078000038e-001 0.0000 1.47434765e-007 0.0154
1.32e-004 4.72997262e-007 0.0109 3.257242238573e-001 0.0000 1.54066666e-007 0.0109
1.39e-004 1.73897002e-007 0.0155 3.342650954992e-001 0.0000 5.81276978e-008 0.0155
1.46e-004 9.79519821e-008 0.0272 3.432627344684e-001 0.0000 3.36232652e-008 0.0272
1.54e-004 1.12621474e-007 0.0258 3.526373281384e-001 0.0000 3.97145355e-008 0.0258
1.60e-004 4.97304710e-008 0.0345 3.598421222810e-001 0.0000 1.78951182e-008 0.0345
1.64e-004 8.15863994e-008 0.0311 3.647667132354e-001 0.0000 2.97600028e-008 0.0311
1.68e-004 8.62810820e-008 0.0310 3.697969042740e-001 0.0000 3.19064770e-008 0.0310
1.72e-004 1.04578514e-007 0.0293 3.749421226900e-001 0.0000 3.92108900e-008 0.0293
1.79e-004 2.85368336e-007 0.0176 3.828975483897e-001 0.0000 1.09266836e-007 0.0176
1.88e-004 3.14186692e-007 0.0153 3.940112649613e-001 0.0000 1.23793096e-007 0.0153
1.97e-004 2.67118797e-007 0.0159 4.058094143984e-001 0.0000 1.08399323e-007 0.0159
2.08e-004 1.76036427e-007 0.0187 4.186328558073e-001 0.0000 7.36946322e-008 0.0187
2.18e-004 2.30817638e-007 0.0200 4.325174142870e-001 0.0000 9.98326478e-008 0.0200
2.29e-004 2.78764173e-007 0.0182 4.472647719475e-001 0.0000 1.24681394e-007 0.0182
2.41e-004 3.96327902e-007 0.0181 4.626528221156e-001 0.0000 1.83362222e-007 0.0181
2.53e-004 4.52649464e-007 0.0129 4.782985058476e-001 0.0000 2.16501562e-007 0.0129
2.66e-004 6.78624338e-007 0.0115 4.936956702759e-001 0.0000 3.35033897e-007 0.0115
2.77e-004 2.24402960e-007 0.0188 5.054227736351e-001 0.0000 1.13418367e-007 0.0188
2.84e-004 1.27901189e-007 0.0219 5.134997963144e-001 0.0000 6.56772343e-008 0.0219
2.91e-004 1.50810743e-007 0.0245 5.219158622694e-001 0.0000 7.87105189e-008 0.0245
2.98e-004 2.01173530e-007 0.0214 5.308026267875e-001 0.0000 1.06783438e-007 0.0214
3.06e-004 2.40813882e-007 0.0228 5.397541155338e-001 0.0000 1.29980284e-007 0.0228
3.14e-004 1.97084340e-007 0.0156 5.486141070615e-001 0.0000 1.08123249e-007 0.0156
3.25e-004 4.41119504e-007 0.0137 5.619685854140e-001 0.0000 2.47895304e-007 0.0137
3.42e-004 6.13579106e-007 0.0092 5.800966527590e-001 0.0000 3.55935186e-007 0.0092
3.60e-004 4.71871973e-007 0.0109 5.989578678036e-001 0.0000 2.82631431e-007 0.0109
3.78e-004 4.93505329e-007 0.0080 6.190738370547e-001 0.0000 3.05516237e-007 0.0080
3.98e-004 5.67927491e-007 0.0087 6.411256251329e-001 0.0000 3.64112868e-007 0.0087
4.18e-004 3.79587743e-007 0.0166 6.645806289057e-001 0.0000 2.52266661e-007 0.0166
4.39e-004 3.93884685e-007 0.0115 6.895441616772e-001 0.0000 2.71600885e-007 0.0115
4.62e-004 4.78797483e-007 0.0154 7.159367253390e-001 0.0000 3.42788702e-007 0.0154
4.86e-004 5.21478185e-007 0.0149 7.434854872593e-001 0.0000 3.87711462e-007 0.0149
5.04e-004 2.84748967e-007 0.0118 7.640202667361e-001 0.0000 2.17553982e-007 0.0118
5.17e-004 2.93294209e-007 0.0169 7.756660989508e-001 0.0000 2.27498375e-007 0.0169
5.30e-004 2.12248395e-007 0.0232 7.868750507406e-001 0.0000 1.67012967e-007 0.0232
5.43e-004 2.71115384e-007 0.0185 7.982479064052e-001 0.0000 2.16417288e-007 0.0185
5.64e-004 5.20005957e-007 0.0120 8.171721999635e-001 0.0000 4.24934412e-007 0.0120
5.93e-004 6.17778158e-007 0.0135 8.424839677855e-001 0.0000 5.20468194e-007 0.0135
6.23e-004 6.44793309e-007 0.0107 8.680193146834e-001 0.0000 5.59693046e-007 0.0107
6.55e-004 5.02936138e-007 0.0137 8.946239536937e-001 0.0000 4.49938716e-007 0.0137
6.89e-004 6.66252152e-007 0.0133 9.233257712960e-001 0.0000 6.15167782e-007 0.0133
7.24e-004 6.39430920e-007 0.0111 9.520869342500e-001 0.0000 6.08793825e-007 0.0111
7.62e-004 5.97287927e-007 0.0126 9.802107011239e-001 0.0000 5.85468018e-007 0.0126
8.01e-004 4.26366956e-007 0.0156 1.010404754244e+000 0.0000 4.30803199e-007 0.0156
8.42e-004 4.75437041e-007 0.0141 1.035366658188e+000 0.0000 4.92251660e-007 0.0141
8.85e-004 4.87530318e-007 0.0111 1.060011033055e+000 0.0000 5.16787516e-007 0.0111
9.30e-004 5.64785069e-007 0.0142 1.088086894057e+000 0.0000 6.14535232e-007 0.0142
9.58e-004 9.44429934e-008 0.0365 1.104594649777e+000 0.0000 1.04321225e-007 0.0365
9.70e-004 1.75737154e-007 0.0181 1.111821908397e+000 0.0000 1.95388418e-007 0.0181
9.90e-004 2.80712898e-007 0.0199 1.124080805964e+000 0.0000 3.15543981e-007 0.0199
1.03e-003 5.15615887e-007 0.0117 1.144468616373e+000 0.0000 5.90106200e-007 0.0117
1.08e-003 5.57924091e-007 0.0129 1.169814408853e+000 0.0000 6.52667641e-007 0.0129
1.14e-003 4.33867162e-007 0.0146 1.198039977730e+000 0.0000 5.19790205e-007 0.0146
```

```
1.18e-003 1.90538476e-007 0.0188 1.219746419489e+000 0.0000 2.32408624e-007 0.0188
1.21e-003 2.13167338e-007 0.0188 1.236371351492e+000 0.0000 2.63553989e-007 0.0188
1.26e-003 4.21081513e-007 0.0141 1.257828651718e+000 0.0000 5.29648392e-007 0.0141
1.32e-003 4.26119681e-007 0.0148 1.268569800117e+000 0.0000 5.40562558e-007 0.0148
1.39e-003 4.03578512e-007 0.0148 1.271984261748e+000 0.0000 5.13345515e-007 0.0148
1.46e-003 3.68374971e-007 0.0129 1.287228043142e+000 0.0000 4.74182594e-007 0.0129
1.51e-003 1.78909917e-007 0.0167 1.313754159568e+000 0.0000 2.35043648e-007 0.0167
1.55e-003 1.67691514e-007 0.0197 1.322724718565e+000 0.0000 2.21809710e-007 0.0197
1.59e-003 1.79254796e-007 0.0173 1.330679860845e+000 0.0000 2.38530748e-007 0.0173
1.63e-003 1.88436894e-007 0.0166 1.337790145652e+000 0.0000 2.52089020e-007 0.0166
1.69e-003 3.45400176e-007 0.0169 1.347333124054e+000 0.0000 4.65369098e-007 0.0169
1.78e-003 3.27835939e-007 0.0149 1.359365069773e+000 0.0000 4.45648724e-007 0.0149
1.85e-003 1.80051111e-007 0.0241 1.369348249338e+000 0.0000 2.46552674e-007 0.0241
1.90e-003 1.61389859e-007 0.0234 1.377248112702e+000 0.0000 2.22273878e-007 0.0234
1.94e-003 1.40841541e-007 0.0259 1.386733773689e+000 0.0000 1.95309721e-007 0.0259
1.99e-003 1.49669899e-007 0.0228 1.398392256125e+000 0.0000 2.09297228e-007 0.0228
2.07e-003 2.79713137e-007 0.0133 1.407646217733e+000 0.0000 3.93737140e-007 0.0133
2.18e-003 2.77679416e-007 0.0152 1.408374225921e+000 0.0000 3.91076532e-007 0.0152
2.25e-003 9.28965366e-008 0.0252 1.404999399716e+000 0.0000 1.30519578e-007 0.0252
2.29e-003 8.35346704e-008 0.0333 1.403097039153e+000 0.0000 1.17207249e-007 0.0333
2.33e-003 8.94062398e-008 0.0330 1.401547338742e+000 0.0000 1.25307077e-007 0.0330
2.36e-003 4.56816042e-008 0.0504 1.400867340337e+000 0.0000 6.39938674e-008 0.0504
2.38e-003 5.18247199e-008 0.0320 1.400750425997e+000 0.0000 7.25934985e-008 0.0320
2.41e-003 9.65321206e-008 0.0290 1.401232456296e+000 0.0000 1.35263941e-007 0.0290
2.45e-003 1.08561448e-007 0.0280 1.403438993204e+000 0.0000 1.52359369e-007 0.0280
2.53e-003 2.25720849e-007 0.0184 1.404295412311e+000 0.0000 3.16978753e-007 0.0184
2.66e-003 2.36715367e-007 0.0193 1.380560704585e+000 0.0000 3.26799934e-007 0.0193
2.79e-003 2.20810796e-007 0.0155 1.357560391744e+000 0.0000 2.99763991e-007 0.0155
2.94e-003 2.05736984e-007 0.0181 1.332260866118e+000 0.0000 2.74095332e-007 0.0181
3.05e-003 9.99222853e-008 0.0305 1.306727172008e+000 0.0000 1.30571165e-007 0.0305
3.13e-003 9.44271444e-008 0.0340 1.293635428293e+000 0.0000 1.22154299e-007 0.0340
3.21e-003 9.07433475e-008 0.0260 1.288176377472e+000 0.0000 1.16893437e-007 0.0260
3.29e-003 9.22233711e-008 0.0294 1.289170845914e+000 0.0000 1.18891681e-007 0.0294
3.41e-003 1.65007357e-007 0.0191 1.299588907170e+000 0.0000 2.14441731e-007 0.0191
3.59e-003 1.59481521e-007 0.0208 1.320515477378e+000 0.0000 2.10597817e-007 0.0208
3.77e-003 1.59694654e-007 0.0244 1.332137078912e+000 0.0000 2.12735170e-007 0.0244
3.97e-003 1.48413163e-007 0.0338 1.309667423128e+000 0.0000 1.94371884e-007 0.0338
4.17e-003 1.38982378e-007 0.0234 1.314349752915e+000 0.0000 1.82671454e-007 0.0234
4.38e-003 1.31737593e-007 0.0258 1.317027303760e+000 0.0000 1.73502007e-007 0.0258
4.55e-003 6.72827041e-008 0.0263 1.314028523840e+000 0.0000 8.84113924e-008 0.0263
4.66e-003 6.20113674e-008 0.0257 1.312598459720e+000 0.0000 8.13960254e-008 0.0257
4.78e-003 5.80677005e-008 0.0406 1.313875458798e+000 0.0000 7.62937266e-008 0.0406
4.90e-003 6.20256483e-008 0.0346 1.320120869992e+000 0.0000 8.18813528e-008 0.0346
5.09e-003 1.12917542e-007 0.0221 1.318494489671e+000 0.0000 1.48881157e-007 0.0221
5.35e-003 1.07545247e-007 0.0253 1.300270155673e+000 0.0000 1.39837876e-007 0.0253
5.63e-003 1.00316787e-007 0.0266 1.290563195720e+000 0.0000 1.29465154e-007 0.0266
5.84e-003 4.35067980e-008 0.0416 1.277878904455e+000 0.0000 5.55964193e-008 0.0416
5.99e-003 4.37682076e-008 0.0378 1.261432992631e+000 0.0000 5.52106611e-008 0.0378
6.14e-003 4.70164859e-008 0.0387 1.250087982105e+000 0.0000 5.87747440e-008 0.0387
6.30e-003 4.72070983e-008 0.0296 1.239204883618e+000 0.0000 5.84992667e-008 0.0296
6.46e-003 4.42864777e-008 0.0380 1.228046007509e+000 0.0000 5.43858321e-008 0.0380
6.56e-003 1.43818788e-008 0.0815 1.220451184982e+000 0.0000 1.75523810e-008 0.0815
6.62e-003 1.44966206e-008 0.0633 1.216604737375e+000 0.0000 1.76366572e-008 0.0633
6.68e-003 1.34439374e-008 0.0809 1.212726062605e+000 0.0000 1.63038133e-008 0.0809
6.79e-003 4.19464681e-008 0.0439 1.204873972335e+000 0.0000 5.05402077e-008 0.0439
6.96e-003 3.93566581e-008 0.0416 1.192846099784e+000 0.0000 4.69464361e-008 0.0416
7.14e-003 4.14898318e-008 0.0321 1.179557125954e+000 0.0000 4.89396268e-008 0.0321
7.32e-003 3.65948532e-008 0.0376 1.165078718060e+000 0.0000 4.26358847e-008 0.0376
7.50e-003 3.84691425e-008 0.0445 1.149887718604e+000 0.0000 4.42351945e-008 0.0445
```

```
7.69e-003 3.23922999e-008 0.0584 1.134317905687e+000 0.0000 3.67431658e-008 0.0584
7.89e-003 3.31303408e-008 0.0449 1.118758556584e+000 0.0000 3.70648523e-008 0.0449
8.09e-003 3.27832719e-008 0.0657 1.105072853395e+000 0.0000 3.62279039e-008 0.0657
8.29e-003 3.32776827e-008 0.0461 1.098149082937e+000 0.0000 3.65438567e-008 0.0461
8.50e-003 3.39844091e-008 0.0488 1.094998096529e+000 0.0000 3.72128632e-008 0.0488
8.72e-003 3.31514081e-008 0.0448 1.091728759505e+000 0.0000 3.61923456e-008 0.0448
8.94e-003 3.02528438e-008 0.0518 1.083821017541e+000 0.0000 3.27886679e-008 0.0518
9.16e-003 3.20980787e-008 0.0419 1.077001021544e+000 0.0000 3.45696635e-008 0.0419
9.39e-003 3.20646780e-008 0.0686 1.075300270046e+000 0.0000 3.44791570e-008 0.0686
9.63e-003 3.06737269e-008 0.0435 1.074601234972e+000 0.0000 3.29620248e-008 0.0435
9.88e-003 2.93781240e-008 0.0450 1.072468654478e+000 0.0000 3.15071171e-008 0.0450
1.01e-002 2.99308336e-008 0.0471 1.068741914916e+000 0.0000 3.19883364e-008 0.0471
1.04e-002 2.74197587e-008 0.0632 1.066178607387e+000 0.0000 2.92343601e-008 0.0632
1.06e-002 2.88986649e-008 0.0491 1.063550814583e+000 0.0000 3.07351986e-008 0.0491
1.09e-002 2.99081808e-008 0.0443 1.060856029044e+000 0.0000 3.17282739e-008 0.0443
1.12e-002 2.70727555e-008 0.0574 1.054755596210e+000 0.0000 2.85551404e-008 0.0574
1.15e-002 2.64758439e-008 0.0537 1.045844696221e+000 0.0000 2.76896209e-008 0.0537
1.18e-002 3.10652870e-008 0.0547 1.036589391157e+000 0.0000 3.22019470e-008 0.0547
1.21e-002 2.85767733e-008 0.0430 1.027678753424e+000 0.0000 2.93677428e-008 0.0430
1.24e-002 2.58873214e-008 0.0413 1.020631294974e+000 0.0000 2.64214103e-008 0.0413
1.27e-002 2.63712103e-008 0.0528 1.018891805355e+000 0.0000 2.68694101e-008 0.0528
1.30e-002 2.68729627e-008 0.0443 1.020008669547e+000 0.0000 2.74106549e-008 0.0443
1.33e-002 2.83871013e-008 0.0568 1.021111023120e+000 0.0000 2.89863821e-008 0.0568
1.37e-002 3.00569304e-008 0.0490 1.018863066629e+000 0.0000 3.06238963e-008 0.0490
1.40e-002 3.02773579e-008 0.0441 1.009931058044e+000 0.0000 3.05780441e-008 0.0441
1.44e-002 2.65495043e-008 0.0509 1.009695333671e+000 0.0000 2.68069106e-008 0.0509
1.47e-002 2.90301035e-008 0.0323 1.010455961787e+000 0.0000 2.93336411e-008 0.0323
1.51e-002 2.84538135e-008 0.0435 1.010000000000e+000 0.0000 2.87383516e-008 0.0435
1.55e-002 2.75522254e-008 0.0531 1.010000000000e+000 0.0000 2.78277477e-008 0.0531
1.59e-002 2.59999921e-008 0.0539 1.010000000000e+000 0.0000 2.62599920e-008 0.0539
1.63e-002 2.51894245e-008 0.0465 1.011411888677e+000 0.0000 2.54768834e-008 0.0465
1.67e-002 2.82734255e-008 0.0597 1.013472977831e+000 0.0000 2.86543527e-008 0.0597
1.71e-002 2.78314769e-008 0.0544 1.015586064797e+000 0.0000 2.82652601e-008 0.0544
1.76e-002 2.57466725e-008 0.0573 1.017752643443e+000 0.0000 2.62037440e-008 0.0573
1.80e-002 2.45185368e-008 0.0712 1.019974220136e+000 0.0000 2.50082755e-008 0.0712
1.85e-002 2.35755885e-008 0.0506 1.024483623786e+000 0.0000 2.41528044e-008 0.0506
1.89e-002 2.63284209e-008 0.0576 1.029227406407e+000 0.0000 2.70979324e-008 0.0576
1.94e-002 2.69083162e-008 0.0551 1.069227621947e+000 0.0000 2.87711149e-008 0.0551
1.98e-002 2.01056283e-008 0.0616 1.112706903177e+000 0.0000 2.23716714e-008 0.0616
3.82e-002 1.25383062e-006 0.0071 1.235921727806e+000 0.0000 1.54963651e-006 0.0071
1.03e-001 8.73832560e-007 0.0110 1.346230218518e+000 0.0000 1.17637980e-006 0.0110
1.79e-001 1.57471996e-007 0.0243 1.447261315932e+000 0.0000 2.27903128e-007 0.0243
2.53e-001 2.28004694e-009 0.1975 1.572388666756e+000 0.0000 3.58511997e-009 0.1975
3.26e-001 0.00000000e+000 0.0000 1.728181322676e+000 0.0000 0.00000000e+000 0.0000
3.99e-001 0.00000000e+000 0.0000 1.898530449851e+000 0.0000 0.00000000e+000 0.0000
4.73e-001 0.00000000e+000 0.0000 2.066559225444e+000 0.0000 0.00000000e+000 0.0000
5.46e-001 0.00000000e+000 0.0000 2.221055088944e+000 0.0000 0.00000000e+000 0.0000
6.19e-001 0.00000000e+000 0.0000 2.341044675672e+000 0.0000 0.00000000e+000 0.0000
6.92e-001 0.00000000e+000 0.0000 2.493481988516e+000 0.0000 0.00000000e+000 0.0000

Convolution integral: 3.05792091e-005  +- 0.167% (Max err: 1.816%)
```

A.2. FLUKA file

This section shows the FLUKA input file which was used to simulate the neutron fluence spectrum for the WENDI-II rem counter in the vicinity of the chopper.

```
TITLE
Chopper
#define E1
#define E2
#define E3
#define E4
#define E5
* Set the defaults for precision simulations
DEFAULTS                                                          PRECISIO
#if E1
* Define the beam characteristics
!@scale=100
BEAM            -0.25                         -1.0      -1.0       PROTON
#elif E2
* Define the beam characteristics
!@scale=100
BEAM            -0.205                        -1.0      -1.0       PROTON
#elif E3
* Define the beam characteristics
!@scale=100
BEAM            -0.23                         -1.0      -1.0       PROTON
#elif E4
* Define the beam characteristics
!@scale=100
BEAM            -0.255                        -1.0      -1.0       PROTON
#elif E5
* Define the beam characteristics
!@scale=100
BEAM            -1.0                          -1.0      -1.0       PROTON
#endif
* Define the beam position
BEAMPOS           0.        0.        40.
GEOBEGIN                                                          COMBNAME
    0    0
* Black body
SPH blkbody    0.0 0.0 0.0 100000.0
* Void sphere
SPH void       0.0 0.0 0.0 10000.0
* Wendi
RCC wendi      -10.5 50.0 170.0 21.0 0. 0. 12.5
#if 0
* Tungsten part wendi
RCC WC         -6.4 50.0 170.0 11.46 0. 0. 5.5
#endif
#if 0
* Inside of tungsten part
RCC WC_i       -4.9 50. 170. 9.96 0.0 0. 4.
#endif
* Outside of the base quader
RPP base_o     -17.25 17.25 -13.023 8.736 100. 146.22
* inside of the base quader
RPP base_i     -6.56 16.05 -10. 5.21 107.3 143.1
RPP dump       -3. 3. -1. 5. 115.2 146.
* Alu pipe after CHO outside
RPP Alupi1o    -3.3 3.3 -3.3 3.3 146.22 156.52
* Alu pipe after CHO inside
RPP Alupi1i    -2.6 2.6 -2.6 2.6 146.22 156.52
* MKC1 outside
RPP endbox_o   -15. 15. -17.15 17.15 156.52 196.72
```

```
* MKC1 inside
RPP endbox_i    -3.3 3.3 -3.3 3.3 156.52 196.72
* Alu pipe after CHO outside
RPP Alupip_o    -3.3 3.3 -3.3 3.3 89.7 100.
* Alu pipe after CHO inside
RPP Alupip_i    -2.6 2.6 -2.6 2.6 89.7 100.
* MKC outside
RPP bebox_o     -15. 15. -17.15 17.15 49.5 89.7
* MKC inside
RPP bebox_i     -3.3 3.3 -3.3 3.3 49.5 89.7
ZCC beamhole    0. 0. 3.3
XYP beamcut1    100.
XYP beamcut2    146.22
* SFX
RPP SFX_a       -4.3 -2.3 8.736 23.736 111. 113.
* SFX
RPP SFX_b       -6.8 0.2 23.736 50.736 108.5 115.5
* SFX
RPP SFX_c       -8.3 1.7 68.736 87.736 107. 117.
* Floor
RPP floor       -275. -125. -400. 400. -200. 400.
* Wall
RPP wall        -125. 800. 400. 800. -600. 1000.
#if 0
RCC TLD1        0.0 38. 128. 0.0 0.0 0.09 0.45
#endif
#if 0
RCC TLD2        0.0 40.66 160.66 0.0 0.0 0.09 0.45
#endif
#if 0
RCC TLD3        0.0 59.34 179.34 0.0 0.0 0.09 0.45
#endif
END
* Black hole
BLKBODY       5 +blkbody -void
* Void around
VOID          5 +void -base_o -wendi -Alupip_o -endbox_o - SFX_a -SFX_b
                -SFX_c- wall -floor -bebox_o -Alupi1o
* Target
WENDI         5 +wendi
#if 0
WC            5 +WC - WC_i
#endif
#if 0
WC_i          5 +WC_i
#endif
REG_ALU       5 +base_o -base_i-beamhole -  dump
REG_DUMP      5 +dump
REG_VAC       5 +base_i-dump
                | +beamhole - dump -beamcut1 +beamcut2
REG_PIPE      5 +Alupip_o-Alupip_i
                | +Alupi1o -Alupi1i
REG_PIP1      5 +Alupip_i
                | +Alupi1i
MAGNET_O      5 +endbox_o -endbox_i
                | +bebox_o -bebox_i
MAGNET_I      5 +endbox_i
                | +bebox_i
SFX           5 +SFX_a
```

```
                    | +SFX_b
                    | +SFX_c
WAFL           5 +floor
                    | +wall
#if 0
TLD_S          5 +TLD1
                    | +TLD2
                    | +TLD3
#endif
END
GEOEND
* ..+....1....+....2....+....3....+....4....+....5....+....6....+....7..
ASSIGNMA   BLCKHOLE   BLKBODY
ASSIGNMA        AIR      VOID
ASSIGNMA        ALU   REG_ALU
ASSIGNMA     VACUUM   REG_VAC
ASSIGNMA       DUMP  REG_DUMP
ASSIGNMA        AIR     WENDI
ASSIGNMA        ALU  REG_PIPE
ASSIGNMA     VACUUM  REG_PIP1
ASSIGNMA    MAGSTEEL  MAGNET_O
ASSIGNMA     VACUUM  MAGNET_I
ASSIGNMA        ALU       SFX
ASSIGNMA      CONCR      WAFL
*ASSIGNMA       LiF     TLD_S
*ASSIGNMA   TUNGSTEN        WC
*ASSIGNMA   POLYETHY      WC_i
MATERIAL        14.            2.33                        SILICON
MATERIAL        12.            1.74                        MAGNESIU
MATERIAL        25.            7.44                        MANGANES
*MATERIAL       22.            4.54                         TITANIUM
MATERIAL        26.           7.874                        IRON
MATERIAL        29.            8.96                        COPPER
MATERIAL        24.            7.18                        CHROMIUM
MATERIAL        30.           7.133                        ZINC
MATERIAL        15.             2.2                        PHOSPHO
MATERIAL        13.          2.6989                        ALUMINUM
MATERIAL        28.           8.902                        NICKEL
MATERIAL        23.            6.11                        VANADIUM
MATERIAL        74.            19.3                        TUNGSTEN
MATERIAL        74.           10.71                        TUNG_POW
MATERIAL         3.           0.534                        LITHIUM
MATERIAL         9.        0.001696                        FLUORINE
MATERIAL        19.   39.093     0.862                     POTASSIU
MATERIAL        16.   32.066      2.06                     SULFUR
MATERIAL        24.  51.9961      7.18                     CHROMIUM
MATERIAL        25. 54.938049     7.21                     MANGANES
MATERIAL                        2.739                      ALU
MATERIAL                          18.                      DUMP
MATERIAL                          2.4                      CONCR
MATERIAL                         7.71                      MAGSTEEL
COMPOUND      -1.05    SILICON      -1.1  MAGNESIU    -0.66 MANGANESALU
COMPOUND     -0.017   TITANIUM     -0.44      IRON    -0.08  COPPERALU
COMPOUND      -0.18   CHROMIUM    -0.065      ZINC  -96.352 ALUMINUMALU
COMPOUND      -0.03     NICKEL     -0.02  VANADIUM               ALU
COMPOUND      -95.0   TUNGSTEN      -2.5    NICKEL     -2.5 COPPERDUMP
COMPOUND      -0.47   HYDROGEN    -10.36    CARBON   -49.28 OXYGENCONCR
COMPOUND      -1.68   MAGNESIU     -0.42  ALUMINUM    -0.08  IRONCONCR
COMPOUND      -1.47    SILICON     -0.03    SODIUM    -35.8 CALCIUMCONCR
```

```
COMPOUND         -0.05  TITANIUM      -0.09  POTASSIU      -0.27     SULFURCONCR
COMPOUND         0.003  CARBON         2.36  SILICON       0.318  MANGANESMAGSTEEL
COMPOUND         0.015  PHOSPHO      0.0054  SULFUR         1.05  ALUMINUMMAGSTEEL
COMPOUND       96.2486  IRON                                             MAGSTEEL
* LiF Crystal
* LiF crystals rapidly become damaged under ion bombardment, and
* there can be up to 8% density change in the surface region.
MATERIAL                              2.635                                  LiF
COMPOUND          1.0   LITHIUM        1.0  FLUORINE                         LiF
USRBIN           10.    DOSE-EQ       -21.     10.5     62.5     182.5Wendi_o
USRBIN          -10.5   37.5         157.5      1.       1.        1. &
*USRBIN          10.    DOSE-EQ       -21.     10.5     51.22    171.22Wendi_i
*USRBIN         -10.5   48.78        168.78     1.       1.        1. &
*USRBIN          12.    DOSE-EQ       -21.    WENDI                    Wendi_reg
*USRBIN         WENDI                                                       &
*USRBIN          10.    DOSE-EQ       -21.     0.45     38.45    128.09TLD1D
*USRBIN         -0.45   37.55         128.      1.       1.        1. &
*USRBIN          10.    DOSE-EQ       -21.     0.45     41.11    160.75TLD2D
*USRBIN         -0.45   40.21        160.66     1.       1.        1. &
*USRBIN          10.    DOSE-EQ       -21.     0.45     59.79    179.43TLD3D
*USRBIN         -0.45   58.89        179.34     1.       1.        1. &
*USRBIN          10.    NEUTRON       -21.     0.45     38.45    128.09TLD1F
*USRBIN         -0.45   37.55         128.      1.       1.        1. &
*USRBIN          10.    NEUTRON       -21.     0.45     41.11    160.75TLD2F
*USRBIN         -0.45   40.21        160.66     1.       1.        1. &
*USRBIN          10.    NEUTRON       -21.     0.45     59.79    179.43TLD3F
*USRBIN         -0.45   58.89        179.34     1.       1.        1. &
*USRBIN          10.    NEUTRON       -21.      5.      100.      1000.alleszam
*USRBIN          -5.   -800.        -600.       1.     1000.      1000. &
*USRBIN          10.    DOSE-EQ       -21.     0.45     38.45    128.09TLD1ndose
*USRBIN         -0.45   37.55         128.      1.       1.        1. &
*AUXSCORE      USRBIN   NEUTRON             TLD1ndose TLD1ndose       1.AMB74
*USRBIN          10.    DOSE-EQ       -21.     0.45     41.11    160.75TLD2ndose
*USRBIN         -0.45   40.21        160.66     1.       1.        1. &
*AUXSCORE      USRBIN   NEUTRON             TLD2ndose TLD2ndose       1.AMB74
*USRBIN          10.    DOSE-EQ       -21.     0.45     59.79    179.43TLD3ndose
*USRBIN         -0.45   58.89        179.34     1.       1.        1. &
*AUXSCORE      USRBIN   NEUTRON             TLD3ndose TLD3ndose       1.AMB74
*USRBIN          10.    DOSE-EQ       -21.     0.45     38.45    128.09TLD1gdose
*USRBIN         -0.45   37.55         128.      1.       1.        1. &
*AUXSCORE      USRBIN   PHOTON              TLD1gdose TLD1gdose       1.AMB74
*USRBIN          10.                  -21.     0.45     41.11    160.75TLD2gdose
*USRBIN         -0.45   40.21        160.66     1.       1.        1. &
*AUXSCORE      USRBIN   PHOTON              TLD2gdose TLD2gdose       1.AMB74
*USRBIN          10.    DOSE-EQ       -21.     0.45     59.79    179.43TLD3gdose
*USRBIN         -0.45   58.89        179.34     1.       1.        1. &
*AUXSCORE      USRBIN   PHOTON              TLD3gdose TLD3gdose       1.AMB74
USRTRACK          1.    NEUTRON       -22.    WENDI  10308.35         W_spec
* Set the random number seed
RANDOMIZ         1.0
* Set the number of primary histories to be simulated in the run
START          1E+06
STOP
```